Advances in Colloid and Interface Science xxx (2015) xxx–xxx

Contents lists available at ScienceDirect

Advances in Colloid and Interface Science

journal homepage: www.elsevier.com/locate/cis

Historical perspective

The science of foaming

Wiebke Drenckhan [a,*], Arnaud Saint-Jalmes [b]

[a] Laboratoire de Physique des Solides, Université Paris-Sud, UMR 8502, Orsay, France
[b] Institut de Physique de Rennes, CNRS UMR 6251, Université Rennes-1, Rennes, France

ARTICLE INFO

Available online xxxx

Keywords:
Foaming
Liquid foam
Bubble generation
Gas/liquid interface
Foaming techniques
Bubble size distribution

ABSTRACT

The generation of liquid foams is at the heart of numerous natural, technical or scientific processes. Even though the subject of foam generation has a long-standing history, many recent progresses have been made in an attempt to elucidate the fundamental processes at play. We review the subject by providing an overview of the relevant key mechanisms of bubble generation within a coherent hydrodynamic context; and we discuss different foaming techniques which exploit these mechanisms.

Contents

1. Introduction

Liquid foams consist of gas bubbles which are closely packed within a liquid carrier matrix [1–4]. Coalescence of the bubbles is hindered by the addition of stabilising agents, which may be low molecular weight surfactants, polymers, proteins, nano-particles, or their mixtures [5]. The resulting network of gas/liquid interfaces provides liquid foams with numerous complex and useful properties. Amongst these are thermal and acoustic properties, or the fact that they strongly scatter light. Most exploited are their rheological properties, since they have the unique feature that the same foam may behave like an elastic/plastic

* Corresponding author.
E-mail address: Wiebke.Drenckhan@u-psud.fr (W. Drenckhan).

http://dx.doi.org/10.1016/j.cis.2015.04.001
0001-8686/

solid or like a viscous liquid depending on how it is manipulated. The result is that liquid foams have found their way into numerous applications of very different kind, including cosmetic and laundry applications, fire fighting, oil recovery, soil remidation or foam fractionation. Liquid foams are also very important as templates for the generation of solid foams. Last but not at all the least, foams may also occur as a byproduct in many natural or industrial processes. In the latter case, their presence may interfere with production in a harmful manner; paper or paint industry being the most prominent examples.

The physical properties of a foam depend crucially on its structural properties — such as the gas fraction Φ (= gas volume / foam volume) or the bubble size distribution. A large number of foaming techniques has been developed in the past in order to obtain control over these parameters. Depending on the technique, bubble sizes may range from micrometres to centimetres, bubbles can be extremely monodisperse or highly polydisperse, and gas fractions can be varied over the entire range. Unfortunately, to most users' despair, each individual technique typically covers only a relatively small range of these parameters. Moreover, the choice of a foaming technique is not only guided by the properties of the obtained foam, but also by how rapidly it can be generated. Hence, any academic or industrial foaming application needs to start with a wise choice of the appropriate foaming technique(s) — which can be a daunting task.

All foaming techniques have one aspect in common: the generation of bubbles within a liquid. This implies the creation of gas/liquid interfaces of interfacial tension γ which, in turn, implies an energy input of at least $U = 4\gamma r_B^2$ per bubble. For typical interfacial tensions and bubble sizes, this is many orders of magnitude larger than thermal energies (kT), which means that bubble formation is not a spontaneous process and that one needs to put a lot of energy into a liquid in order to create a foam. What distinguishes the different foaming techniques is how exactly one chooses to put this energy into the liquid. This may be done by physical, chemical or even biological means (see Table 1). Physical means include mechanical action (gas sparging, whipping, shaking, etc.) or phase transitions (boiling, cavitation, effervescence, etc.). Chemical techniques create bubbles either by a gas-releasing chemical or electro-chemical reaction (electrolysis), while the most common biological approach relies on gas-generating species such as yeast.

These different techniques lead to the final foam in a one-step or in a two-step process. In a one-step process, the mechanism which generates the bubbles leads directly to the final foam with a well-defined gas fraction. Only few foaming techniques allow for this. Most techniques rely on two types of two-step processes. In the first case, loose bubbles are generated in the liquid which are then compacted to give the final foam — for example through gravity or pressure-driven drainage of the liquid. In the second case, the initial bubbling mechanism creates a coarse foam containing large bubbles, which are then broken into smaller bubbles to create the final foam.

Table 1
Classification of different foaming techniques.

Global mechanism	Sub-mechanism	Examples
Physical foaming	Mechanical foaming	Bubbling, sparging, foam generation in porous media, wave breaking, shaking, rotor–stator mixers, kitchen blender, double syringe technique
	Phase transition	Champagne, beer, extrusion, cream dispenser, shaving foam
Chemical foaming	Chemical reaction	Fizzy drink tablets, baking powder, polyurethane foaming
	Electro-chemical reaction	Microflotation
Biological foaming	Yeast	Baking

In order to describe the science of foaming we have decided to take the following approach: First of all, we concentrate on the description of physical foaming techniques, leaving out considerations of chemical and biological foaming (with the exception of electro-chemical foaming). We provide first a detailed description of the different fundamental mechanisms which lead to the creation of isolated bubbles in a liquid (Section 2). We then continue with the description of commonly used foaming techniques (Section 3). Considering the large number of available foaming techniques, we have decided to stay on the level of a general overview, providing the reader mostly with the main ideas of the different concepts or techniques, rather than with an in-depth analysis. We hope that this can help the reader to orient his general reflexions before going into detail by following the provided references.

Before entering into the analysis, some comments on the physico-chemical aspects of foaming are required. Any foaming solution needs to contain stabilising agents in order to control the stability of the obtained foam. It is evident that the properties of the obtained foam depend sensitively on the fact whether bubble coalescence occurs during the foaming process. In fact, in many of the more complex foaming techniques, the final foam properties are given by a subtle equilibrium between bubble generation and bubble coalescence. Moreover, the stabilising agents may have characteristic adsorption times or energy barriers, which need to be compared with the characteristic generation times and energy input of the foaming process. For example, adsorption times play an important role in setting the interfacial tension during bubble generation. If the bubbling process is faster than the equilibration time of the interface, the surface tension will be between that of the pure solvent and the equilibrium surface tension, its precise value depending on the bubbling speed [6]. Last but not least, the stabilising agents often confer visco-elastic properties to the gas/liquid interfaces [7]. This may add important interfacial stresses during the process of bubble creation, which may alter significantly the finally obtained foam. For the sake of simplicity, we shall neglect all these different effects in most of our argumentations by assuming that bubbles are indefinitely stable and that their interfaces have one constant value γ for the interfacial tension which is obtained instantaneously upon bubble creation.

The formulation of the bulk liquid can also modify significantly the rheology of the liquid phase, leading eventually to non-Newtonian behaviour and very different conditions for bubble formation [8,9]. For the sake of clarity we will limit our description to the foaming of simple, i.e. Newtonian fluids.

2. Fundamentals of foam formation

2.1. Introduction

In this section we shall concentrate on the description of the fundamental mechanisms which lead to the generation of individual bubbles. We have chosen to group them into two conceptually different categories. In the first category, the gas/liquid interface needs to undergo a topological change in order to create the final bubble. This topological change can occur in many different ways. The most common ones are sketched in Fig. 1. For example, a bubble may detach from a nozzle or from a deformed free surface; or a large bubble may break into smaller ones. What differentiates these mechanisms is which of the two phases is flowing and under which conditions. The different mechanisms are discussed in more detail in Section 2.4. Even if the initial mechanism of creating a pocket-like gas/liquid interface may be very different, the final break-up mechanism which leads to the topological change is the same: the gas/liquid interface has to be deformed into a slender filament which is physically unstable and breaks to make the topological transition. The physics of this instability is described in more detail in Section 2.3.

Please cite this article as: Drenckhan W, Saint-Jalmes A, The science of foaming, Adv Colloid Interface Sci (2015), http://dx.doi.org/10.1016/j.cis.2015.04.001

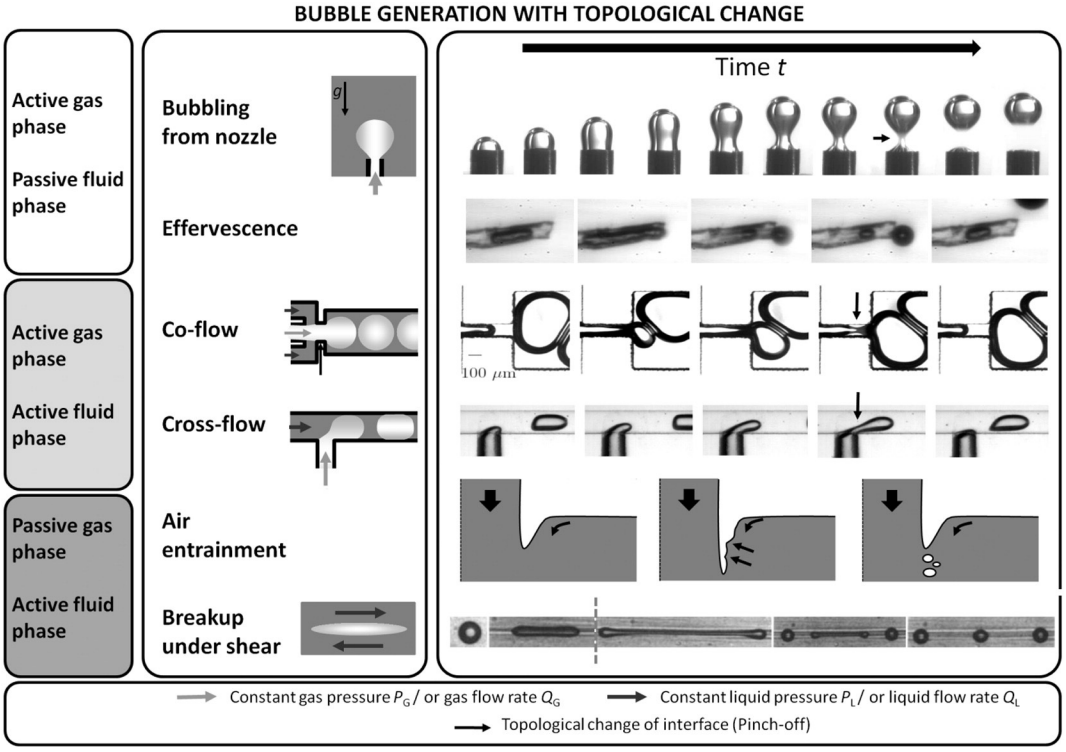

Fig. 1. Different routes of bubble generation which require a topological change to "pinch-off" one or more bubbles from a main gas body (bubbling from nozzle from [10], effervescence from [11], co-flow from PhD thesis Jan-Paul Raven, cross-flow from [12], air-entrainment inspired by [13], breakup under shear from [14]). "Active" or "Passive" refers to whether or not the corresponding phase is flowing actively in the process.

In the second category, no topological change of the gas/liquid interface is required, as a freely floating bubble is directly created within the liquid by a phase transition or by a chemical reaction (Table 1 and Fig. 2). The different physical mechanisms of this kind of bubble creation are discussed in more detail in Section 2.5. Some mechanisms may belong to both classes. For example, phase transitions are often favoured by the presence of walls or impurities from which the bubbles need to detach via a topological change.

In both categories, a number of different stresses are involved in the process of bubble creation. We briefly review these in Section 2.2 and discuss how they may be grouped into non-dimensional numbers for a coherent description of different bubbling processes.

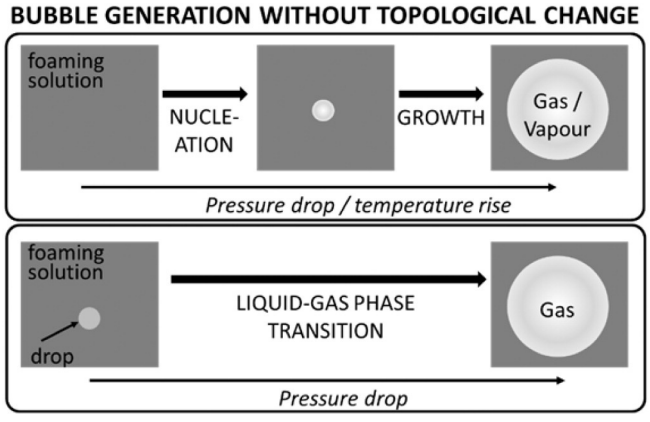

Fig. 2. Sketch of the two main routes of bubble generation by physical means which do not require a topological change of the interface. The first creates bubbles via cavitation, boiling or effervescence. In the second, the drops of an emulsion turn into a gas, generally upon pressure release.

2.2. The physics of deforming interfaces

Any process of bubble formation involves the creation and deformation of a gas/liquid interface. Even if the fundamental mechanism may be non-mechanical in nature (like chemical reactions), the actual creation process involves a number of mechanical stresses (= force per area) which need to be considered. One of the most important contributions is that of the surface tension γ, which leads to a normal stress σ_γ and therefore to a pressure drop Δp across a curved surface of mean curvature κ described by the Young–Laplace law [15]

$$\sigma_\gamma = \Delta p = 2\gamma\kappa. \tag{1}$$

Of similar importance is the influence of a hydrostatic pressure difference, which leads to the well-known buoyancy force F_B on a bubble of volume V_B, which plays a major role in bubble detachment and compaction. The buoyancy force is given by

$$F_B = \Delta\rho g V_B. \tag{2}$$

Surface tension and gravitational stresses are "static" stresses since they do not require fluid motion. In a dynamic context important "dynamic stresses" may arise. The first one is a tangential viscous stress σ_V, which results from a viscous shear flow at the interface. It depends on the fluid viscosity η_L and the deformation rate dU/dL of the fluid and is commonly approximated as

$$\sigma_V = \eta_L \frac{U}{L}, \tag{3}$$

where U is the characteristic flow velocity and L a characteristic length scale of the flow. Generally one has two viscous contributions, one from the gas and one from the liquid phase. Viscous flow can also lead to the occurrence of a dynamic pressure, hence exerting additional

Table 2
Summary of the most important dimensionless numbers used to classify different regimes of bubble generation and their cross-relations.

Name	Sym.	Definition	Ratio of stress	Equ.
Bond number	Bo	$\frac{\Delta\rho\, g\, L^2}{\gamma}$	$\frac{Graviational\ stress}{Interfacial\ stress}$	(5)
Capillary number	Ca	$\frac{\eta U}{\gamma}$	$\frac{Viscous\ stress}{Interfacial\ stress}$	(6)
Reynolds number	Re	$\frac{\rho U L}{\eta}$	$\frac{Inertial\ stress}{Viscous\ stress}$	(7)
Froude number	Fr	$\frac{U}{\sqrt{gL}}$	$\frac{Inertial\ stress}{Graviational\ stress}$	(8)
Weber number	We	$\frac{\rho U^2 L}{\gamma}$	$\frac{Inertial\ stress}{Interfacial\ stress}$	(9)
Ohnesorg number	Oh	$\frac{\eta}{\sqrt{\rho\gamma L}}$	$\frac{Viscous\ stress}{\sqrt{Interfacial * inertial}}$	(10)
Galilei number	Ga	$\frac{g\rho^2 L^3}{\eta^2}$	Gravity vs viscosity	(11)

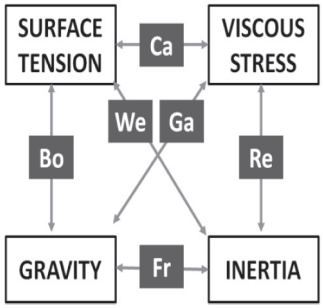

normal stresses on an interface. Gases or liquids in motion also exert normal inertial stresses σ_I on an interface due to the momentum of the flow. These stresses may be approximated as

$$\sigma_I = \rho U^2. \tag{4}$$

As discussed in Section 2.1, the presence of stabilising agents can give rise to important interfacial stresses [16] which can interfere with bubble generation in non-negligible manner [17,18]. Other stresses may act in specifically designed systems which make use of acoustic, electric or magnetic forces. For simplicity, we will not consider explicitly any of these latter stresses here.

Generally, all the above-mentioned stresses act simultaneously during the process of bubble generation. However, in most cases, some of the contributions dominate while others can be neglected. One commonly distinguishes between a "quasi-static" and a "dynamic" regime. In the quasi-static regime, the flow velocities are sufficiently small so that the system can be assumed to progress via a sequence of static states. Such processes are therefore independent of the flow velocities. In the dynamic regime, viscous and/or inertial forces need to be taken into account. In this regime the bubble formation is often dominated by one of the two contributions, which is why one commonly distinguishes between a "viscosity-dominated" and an "inertia-dominated" regime.

One way to navigate the complexity of the different stresses is to work with non-dimensional numbers which allows to measure in a (somewhat) more quantitative way the relative importance of each of the acting stresses. Table 2 summarises the most important non-dimensional numbers which are used in the description of bubble formation. The use of these numbers can be extremely powerful since they provide an important degree of abstraction by grouping together different parameters using simple "scaling arguments". Most of these numbers are used throughout this article in order to classify different regimes of foaming techniques.

The definition of the dimensionless numbers involves the following parameters: surface tension γ, density ρ, viscosity η and the gravitational acceleration g. Moreover, it relies on a characteristic velocity U and a characteristic length scale L. The latter two parameters need to be chosen with care, as most flow problems involve complex flow fields and flow geometries, hence a wide range of velocities and length scales. Moreover, the problems deal with two-phase flows; one therefore needs to choose wisely, if the stresses of one of the phases dominate the behaviour, or if both need to be taken into account. Good choices of these parameters are discussed in more detail throughout this article.

Another frequently used parameter is the capillary length

$$l_c = \sqrt{\frac{\gamma}{\Delta\rho\, g}}, \tag{12}$$

which is a dimensional expression of the Bond number. It provides a characteristic length beyond which gravitational effects need to be taken into account in comparison to surface tension effects. Last but not least, the viscosity, density and flow rate ratio of the gas ("*G*") and the liquid ("*L*") phase

$$\lambda_V = \frac{\eta_G}{\eta_L},\ \lambda_D = \frac{\rho_G}{\rho_L},\ \text{and}\ \lambda_Q = \frac{Q_G}{Q_L}, \tag{13}$$

are often taken into account in the description of bubble formation.

Numerous other non-dimensional numbers exist, for example, if the visco-elasticity of the interfaces was to be taken into account. The *interfacial mobility* may be used to as a measure of the interfacial viscosity, while the *Marangoni number* captures the importance of an interfacial elasticity [3,7].

2.3. The physics of rupturing gas ligaments

Here we shall discuss in detail the physics of how the bubble under creation undergoes the topological change to detach from an object, a free surface or a "mother" bubble. Many different configurations can lead to this final stage and a selection is discussed in detail in Section 2.4. However, in all cases, the physics of the final step leading to the topological change is the same (Fig. 3): the bubble has to be deformed into an elongated cylinder (or "gas thread", or "ligament"), which becomes physically unstable and breaks. If the cylinder is relatively short with respect to its width, it breaks in one point to liberate one bubble (Fig. 3a). If it is very long, it can break into many bubbles (Fig. 3b).

To understand this break-up let us consider the physics of a long cylindrical ligament of one fluid within another. This can be a gas ligament in a liquid, a liquid ligament in a gas, or a liquid ligament in a second immiscible liquid. The thinner such a ligament is, the higher is its

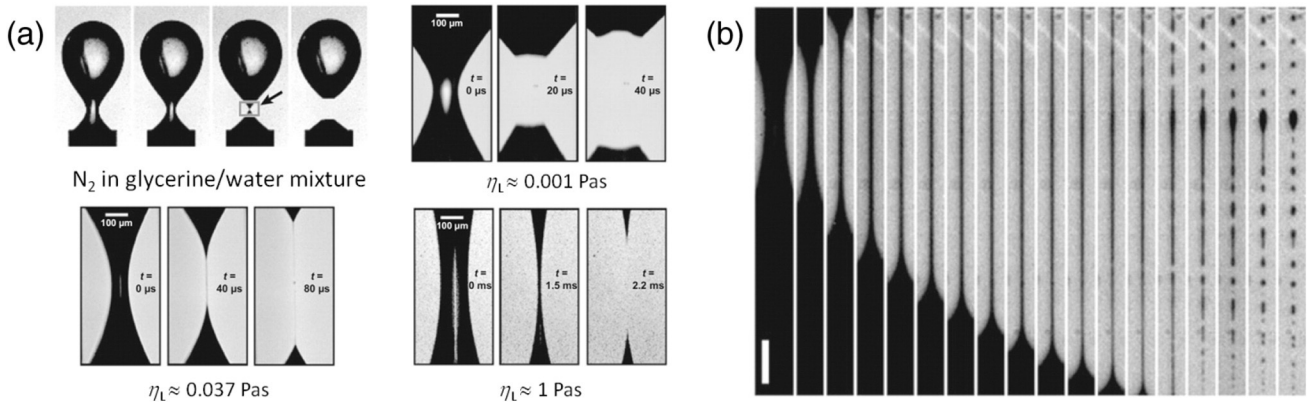

Fig. 3. The instability of thin gas ligaments leads to the topological change of the gas/liquid interface required to create one or more separate bubbles. (a) Bubble pinch-off in water/glycerol mixtures of increasing liquid viscosity η_L (from [19]). (b) Pinch-off of a gas bubble containing insoluble SF_6 for $\eta_L = 0.03$ Pa s, showing the generation of many tiny satellite bubbles during the detachment of the main bubble (time between images: 5 µs. Scale bar 50 µm) (from [20]).

surface-to-volume ratio. It would therefore energetically be more favourable to turn the cylinder into a number of spherical objects. But the key question is: how does the system get there? This transition happens via an instability which links the ligament curvature and pressure via the Young–Laplace equation (Eq. (1)). This issue has been widely studied, and the understanding of the key mechanisms goes back to the 19th century and the pioneering works of Savart, Plateau and Rayleigh who were trying to understand the destabilisation of a water jet as it falls out of a faucet. Implementing the ideas of Savart [21] and Plateau [22], Rayleigh developed a first basic model [23], which is now known as the "Rayleigh–Plateau instability". Rayleigh considered a cylindrical, infinite thread of an inviscid fluid in air, without external flow. Such a fluid column experiences spontaneous thickness undulations (called "varicosity", Fig. 4a) which are generally damped. However, Rayleigh could show that under certain conditions, some of the undulations can actually grow with time rendering a certain range of "varicose" modes unstable. This cannot be understood if one considers only the pressure gradients arising from modulations of the cross-section (of radius r) of the ligament. In fact, as sketched in Fig. 4a, the Young–Laplace law includes also the radius r', in the plane orthogonal to the cross-section, and associated with the deformation mode (and with the deformation wavelength λ). In particular, when the cross-section gets small, there is a saddle point and the two curvatures have different signs. Thus, depending on which radius (r or r') is the biggest, a different behaviour will be found. Qualitatively, modes associated with large r' (wavelength longer than the ligament section) will be unstable, and vice versa. Performing the detailed mathematical analysis assuming that inertia is balancing surface tension, one obtains that the modes having a positive growth rate (sketched in Fig. 4b) are those whose wave number k ($k = 2\pi / \lambda$) fulfils

$$kr<1. \tag{14}$$

The maximum in Fig. 4b corresponds to the most "dangerous" mode which is called the "Rayleigh mode". It is given by

$$kr = 0.697 \text{ and } \lambda = 9.02r. \tag{15}$$

An important point is that all the unstable modes are finite and of the order of the thread radius (but somewhat larger than the thread radius). Since the final bubble or droplet size is of the order of the wavelength of the most unstable mode, it is generally a linear function of the thread radius at which the instability occurs. Another interesting output is the capillary timescale associated with these deformations [24]

$$\tau_{cap} = \sqrt{\frac{r^3\rho}{\gamma}}, \tag{16}$$

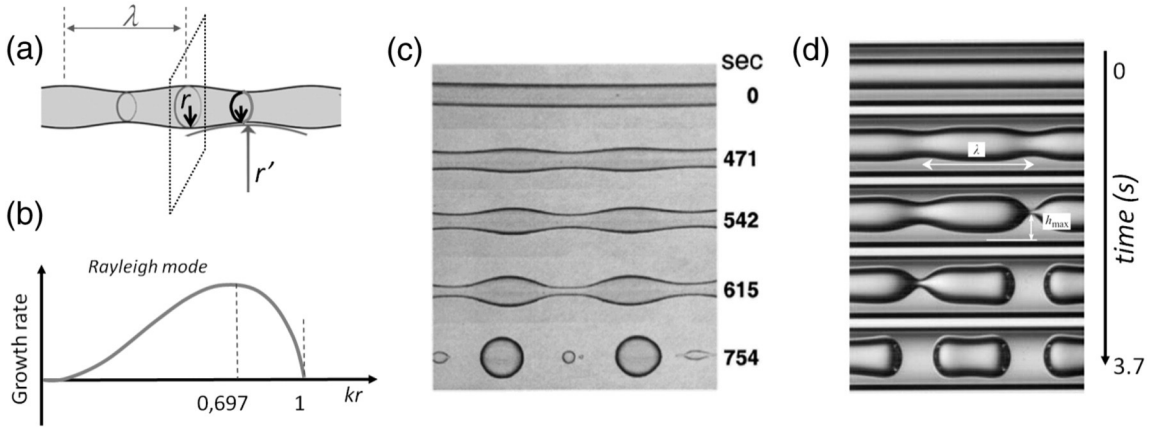

Fig. 4. The Rayleigh–Plateau instability: (a) Scheme showing the different radii of curvature. (b) Growth rate as a function of the undulation wave number $k = 2\pi / \lambda$ multiplied by the thread radius r. (c, d) Time evolution of unstable ligaments of (c) two polymeric fluids [27], of a (d) gas ligament in a viscous liquid confined in a tube (from [28]).

Please cite this article as: Drenckhan W, Saint-Jalmes A, The science of foaming, Adv Colloid Interface Sci (2015), http://dx.doi.org/10.1016/j.cis.2015.04.001

which provides an approximation as to how rapidly a thread will become unstable.

Rayleigh's simple model was expanded in many different ways in order to describe more realistic scenarios. Weber [25] was one of the first to take into account the viscosity of the fluid of the cylinder. His results can be rationalised using the Ohnesorge number *Oh* (Eq. (10) in Table 2) which can also be considered as the ratio of the viscous timescale over the capillary time scale ([24,26] and references therein). The stability of the fluid cylinder decreases with decreasing *Oh*, and the growth rate and the wavelength of the most unstable mode can be calculated using this "viscous" Rayleigh–Plateau instability ([24,26] and references therein).

Remaining in the situation of stationary liquids (no flow inside or outside the cylinder), the ratio λ_V of the viscosities of the inner and outer fluid can be taken into account [29]. The most unstable wavelength depends on the viscosity ratio, being maximum when $\lambda_V \approx 1$. Considering the case of a gas cylinder inside a liquid ($\lambda_V \approx 1/55$) the most unstable wavelength is predicted to be $\lambda = 12.5r$ — which remains close to the basic prediction (Eq. (15)) of Rayleigh.

Most situations which lead to the formation of long cylindrical ligaments require that the fluid inside and/or outside the ligament is flowing (Fig. 1). In this case, the "temporal instability" discussed up to now is often not sufficient. One must also consider the "spatial instability", meaning that an initially localised deformation propagates also along the ligament axis. Researchers have therefore identified two different scenarios for the instability to occur: the "absolute" and the "convective" instability ([30] and references therein).

An absolute instability corresponds to a deformation which grows too fast in time and space to be convected by the main flow, it thus propagates both downstream and upstream, invading the whole ligament, independently of the flow. At a fixed point in space, the growth of an unstable mode is never limited. By contrast, the convective instability implies perturbations which are convected downstream while they grow. At a given point in space, the amplitude of the deformation remains finite, as the flow is fast enough to sweep the deformation away before it becomes exponentially large. The convective regime allows for a continuous and longer fluid ligament to survive, when compared to the absolute regime. Within the same bubbling conditions one can typically switch between both scenarios by appropriately adjusting the flow rates of both phases. The consequences of these different behaviours are particularly well evidenced and discussed in more detail when bubbles are blown from nozzles (Sections 2.4.1 and 2.4.2.)

Let us finish with two important remarks. A ligament does not necessarily break into equal-volume bubbles. Small bubbles (called "satellite bubbles") can result from the final step of rupture (Figs. 3b and 4c). This is discussed in more detail in Section 2.4.3. Last but not least, it is important to keep in mind that geometrical confinement has a dramatic effect on ligament curvatures and therefore on its stability. In fact, if a ligament is confined in one direction (for example in a flat channel) it remains stable until the confinement is released [27,31]. This can provide an important degree of control over bubble formation and is often used in microfluidic contexts.

2.4. Bubble generation requiring topological changes

Many different mechanisms exist which allow to detach a bubble from a gas pocket. One of the most common approaches uses the gravity-driven detachment of a bubble which is blown at constant pressure or flow rate into a stationary solution via an orifice (Fig. 1 and Section 2.4.1). Since gravity is not very efficient when small length scales are involved (small Bond numbers *Bo* — Table 2), many bubbling mechanisms involve a co-flow of the liquid in order to make use of viscous or inertial forces to influence the break-up process. This co-flow may occur in unconfined conditions — for example one can move a nozzle through the foaming solution. But in many cases it is more suitable to work in confined geometries in which dynamic stresses can be imposed more efficiently and in a better controlled manner. We discuss here in particular the case of confined co-flow and cross-flow (Fig. 1 and Section 2.4.2).

Another important mechanism includes the entrainment of air at free surfaces (Fig. 1 and Section 2.4.1) and the breakup of large bubbles into smaller ones under shear flow (Fig. 1 and Section 2).

For simplicity, we shall discus the various flow problems in terms of "flow rates *Q*" and "flow velocities *U*". This means that the pressures adjust to ensure a constant flow rate. In many experimental scenarios it is more practical to control the pressures and measure the flow rates, for example to avoid long equilibration times. This means, however, that flow rates are not constant and the physical description is sometimes more awkward. It can also change non-negligibly the behaviour of a device.

2.4.1. Bubbling into a stationary liquid

Due to the technical importance of the process of bubbling through orifices, the subject has been investigated intensively in the past. While slow bubbling can be described in a fairly straightforward manner (Section 2.4.1.1) the description of the dynamic case has proven to be highly complex (Section 2.4.1.2). This complexity is due to different feedback mechanisms within the system, the most important one being the intricate coupling between the dynamic forces and the bubble shape. Moreover, the physics of the dynamics of the contact angle between the interface and the orifice, and of the final break-up mechanism(s) are only being elucidated now. The result is that despite the availability of some review articles [32,33], the subject remains quite scattered with different authors presenting different parameter ranges (surface tension, orifice dimensions and shape, wetting conditions, liquid viscosity, gas and liquid density, etc.). Sometimes the results seem contradictory. However, in most cases these contradictions result from the fact that experiments are done in different regimes where different parameters may have a very different — even opposite — influence. The same challenge holds for modelling attempts which necessarily need to simplify the problem. The appropriate approximations depend once again on the bubbling regime, which has led to a vast number of theoretical and (semi-)empirical models, each describing generally a certain parameter range only. An extensive overview of existing models is given in Table 3 in reference [33]. We shall present here some of the key ingredients.

2.4.1.1. The quasi-static regime. At the outset, let us discuss the simple scenario of bubbling at constant gas flow rate Q_G into a stationary foaming solution using a vertical orifice of circular cross-section and radius R_O (see Figs. 1 and 5). Let us assume that the bubbling occurs sufficiently slowly to be in the quasi-static regime (Fig. 5), i.e. $Ca \ll 1$ and $We \ll 1$ (Table 2), and that the generation process is therefore dominated by surface tension and gravitational forces (buoyancy).

Photographs and simulations of a typical quasi-static blowing process are shown in Fig. 6a. During this process the bubble goes through a well-defined series of pressure states which are sketched in Fig. 6b. The pressure initially increases (which some refer to as the "nucleation stage") before reaching a maximum when the bubble is a hemisphere, i.e. when the bubble radius R_B is equal to the orifice radius R_O. At this point

$$\Delta P_{max} = \frac{2\gamma}{R_O}, \tag{17}$$

which follows naturally from the Young–Laplace law (Eq. (1)). This pressure is important, as any bubbling application needs to provide pressures above this value. Due to the inverse dependence of the blowing pressure on the orifice radius, the pressures for very small orifices may become of the order of a few bar, which can be unfeasible for certain applications.

Please cite this article as: Drenckhan W, Saint-Jalmes A, The science of foaming, Adv Colloid Interface Sci (2015), http://dx.doi.org/10.1016/j.cis.2015.04.001

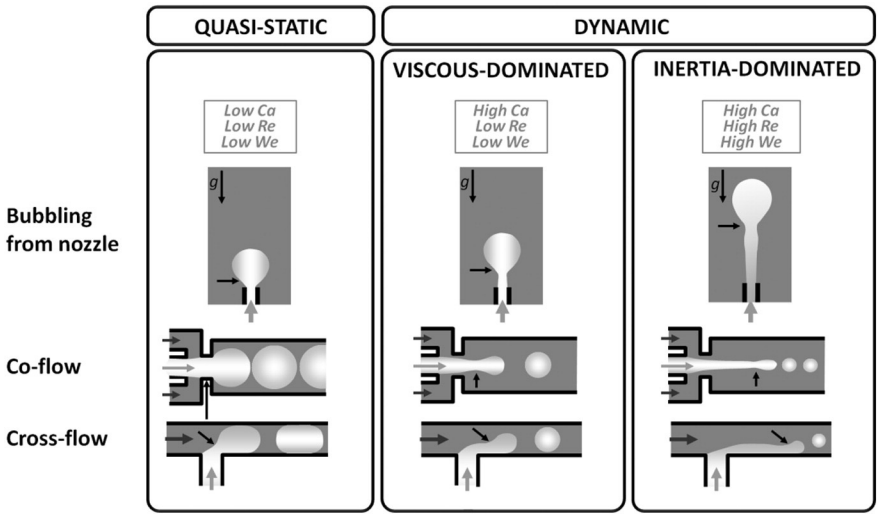

Fig. 5. Variation of bubbling regime with increasing flow velocities. The black arrow indicates where break-up occurs.

A certain reduction of the maximum pressure may be obtained using orifices with more complex geometrical cross-sections [159].

If the applied pressure is higher than the maximum pressure, the bubble grows beyond the hemispherical shape (leading to a pressure decrease) and detaches via the instability mechanisms discussed in Section 2.3 when the surface tension force F_γ (which keeps the bubble "stuck" to the orifice) is of the order of the buoyancy force F_G. If the orifice size R_O is much smaller than the capillary length (Eq. (10)), i.e. if $R_O \ll l_c$, one may approximate the shape of the detaching bubble by a sphere of volume $4/3\pi R_B^3$. This leads to a buoyancy force of $F_G = 4/3\Delta\rho g R_B^3$, while the surface tension force can be written as $F_\gamma = 2\pi\gamma R_O$. R_B may therefore be approximated as

$$R_B \sim \left(\frac{\gamma}{\Delta\rho g}\right)^{2/3} R_O^{1/3} = l_c^{2/3} R_O^{1/3} = R_O\, Bo^{-1/3} \quad (\text{for } R_O \ll l_c), \tag{18}$$

where the length scale L in the definition of the Bond number Bo (Eq. (5)) has been chosen to be the radius of the orifice R_O. In order

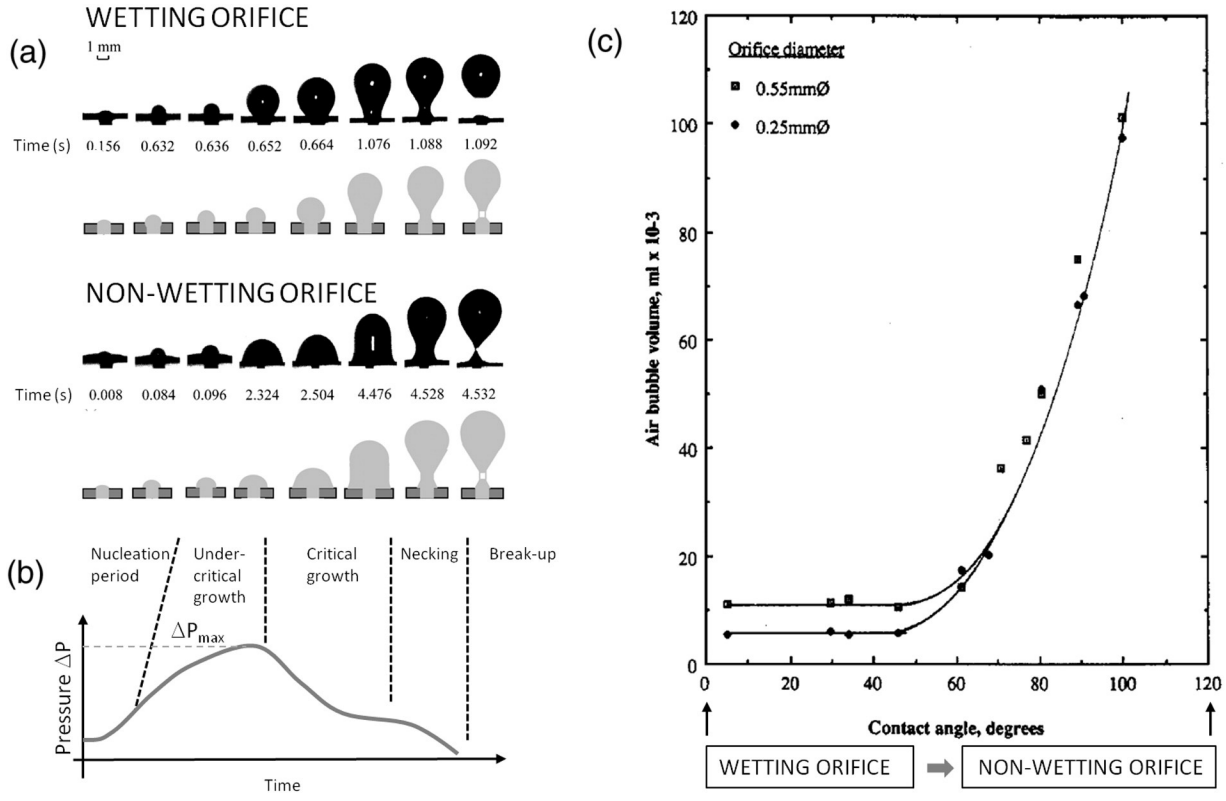

Fig. 6. Blowing bubbles from an orifice into a stationary solution. (a) Bubble evolution as a function of time for two different orifice materials (wetting and non-wetting) comparing each time photographs from an experiment (top row) and computer simulations (bottom row) (adapted from [36]). (b) Schematic pressure evolution during the generation. (c) Final bubble volume as a function of orifice wetting properties (expressed in contact angle) for two different orifice diameters (adapted from [37]).

Please cite this article as: Drenckhan W, Saint-Jalmes A, The science of foaming, Adv Colloid Interface Sci (2015), http://dx.doi.org/10.1016/j.cis.2015.04.001

for the bubble to detach, *Bo* therefore needs to be at least of the order of unity.

If the orifice radius is of the order of the capillary length, i.e. $R_O \geq l_c$, one needs to take into account the gravity-driven deformation of the bubble before detachment. Researchers find that this is well captured by slightly modifying the exponent in Eq. (18) such that

$$R_B \sim R_O Bo^{-\alpha/3} \quad (\text{for } R_O \geq l_c), \tag{19}$$

with $\alpha \approx 1.06$ [34]. In both cases, it is clear that the bubble size is set by the orifice dimensions and by the capillary length l_c with smaller orifices leading to smaller the bubbles. Since this is not a strong dependence it is often more appropriate to work with co-flow scenarios (Section 2.4.2), especially if small bubbles and high production rates are needed.

The pinch-off process (see also Section 2.3) is generally much faster than the bubble blowing process, which is why its duration is commonly neglected in models. After the pinch-off the gas thread retracts fully back to (often even into) the orifice and the periodic process restarts. Due to the periodicity of this process, foams generated via bubbling in the quasi-static regime tend to be highly monodisperse. Typical bubble sizes which can be produced with this approach are between a few hundred micrometres and a few millimetres.

In some cases, one may be looking to produce large bubbles. A look at Eq. (18) suggests the use of a large orifice for this purpose. However, when the size of the orifice is larger than the capillary length l_c one has to deal with gravity-driven instabilities of the gas/liquid interface leading to an effect called "weaping" (liquid enters the orifice). An elegant approach is to "tune" gravity instead by letting the bubble grow underneath an inclined plane (Fig. 7) [35].

The pre-factors in Eqs. (18) and (19) are of the order of unity, but depend sensitively on the geometry of the orifice and on its wetting properties with respect to the foaming liquid. The more the liquid wets the orifice, the more the gas thread remains confined within the orifice boundaries, leading to smaller bubbles and to a clearer dependence of the bubble size on the orifice dimensions. This is shown in the image sequences in Fig. 6a (adapted from [36]) and also in the final bubble size measurements of Fig. 6c (adapted from [37]), which shows how the bubble size depends on the wetting conditions (expressed by the contact angle of the liquid on the nozzle material). It also shows that the orifice size plays a less important role in the case of a non-wetting orifice.

Eq. (18) allows us to approximate in which range of flow rates we can approximate the bubbling process as quasi-static. Since viscous forces tend to play a more important role at lower velocities than inertial forces, we may require that Ca ≪ 1, hence

$$Q_G = U\pi R_O^2 \ll \frac{\gamma}{\eta}\pi R_O^2. \tag{20}$$

Using Eq. (18), we can calculate a corresponding bubbling frequency f_B

$$f_B = \frac{Q_G}{V_B} \ll \frac{\Delta\rho\, g}{\eta} R_O. \tag{21}$$

This gives $f_B \ll 100$ for a nozzle with $R_O = 100\,\mu m$. Bubbling frequencies in the truly quasi-static regime are therefore rarely above a few bubbles per second, which is too slow for most applications which therefore tend to be run in a dynamic regime (Section 2.4.1.2).

2.4.1.2. The dynamic regime. Upon moving away from quasi-static bubbling conditions, different dynamic forces need to be considered in the bubbling process which are sketched in Fig. 8a. For example, viscous drag exerted by the liquid on the bubble slows down the detachment and therefore leads to larger bubbles. Bubble detachment is also resisted by inertial forces of the liquid, while the inertial forces of the gas help in pushing the bubble away from the orifice.

Images of the bubble generation process with increasing gas flow rate are sketched in Fig. 5 and some corresponding graphs in Fig. 8b. If surface tension and inertial forces can be neglected, researchers find [38] that the resulting bubble size may be approximated by

$$R_B \sim \left(\frac{\eta_L Q_G}{\Delta\rho g}\right)^{1/4} \sim R_O \left(\frac{Ca}{Bo}\right)^{1/4}, \tag{22}$$

where the constant of proportionality is of order 1 and depends on the orifice conditions (geometry, wetting). The important observation here is that unlike in the quasi-static regime, the bubble size now depends on the viscosity η_L of the liquid and the gas flow rate Q_G. More specifically, the bubble size increases with η_L and Q_G.

Upon further increase of Q_G, inertial forces begin to play a non-negligible role ($We_G > 1$). With growing Weber number We_G of the gas, the forming bubble becomes more elongated, since inertial forces become increasingly important with respect to the restoring surface tension forces. The pinch-off point of the gas thread moves increasingly away from the orifice, leading eventually to the formation of a gas-jet which breaks up into bubbles at its tip. This jet widens away from the nozzle, as the gas is decelerated due to viscous friction. For sufficiently high We_G, bubble detachment is entirely driven by the dynamically generated bubble shape. The influence of gravity becomes therefore negligible, which has also been confirmed in micro-gravity experiments [39].

One can therefore think of two extreme scenarios, one in which bubble pinch-off is driven entirely by gravity ($Bo > 1$) versus one where it is driven by inertial forces. When the bubble formation is dominated by gravity and viscous forces, one generally speaks of the "dripping" regime (in analogy to the dripping tap problem). When inertial forces dominate, one speaks of the "jetting regime". A number of theoretical and experimental studies have shown that inertial forces dominate the pinch-off when $We_G > 1$–10 [33,39–41]. In most situations, gravity and inertia act together, which is shown in the phase diagram in Fig. 8b, which uses the *Bo* and the We_G number to predict under

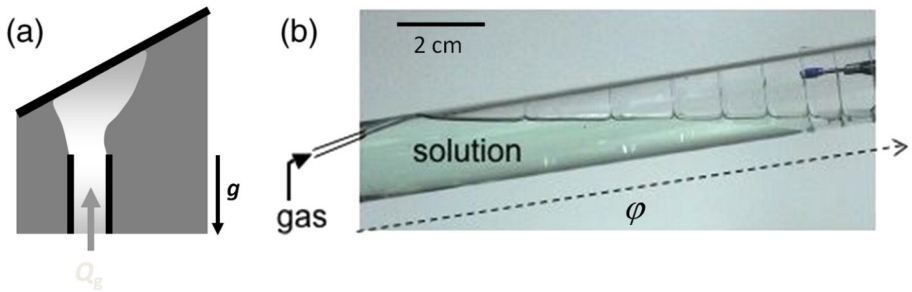

Fig. 7. Blowing large bubbles via tuning the effective gravity acting on the bubble. (a) Schematic representation. (b) Experimental realisation from [35].

Please cite this article as: Drenckhan W, Saint-Jalmes A, The science of foaming, Adv Colloid Interface Sci (2015), http://dx.doi.org/10.1016/j.cis.2015.04.001

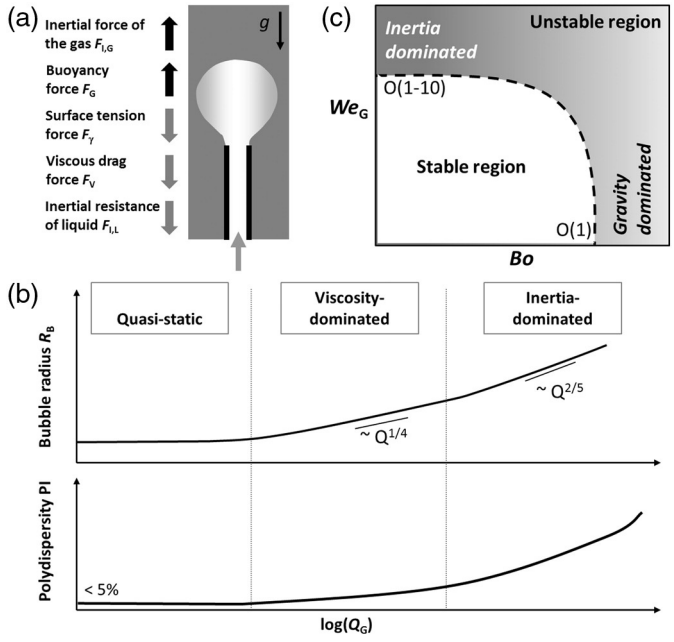

Fig. 8. (a) Summary of the different forces acting on a bubble during creation. (b) Sketch of variation of bubble radius R_B and polydispersity PI with gas flow rate Q_G. Corresponding images are shown in Fig. 5. (c) Stability diagram of the bubbling process. Bubbles detach from the orifice if either the Bond number *Bo* or the Weber number We_G of the gas are sufficiently high.
Inspired from [40].

which flow conditions bubble detachment occurs (unstable region). A number of studies have investigated the transition from the dripping to the jetting regime — and we will discuss the physics of these transitions in more detail when discussing bubbling under co-flow conditions in Section 2.4.2. What is important to note at this point is that at the transition, important non-linear effects can play a role, leading to multiple bubble periods and even chaotic bubbling. This leads to foams with bubbles of multiple or polydisperse sizes and is discussed in more detail in Section 3.2.1.1.

If surface tension and viscous forces can be neglected, the bubble size in the inertial regime may be approximated by [32,38]

$$R_B \sim \frac{Q_G^{2/5}}{g^{1/5}} \sim R_O Fr_G^{2/5} = R_O \left(\frac{We_G}{Bo}\right)^{1/5}, \tag{23}$$

where the factor of proportionality is of order one, its value depending on the model used. In this regime polydispersity of the bubbles tends to increase significantly.

In most practical cases, gravity, surface tension, viscosity and inertia act simultaneously. In this case, the model needs to take into account the various contributions, rendering it quite complex. One of the frequently used models is the one proposed by Jamialahmadi et al. [42]

$$R_B = R_O \left[\frac{5.0}{Bo^{1.08}} + \frac{9.261 Fr_G^{0.36}}{Ga_G^{0.39}} + 2.14 Fr_G^{0.51}\right]^{1/3}. \tag{24}$$

Notice the importance of the Froude number *Fr*, which captures the ratio of inertial and gravitational stresses and which can also be expressed as $Fr^2 = We / Bo$ in order to make the link with previous discussions.

2.4.2. Bubbling into a flowing liquid

Scientists have developed a large number of bubbling techniques which involve the active flow of the liquid phase. This creates additional viscous and inertial forces which can play a very important role in bubble detachment. The first group of techniques involves the co-flow (Fig. 9a, b) or the cross-flow (Fig. 9c) in unconfined conditions. The latter may be achieved by dragging the orifice through a large liquid pool, an approach originally used by Bragg [43] to blow small bubbles. The influence of the flowing liquid phase can be increased if co- or cross-flow take place under confined conditions (Fig. 9d–g), since high shear rates and high flow velocities can be obtained in the confined flow regions. The confining geometry therefore plays an important role in the bubbling process, as it fixes the flow field and therefore the dynamic forces acting on the bubble. Smith was one of the first scientists to use this approach systematically in order to blow small(er) bubbles for Bragg [44]. Towards the end of the 20th century the subject has found an explosive rebirth with emerging microfluidic techniques [45–49]. A more substantial body of work has been done on droplet, rather than bubble generation, but with many physical mechanisms being the same, the interested reader will find important inspiration in the droplet literature [50–52]. In most of the confined co/cross-flow devices, the influence of gravity can be neglected because of the small device dimensions (i.e. $Bo \ll 1$) or the importance of the dynamic forces ($Ca \gg 1$, and/or $We \gg 1$, etc.). This is why we will not discuss the influence of gravity in the following.

2.4.2.1. The quasi-static regime. When both, the gas and the liquid flow rate, are small enough so that the dynamic forces can be neglected, unconfined flow gives the same results as bubble blowing into a stationary liquid (Section 2.4.1). In the absence of gravity there is no detachment force, hence bubbles cannot be generated. This is very different when the bubble is generated under appropriately confined conditions. In this case, the bubble can block the entire channel or constriction in which it is generated. The liquid flow then leads to a filling of the channel or the constriction, which pinches off the bubble (Fig. 1). The bubble is carried away by the slow flow and the periodic process restarts. This regime has been called the "squeezing" regime [48] since it is entirely controlled by the normal pressures acting on the interface. Since the bubble continues to be blown at constant flow rate Q_G while the liquid fills the constriction of volume V_c at constant flow rate Q_L, one finds a simple relationship which relates the final bubble volume to the channel geometry and the flow rates to a good approximation [53,54]

$$V_B \sim V_C \frac{Q_G}{Q_L}. \tag{25}$$

The prefactor depends on the precise geometry. The volume of the constriction may be replaced by the 3rd power of a characteristic channel dimension, if the geometry does not contain a well-defined constriction. With this approach, one can therefore generate foams over a wide range of bubble sizes (10–1000 μm) and gas fractions Φ, since

$$\Phi = \frac{Q_G}{Q_G + Q_L}. \tag{26}$$

The squeezing regime leads to highly monodisperse foams (PI < 2%). Some examples of obtained foams are shown in Fig. 10.

2.4.2.2. The dynamic regime. The simplest case in the dynamic regime is when the viscous drag which is exerted on the bubble by the fluid overcomes the capillary force which attaches the bubble to the orifice (Fig. 8a). An example from an experiment is shown in Fig. 11b. The viscous Stokes force, which may be approximated as $F_V = 6\pi R_B \eta_L U_L$, plays the same role as gravity in Section 2.4.1. Equating the viscous and the capillary force ($2\pi\gamma R_O$) leads to a simple expression for the obtained bubble size

$$R_B \sim \frac{\gamma}{\eta_l U} R_O = Ca_L^{-1} R_O. \tag{27}$$

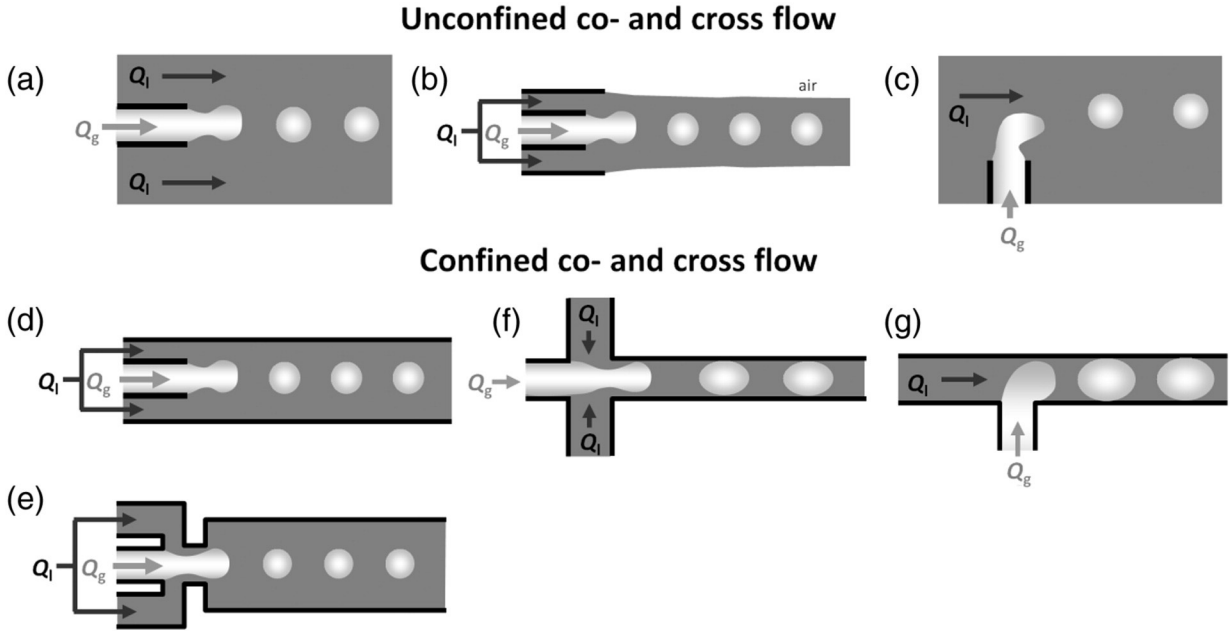

Fig. 9. Selection of the most commonly used geometries to generate bubbles in conditions where both, the gas and the liquid are flowing. The flow may either be unconfined (a–c) or confined (d–g). Flow patterns are typically that of co-flow of both phases (a, b, d–f) or of cross-flow (c, g).

Hence, the obtained bubble size is inversely proportional to the capillary number Ca_L of the liquid and depends linearly on the orifice radius R_O. In the case of confined geometries one observes a well-defined transition from the "squeezing" (Section 2.4.2.1) to the "dripping" regime when viscous forces start to win over surface tension forces, i.e. above a critical Ca_L [57,58].

Upon increasing the gas or the liquid flow rate, one observes that the point of bubble detachment moves away from the orifice, leading to the creation of a jet whose length depends on the flow velocities. This change of behaviour marks an important transition from the "dripping" (or "bubbling") to the "jetting" regime [51,59,60]. This transition is generally rationalised using the concept of absolute and convective instabilities, which we discussed at the end of Section 2.3. In the squeezing and dripping regimes, the break-up of the gas ligament is caused by an absolute instability, which invades the entire system and therefore occurs always at the orifice. With the presence of non-negligible viscous and/or inertial forces, the evolution of the instability can be slowed down and hence be "convected" with the flow. The system can therefore create a jet which breaks at the point where the jet is "old enough" so that the capillary instability had enough time to develop. Two different extremes of jetting scenarios exist. In the first case, the jetting is dominated by the external flow (Fig. 11c). This leads to the formation of a jet which thins away from the orifice as the inner fluid is being accelerated, leading to the formation of bubbles which are smaller than the orifice diameter (since the bubble diameter is of the order of the jet diameter as discussed in Section 2.3). In the second case, the jetting is dominated by inertial contributions of the inner fluid, leading to a jet of increasing thickness as the inner fluid is decelerated by the outer fluid (Fig. 11d), and to bubble sizes which are larger than the orifice diameter. This case was already discussed in Section 2.4.1.2.

In the first case, researchers have been able to show that the transition between dripping and jetting is well defined by the We_{out} and Re_{out} numbers of the outer fluid [61]. This is shown in a phase diagram in Fig. 11e (redrawn from [61]). The transition depends strongly on the density ratio λ_D and on the viscosity ratio λ_V of both fluids. Interestingly, one can see that We_{out} and Re_{out} are proportional at low Re number, meaning that the transition occurs at a fixed Ca number since $Ca = We / Re$. This observation was confirmed by different experiments and a wide range of fluid couples and flow conditions [51,61]. Fig. 11f shows an example of a typical phase diagram obtained for the geometry shown in Fig. 11a (from [61]). What this phase diagram also shows is that the capillary number of the outer flow defines the transition only if inertial forces of the inner fluid can be neglected. In the limit of small Ca_{out}, the transition seems to be defined by a critical Weber number We_{in} of the inner fluid. For intermediate cases (and if Reynold numbers are sufficiently low) one observes that the transition occurs when $We_{in} + We_{out} \approx O(1)$ [61].

The discussion between dripping and jetting may seem somewhat academic. However, it is very useful even for the practitioner. The first reason is that as one enters the jetting regime, monodispersity commonly drops. This is due to the fact that the maximum of the curve giving the unstable wavelengths (Fig. 4b) is quite smooth, meaning that the system may select a wider range of bubble sizes. Moreover, when the system is in the jetting state, the bubbles do not need to be "nucleated" with the associated problems of the initial entry pressure, helping with pressure reduction in devices and for parallelisation. Last but not least, with bubble sizes being of the order of the jet diameter at break-up (Section 2.3), creating thin jets is an efficient way to create a large number of small bubbles, down to a few micrometres [62,63].

The obtained bubble sizes depend on the operating regime of the device. Bubble sizes in the dripping regime tend to be well described by Eq. (27). Bubble sizes in the jetting regime dominated by the outer fluid phase are found to be well captured by simple scalings of the type

$$\frac{R_B}{R_O} \sim \left(\frac{Q_G}{Q_L}\right)^{\beta}, \tag{28}$$

with the pre-factor and β depending on the flow geometry and on the viscosity ratio λ_V. Typically, β has been found to lie between 0.4 and 0.5. For example, researchers found experimentally and theoretically that $\beta = 0.5$ if $Q_G / Q_L \to 0$, and $\beta = 2 / 12$ if $\lambda_V = \eta_G / \eta_L \to 0$ [26]. For high Reynolds and Weber numbers it was found that $\beta = 2 / 5$ [64].

Up to now we have only discussed periodic bubbling regimes. It needs to be said that just as in the case of bubbling from an orifice into a stationary liquid (Section 3.2.1) co-flow can lead to period-

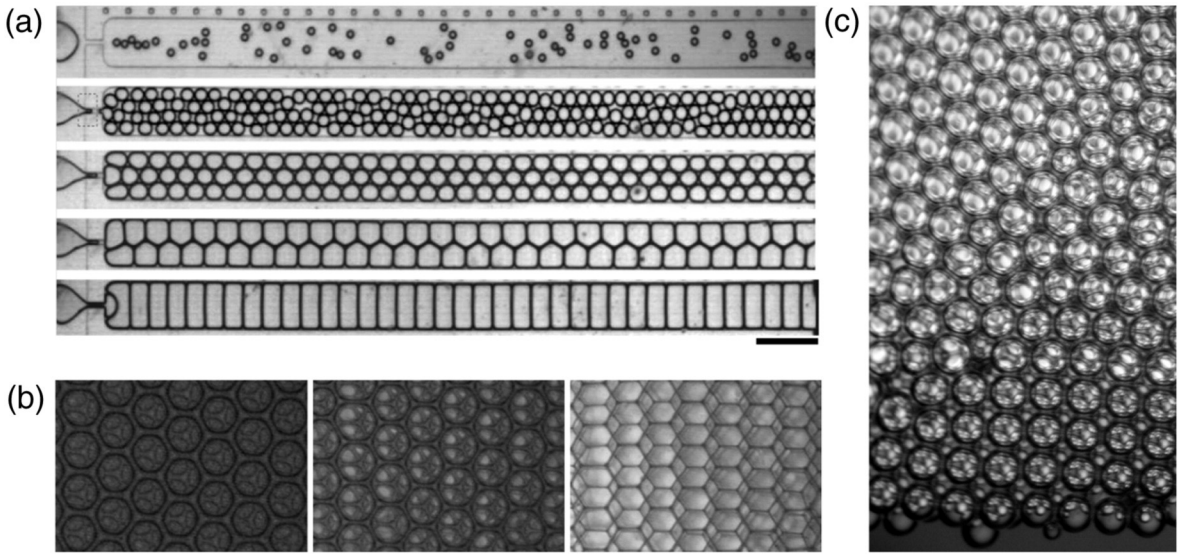

Fig. 10. Examples of monodisperse foams generated via co-flow of gas and foaming solution through a constriction. (a) Examples of foams of different bubble size and liquid fraction in a channel just after the generation (from [55]). (b) Ordered foams with different liquid fraction (from [56]). (c) Monodisperse foam under gravity (courtesy A. van der Net) (all bubble sizes 200–500 μm).

doubling and chaotic bubbling [65] (Section 3.2.2). Such phenomena occur often at the transition between regimes.

2.4.3. Breakup of bubbles under shear

In this section we consider the bubbles as *passive objects*, which are already in the liquid. We ask ourselves how these can be broken into smaller bubbles by the stresses imposed by an *active* external shear flow (Fig. 1). This process has been widely studied. Even though it is conceptually simple, a proper physical description turns out to be highly complex. However, the general phenomenology is well documented, and can be summarised. Since most of the experimental work has been done on drops rather than on bubbles, and since the concepts are very similar, we shall stay on a rather general level here by simply considering two immiscible fluids

Let us consider a drop of a fluid (gas or liquid) of viscosity η_D suspended in a fluid of viscosity η_C exposed to a shear flow (Fig. 12a). The bubble/drop is first deformed into an elongated, steady shape whose geometry depends on the capillary number *Ca* of the imposed shear flow [66–70]. Examples of resulting bubble shapes are shown in Fig. 12b (adapted from [70]). With increasing *Ca* and η_C the bubbles become increasingly elongated — but still reach a steady equilibrium shape. Note how strongly such a bubble can be steadily deformed without "breaking". The deformation is commonly measured by the aspect ratio $D = (A - B)/(A + B)$ (Fig. 12a).

Upon further increase of the capillary number, a critical capillary number Ca^* (and hence a critical deformation D^*) is reached beyond which the bubble can no longer sustain a steady shape. As a consequence, D increases and eventually reaches a point where capillary instabilities (Section 2.3) break the elongated object into pieces. Thus, the instability of the aspect ratio is directly linked to the breakup of the bubble — even though they are not simultaneous.

What sets the critical capillary number Ca^*? An important piece of work was done by H.P. Grace [71] for the case of droplets. He showed that Ca^* depends strongly on the viscosity ratio λ_V, which is shown in the graph in Fig. 13a and by corresponding photographs of bubbles and drops taken just before Ca^* is reached in Fig. 13b. It is straightforward to see the asymmetry of the curve: with two given fluids of different viscosities, results are different depending on which fluid is inside or outside the drop. When the inner fluid has a much lower viscosity (as for a bubble inside water, where $\lambda_V \sim 10^{-2}$), the results show that the bubble can support reasonably high $Ca^* \approx 3$ before being irreversibly extended and ruptured.

Once the elongated mother-bubble (or mother-drop) has ruptured just above Ca^*, the resulting size of the created objects is directly linked

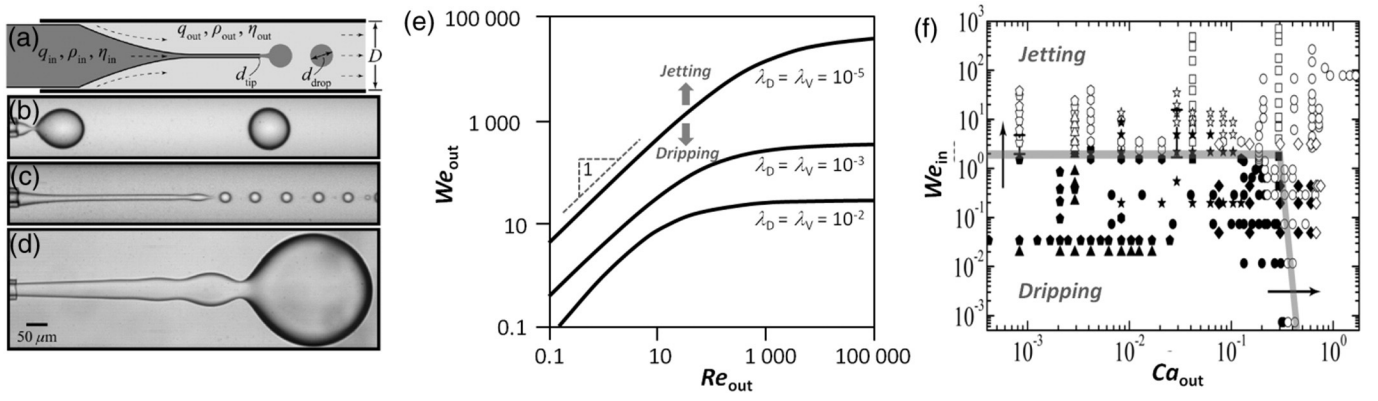

Fig. 11. The dripping to jetting transition in co-flow conditions. (a) Scheme of a commonly used setup. (b) Dripping regime — the bubble/drop is created at the tip of the orifice. (c) Jetting regime dominated by the external flow. (d) Jetting regime dominated by the internal flow. (a–d from [59]) (e) Transition between dripping and jetting for different density and viscosity ratios when the behaviour is dominated by the flow of the external fluid (redrawn from [61]). (f) Transition between dripping and jetting when at low Reynolds number and when both, the internal and the external flow are important (from [59]).

Please cite this article as: Drenckhan W, Saint-Jalmes A, The science of foaming, Adv Colloid Interface Sci (2015), http://dx.doi.org/10.1016/j.cis.2015.04.001

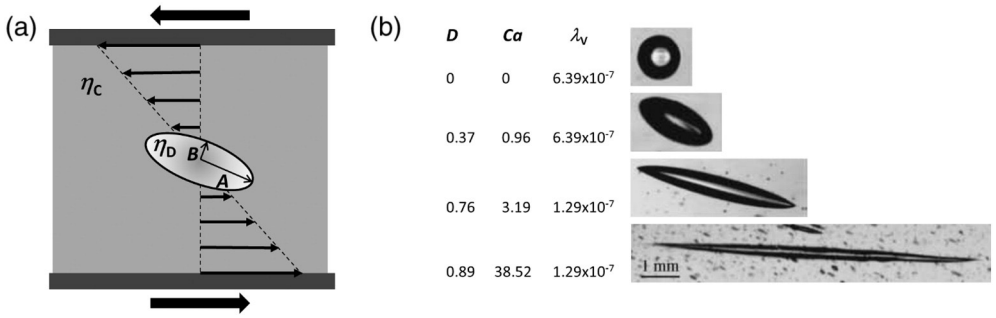

Fig. 12. (a) Scheme of a bubble being deformed in a shear flow. (b) Photographs of the equilibrium shape of a sheared bubble at different Capillary numbers *Ca* and at different viscosity ratios λ_V (adapted from [70]). *D* is a measure of the deformation given by $D = (A - B)/(A + B)$.

to the critical elongation D^*: the ligament radius at Ca^* provides an estimation of the diameter of the newly created entities (see Section 2.3). Since both the critical capillary number Ca^* and the associated deformation D^* increase with decreasing λ_V for $\lambda_V < 1$ (Fig. 13), this implies that the size of the resulting objects decreases for decreasing λ_V.

The above descriptions correspond to deformations generated by a pure shear flow. In fact, it was rapidly discovered that the deformation and stability of bubbles and drops in a flow field depend strongly on the type of imposed flow [68,72,73]. Elongational, rotational or simple shear flow does not deform a bubble in the same way, and consequently, the critical capillary number Ca^* depends on the type of flow. A vast body of theoretical and numerical research deals with such issues, considering gradually varying types of flow, which are shown in Fig. 14a. Such flow fields can be expressed via the velocity gradient

$$\nabla \boldsymbol{u} = \frac{1}{2} G \begin{bmatrix} 1+\alpha & 1-\alpha & 0 \\ -1+\alpha & -1-\alpha & 0 \\ 0 & 0 & 0 \end{bmatrix}, \tag{29}$$

where G fixes the amplitude of flow field. The balance between shear and vorticity of a flow can then be simply described by the factor α, which gives purely extensional flow in the case of $\alpha = 1$ and simple shear flow for $\alpha = 0$ (see flow patterns in Fig. 14a). Experimentally, such kind of flows can be generated by four independently rotating cylinders. The capillary number of these flows is then typically expressed as

$$Ca = \frac{G\eta R_B}{\gamma}, \tag{30}$$

where R_B is the radius of the undeformed bubble/drop.

As shown in Fig. 14b, the dependence of Ca^* on the viscosity ratio λ_V depends non-negligibly on α. In the limit of bubbles (small λ_V), the critical capillary number Ca^* decreases as one goes from $\alpha = 0$ (pure shear flow) to $\alpha = 1$ (purely extensional flow). For curiosity, note the differences with the regime at high λ_V: with only simple shear ($\alpha = 0$) one cannot break very viscous drops, while with extensional shear it is possible (α approaching 1).

Besides the Rayleigh–Plateau instability (Section 2.3) which breaks the elongated ligaments, there are two other important mechanisms which can also lead to the creation of smaller bubbles/drops. The first phenomenon is called "tip streaming" and is shown in Fig. 15. It creates a thin thread which starts at the tip of an elongated bubble/drop, where it has a non-trivial shape [74]. This thread breaks into tiny bubbles/drops. This is very different from the rupture of the main bubble (drop) [75]. As shown in the graph of Fig. 13a, this phenomenon occurs well below the critical capillary number Ca^* for breakup. The presence of surfactants plays an important role in this process and numerous important advances have been made recently in order to elucidate the key mechanisms at play in this process [[]].

Another mode of rupture of the elongated bubble/drop which occurs well before the onset of the capillary instability takes place when the flow is suddenly stopped, or if the bubble/drop is convected towards a region of lower capillary number [14,26,69]. As show in Fig. 16a, in the absence of deforming stresses, the bubble/drop tends to go back to its minimal surface shape, which is a sphere. In this process of contraction, an effect called "end-pinching" can occur: a bulbous head forms at each end of the filament. The filament becomes unstable in the vicinity of the head, creating two smaller heads at the remaining filament and so forth. This can be nicely seen in the right image sequence of Fig. 16a. Whether end-pinching occurs depends on a number of parameters. Recently, a phase diagram was proposed by Driessen et al. [26] (Fig. 16b), showing under which condition the relaxation of stretched drops of different viscosities in air are stable or not. It seems that as in the case of infinitely long fluid cylinders (Section 2.3), one of the control parameters is the Ohnesorge number *Oh* (Table 2). The second control parameter is the deformation of the drop at the moment when the deforming shear flow is stopped. Once again, most of the

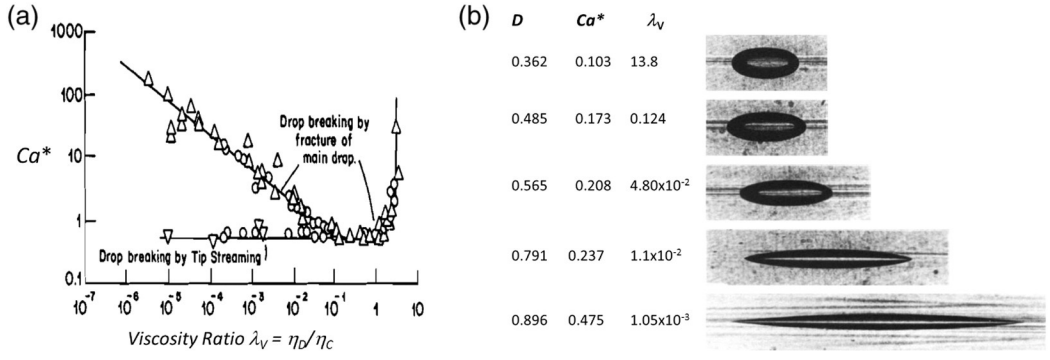

Fig. 13. (a) The "Grace plot": Critical capillary number Ca^* beyond which the drop/bubble becomes unstable in a pure shear flow as a function of the viscosity ratio λ_V of the dispersed and continuous phase (adapted from [71]). (b) Photographs of drop/bubble shapes at the critical point, generated in an extensional flow for a wide range of viscosity ratios λ_V (adapted from [68]).

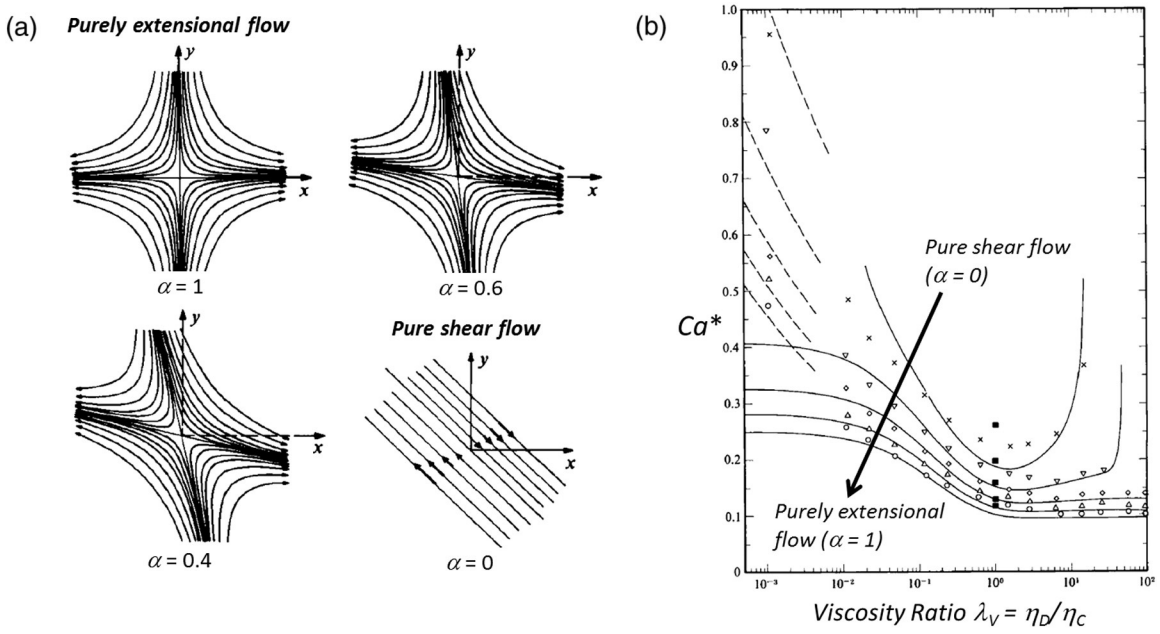

Fig. 14. (a) Different types of flow fields in which the bubbles/drops are deformed, ranging from purely extensional ($\alpha = 1$) to pure shear flow ($\alpha = 1$) (adapted from [68]). (b) Effect of the flow type on the critical capillary number Ca^* beyond which the bubble/drop shape becomes unstable (adapted from [68]).

experiments have been performed with drops, rather than with bubbles, but the physical phenomena concerned here are valid for both systems.

2.4.4. Gas entrainment at free surfaces

If one considers the flow of liquid with a free surface, many sources of perturbations of the interface can lead to the entrainment of the surrounding, passive air. This phenomenon is generally related to the presence of a geometrical constraint or an abrupt change of cross-section or speed between neighbouring fluid zones [13]. Well-known examples include the plunging jet (Fig. 17a) [80], in which the region of gas incorporation opens like a cone, or the hydraulic jump (Fig. 17c) (Section 3.2.3), where air is entrained when the average flow speed of a liquid slows down suddenly. Similar situations arise when the flow is accelerated temporarily as it passes over obstacles or when the free interface with air vanishes, for example when flow disappears under an inclined plane (Fig. 17d).

The plunging jet is the most documented situation in foam-related work [80]. Due to its practical relevance (for example in the kitchen sink and the bathtub), it is used as a standardised foamability technique (Ross–Miles test, Section 3.2.3). Moreover, it corresponds to a prototype (or paradigm) experiment, with which one can probe the basic mechanisms at work in more complex hydrodynamic processes [80]. One of the key parameters in this process is the impact velocity of the jet U, i.e. its capillary number $Ca = \eta_L U / \gamma$. Below a threshold value, a steady deformation of the interface is obtained without the incorporation of gas (inset of Fig. 18). An important feature is that the radius of curvature r at the edge of the gas "cusp" vanishes exponentially with the capillary number Ca, i.e. $r \sim \exp(-Ca)$ [80]. This steady interfacial deformation becomes unstable beyond a critical capillary number Ca_c (and an associated critical cusp radius r_c): a viscous pumping of the entrained fluid into the narrowing nose generates a lubrication pressure, which finally prevents any steady force balance [80]. As in the case of bubble break-up under shear, above this Ca_c the cusp is increasingly stretched until it eventually breaks into smaller bubbles by the mechanisms discussed in Section 2.3. The entire process is sketched in Fig. 1. It can produce quite monodisperse foams with bubble-sizes and monodispersity depending on the jet speed — as the regular bath tuber or dish washer may confirm.

The physics of plunging jets has been investigated in detail for high-viscosity liquids in air, as both experiments and modelisation turn out to be easier to perform than for low-viscosity fluids. Different investigations lead to the prediction that, as long as inertia can be neglected (small Re), the critical capillary number Ca_c scales logarithmically with the viscosity ratio λ_V [80,81]

$$Ca_c \sim -\ln\left(\frac{\eta_G}{\eta_L}\right) = \ln(\lambda_V). \tag{31}$$

This is shown in Fig. 18 (adapted from [80]). Lorenceau et al. [81] have shown that this relationship can be extended over five orders of magnitude to smaller viscosity ratios when working with two liquids.

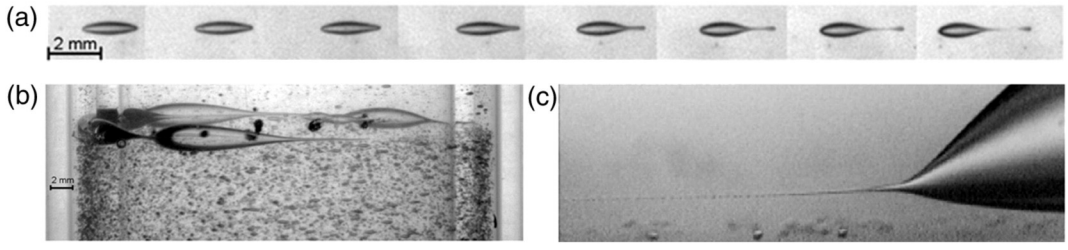

Fig. 15. Tip-streaming: production of tiny bubbles at the tip of bubbles sheared in a Couette cell (a and b from [79]) and at the tip of a drop (c from [24] — Leonhard, H., 1996, "Experiments on tipstreaming," unpublished).

Please cite this article as: Drenckhan W, Saint-Jalmes A, The science of foaming, Adv Colloid Interface Sci (2015), http://dx.doi.org/10.1016/j.cis.2015.04.001

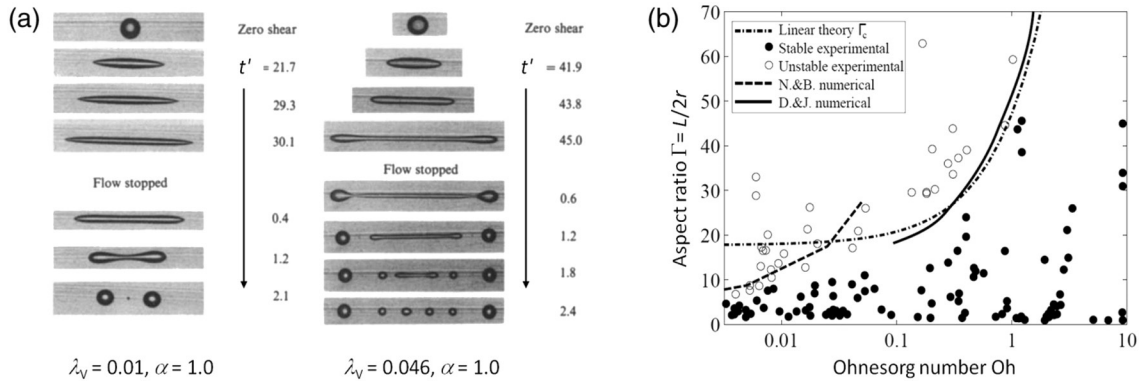

Fig. 16. (a) A bubble breaks as it relaxes from an elongated shape when the applied shear is stopped (from [68]). The way it ruptures depends on its initial aspect ratio and the viscosity ratio of the two fluids. This is shown in a phase diagram in (b) which shows a stable and an unstable zone for deformed droplets of different viscosities in air using the aspect ratio and the Ohnesorge number *Oh* as key parameter (from [26]). Here the full circles correspond to droplets which contract without breaking. The empty circles are obtained for more stretched and viscous drop, which finally break as they relax.

Another non-trivial result concerns the rate of gas entrained. It turns out that it depends only on the gas viscosity, and, surprisingly, not on the fluid viscosity [80]. This is due to the fact that the gas film decouples the jet from the rest of the fluid.

In contrast to the previously described visco-capillary entrainment modes, the physics of low-viscosity plunging jets is commonly characterised by high Reynolds numbers ($Re > 100$) and low capillary numbers ($Ca < 1$). Under such conditions, different inertial instabilities of the gas/liquid interface can develop already before the impact, so that the cross-section of the jet is no longer constant. One of these instabilities is the Kelvin–Helmholtz instability [82]. It arises when two immiscible fluids with different densities flow side by side at very different velocities (Fig. 19a). Beyond a critical velocity difference certain wave lengths of natural interfacial fluctuations become unstable and are amplified by the flow [82]. An example of this instability on a simple water jet in air is visible on the left side of the jet in Fig. 19b. If this instability develops before the viscous pumping effect starts to be important they modify in a non-trivial manner the entrainment and break-up mechanism. Different scenarios arise which are often studied in separate regimes depending on the initial amount of disturbance relative to the speed of the jet [80].

The Kelvin–Helmholtz instability can lead to another type of air entrainment when it is driven to sufficiently high Weber numbers *We* (i.e. both *Re* and *Ca* need to be high since $We = ReCa$). In this case the destabilisation of the interface is greatly amplified, leading to complex flow structures which tend to lead to the formation of smaller ligaments which then again undergo the type of capillary instabilities discussed in Section 2.3. This kind of fluid break-up is called "atomisation" or "fragmentation" (right side of the jet in Fig. 19b and wave breaking in Fig. 19c) [30,83–86]. Under the right flow conditions, it can lead to the entrainment of a significant amount of air and hence to foam generation, as shown by the example of breaking waves in Fig. 19c and discussed briefly in Section 3.2.3.

Gas entrainment does not necessarily require high velocity flow: trapping pockets of gas in a fluid can occur at low flow velocities in the presence of confined geometries and when flow conditions vary fast enough so that the free interface gets locally sufficiently deformed to entrain a gas pocket. Washing your hands with soap is probably enough of an experiment to convince yourself of this effect. Highly viscous fluids may also simply be folded in a way to trap air.

2.5. Bubble generation without topological changes — phase transitions

One of the main techniques to obtain bubbles without the necessity of a topological transition of the interfaces is their generation via a liquid → gas phase transition which occurs locally in the fluid to create bubbles. There are two different classes of phase transitions which are commonly used for bubble generation [88–90]. The first class occurs in pure fluids, where the liquid phase turns into vapour. As indicated in the phase diagram of Fig. 20a, this can either be triggered by a pressure drop ("*cavitation*") or by a temperature rise ("*boiling*"). Cavitation is commonly created by rapid flows which create localised pressure drops through constrictions or rotating propellers or by high energy pressure waves, such as encountered in ultrasound. Bubble and foam generation by boiling is known to most of us for the case of water or milk in the kitchen.

The second class of liquid → gas transitions occurs in supersaturated liquids within which a gas is dissolved which comes out of solution upon a pressure drop (Fig. 20b) or a temperature increase. By far the most commonly used mechanism in the case of foam generation is the one encountered upon a pressure drop, which is called "effervescence" and which is particularly well known to lovers of fizzy drinks, beer or champagne.

These different ways of generating bubbles in an originally homogenous fluid have a common physical mechanism: the system needs to be driven into a supercritical state, in which small bubbles nucleate spontaneously and then grow (Fig. 2). Understanding the nucleation of bubbles in a liquid has a long-standing history [88–91], with a number of open questions that remain to be answered. The complexity of this

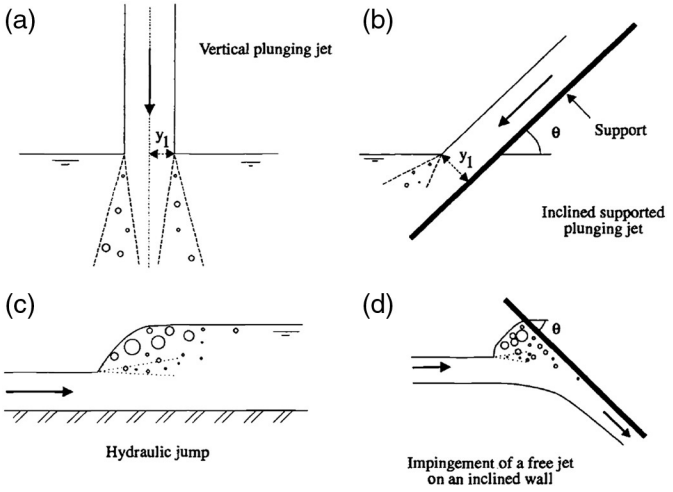

Fig. 17. Different configurations leading to gas entrainment at free surfaces. Adapted from [13].

Please cite this article as: Drenckhan W, Saint-Jalmes A, The science of foaming, Adv Colloid Interface Sci (2015), http://dx.doi.org/10.1016/j.cis.2015.04.001

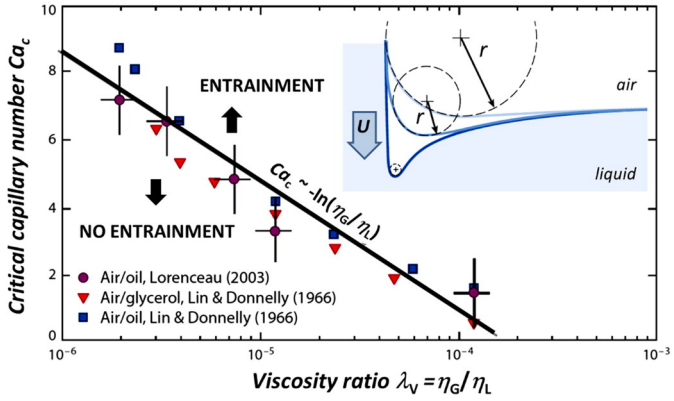

Fig. 18. Critical capillary number Ca_c as a function of the viscosity ratio λ_V beyond which air is entrained by an impacting liquid jet. Inset: sketch of the initial entrainment steps. Adapted from [80].

subject results from the fact that bubble nucleation needs to start with the creation of a singularity within the fluid, which calls upon a molecular description of the process (challenge for theory) and which is extremely sensitive to the presence of impurities (challenge for experiments).

If one neglects the very initial stage of the hole opening, one may assume that the created bubble is large enough so that one can apply the concept of a surface tension and a bulk description of the gas and the liquid phase. In this case one can consider the two key contributions to the free energy of the bubble formation. On the one hand, once the system is in a supercritical state, it will reduce its free energy by the phase transition with an associated change in the free energy density ΔG_V

$$\Delta G_{bulk} = -V_B \Delta G_V = -\frac{4}{3}\pi R_B^3 \Delta G_V. \quad (32)$$

At the same time, the creation of a bubble requires the creation of a vapour/liquid or gas/liquid interface, which leads to an increase in free energy

$$\Delta G_{surf} = A_B \Delta G_S = 4\pi R_B^2 \gamma. \quad (33)$$

Hence, the total change in free energy may be approximated by

$$\Delta G_{tot} = \Delta G_{surf} + \Delta G_{bulk} = \pi R_B^2 \gamma - \frac{4}{3}\pi R_B^3 \Delta G_V. \quad (34)$$

Making the approximation that the surface tension and the volume free energy are independent of the bubble size, one obtains a free energy function which is characterised by a well-defined maximum, as sketched in Fig. 21. This maximum sets a critical nucleation barrier ΔG_C which is associated with a critical bubble radius R_c. A spontaneously generated bubble which is smaller than this critical size will shrink and disappear, while a bubble which is bigger than this critical size will grow. The nucleation rate n of bubbles may be approximated by

$$n \sim \exp\left(-\frac{\Delta G_C}{kT}\right). \quad (35)$$

The growth rate of these bubbles depends on the saturation conditions and can be approximated [88–92] — but this is beyond the scope of the article.

A more mechanical way to approximate the critical radius directly is to use the Laplace law

$$R_C = \frac{2\gamma}{\Delta P} = \frac{2\gamma}{\sigma P_f} \quad (36)$$

where σ is the "supersaturation" of the liquid ($\sigma = \alpha - 1$, with α being the "saturation") and P_f is the final pressure. The definition of this supersaturation depends on the considered scenario and can be obtained from the physical parameters of the system. In the presence of one phase only (cavitation and boiling, index "1Ph") one needs to take into account the vapour pressure P_V of the liquid. One may therefore define

$$\Delta P = P_V - P_f = \sigma_{1Ph} P_f \quad (37)$$

$$\sigma_{1Ph} = \alpha - 1 = \frac{P_V}{P_f} - 1. \quad (38)$$

In the case of two phases (index "2Ph"), i.e. a liquid being supersaturated by a dissolved gas (effervescence), one needs to take into account the vapour pressure of the solvent and the partial pressure of the dissolved gas. The latter being generally much higher, one can neglect the vapour pressure and express the supersaturation using Henry's law

$$\Delta P = P_i - P_f = H(X_i - X_f) = \sigma P_i \quad (39)$$

$$\sigma_{2Ph} = \alpha - 1 = \frac{X_i}{X_f} - 1 \quad (40)$$

where $H = P_f / X_f$ is Henry's constant and X_i and X_f are the mole fractions of the dissolved gas in the initial and final state, respectively.

Due to the nucleation barrier ΔG_C, one generally finds that supersaturations of a few 1000 are required in very pure liquids. The reason why we see nucleation and growth at much lower supersaturations in everyday life is due to the presence of impurities or pre-formed bubbles which act as nucleation sites (Fig. 22) and which may dramatically decrease the nucleation barrier. As sketched in Fig. 22 (inspired by [90]), scientists group the different nucleation scenarios in two main groups of nucleation. **"Homogeneous nucleation" (Type I)** occurs without the presence of any nucleation agents and therefore at very high supersaturations. "Heterogeneous nucleation" occurs in the presence of nucleation agents. In this case one differentiates between three types, following the kind of agents present and the specific physical conditions [90]:

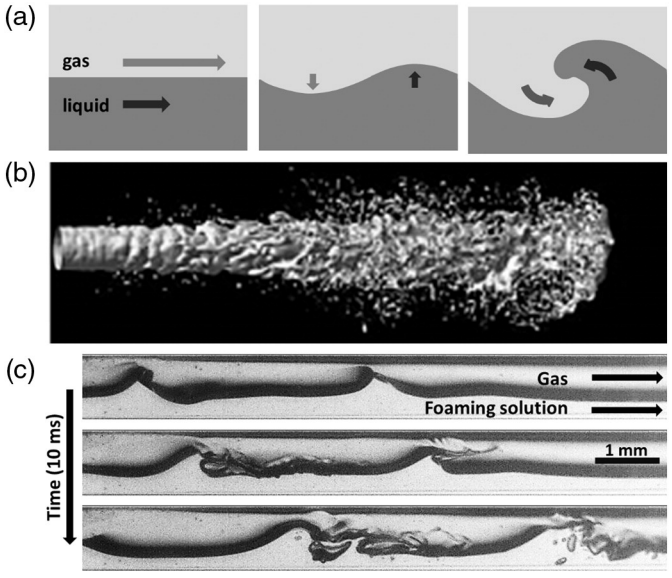

Fig. 19. (a) Destabilisation of a gas/liquid interface due to the Kelvin–Helmholtz instability. (b) Kelvin–Helmholtz instability on a liquid jet. The growth of the instability at sufficiently high *We* leads to the formation of complex patterns which can lead to the creation of small drops (atomisation, from) or the entrainment of air bubbles, as shown by breaking waves in (c) (from [87]).

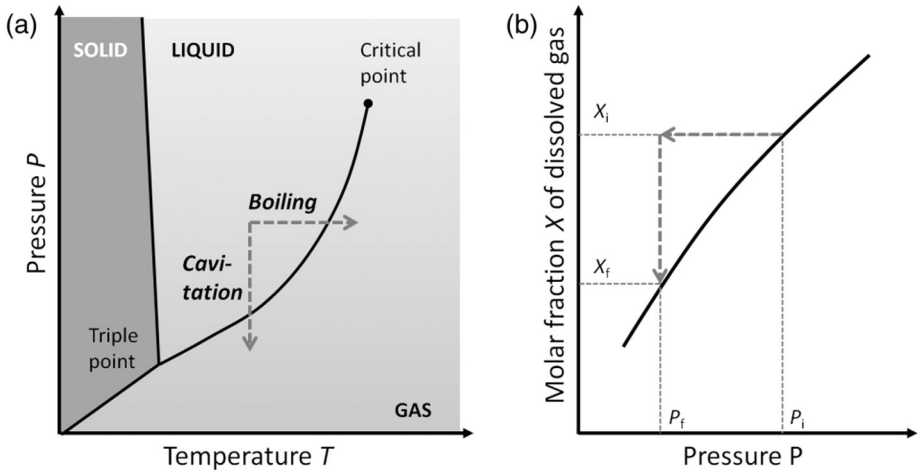

Fig. 20. Different possibilities to nucleate bubbles in a solution. (a) Liquid → gas transition of one phase via pressure drop ("cavitation") or a temperature rise ("boiling"). (b) Liquid → gas transition upon change of solubility of a gas dissolved in a liquid, here by a pressure drop (effervescence).

Heterogeneous nucleation — Type II (classical): Nucleation occurs in the presence of solid impurities which can either be small particles dispersed in the liquid or the solid wall of the container. Reasonably high supersaturations of order 100 are required for bubble generation in this case.

Heterogeneous nucleation — Type III (classical): Nucleation occurs in the presence of pre-existing gas cavities (on the container surface, on suspended particles or freely floating in the liquid) of radius of curvature smaller than the critical radius R_C. Hence one still needs to nucleate, but supersaturations are significantly lower than in the case of type I and II nucleation since the "holes" in the liquid are already made.

Heterogeneous nucleation — Type IV (non-classical): Bubbles are generated from pre-existing gas cavities (on the container surface, on suspended particles or freely floating in the liquid) of radius of curvature larger than the critical radius R_C. Since there is no energy barrier to overcome it is referred to as "non-classical" nucleation. These cavities grow as soon as a small [93] level of supersaturation is reached. Type IV nucleation may follow type III nucleation, for example if bubbles nucleate in cavities on the wall leaving behind a bubble large than the critical radius.

In the case of heterogeneous nucleation, the bubble generation at a wall or at an impurity becomes one which requires a topological change to detach the bubble from the nucleating agent. This provides the same conditions as discussed in Section 2.4.1 with the difference that the bubble is blown by a phase transition.

3. Techniques of foam formation

3.1. Introduction

In this section we discuss some of the most commonly used foaming techniques. These techniques make use of the fundamental mechanisms of bubble generation discussed in Section 2. However, to the despair of those who want to model their behaviour, they commonly combine different mechanisms. Moreover, they are commonly run in a way that the generation of one bubble cannot be considered as isolated from the generation of the others (as we did throughout most of Section 2). Hence, even though the main mechanisms of most techniques may be identified, predicting the properties of the obtained foam as a function of the different device parameters is not simply a question of extrapolating our discussion from the previous section and therefore remains a major challenge. Moreover, only few of the complex foaming techniques have been investigated systematically in the past.

It is for this reason that the description of the different foaming techniques remains here on a somewhat qualitative level. We have tried to group the different techniques by their main mechanisms, going every time from the simplest configuration — where some of the acting physics is understood — to the most complex one. In order to guide the reader who may consult this article in the search for an appropriate technique for his application, we have compiled some of the key features of commonly used techniques in Table 3.

3.2. Mechanical foaming techniques

3.2.1. Foaming by bubbling into a stationary liquid

The process of bubbling into a stationary liquid is of great importance in a number of industrial processes, the most common examples being bubble column reactors [94,95] or foam flotation/fractionation tanks [96,97]. In most applications, bubbling occurs through many orifices in parallel, through a perforated plate (regular distribution of equal-sized holes) or through a porous disc (irregular arrangement of orifices of irregular cross-section, but typically with a characteristic size). Researchers find that even though — in principle — the bubbling process on each individual orifice can be described as in the case of an

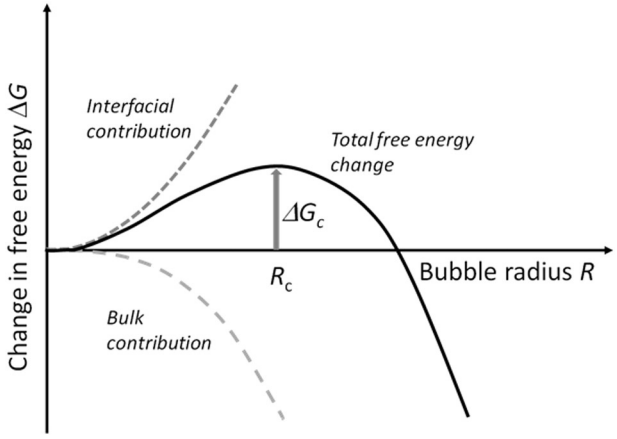

Fig. 21. Change of free energy during bubble generation from a supercritical liquid.

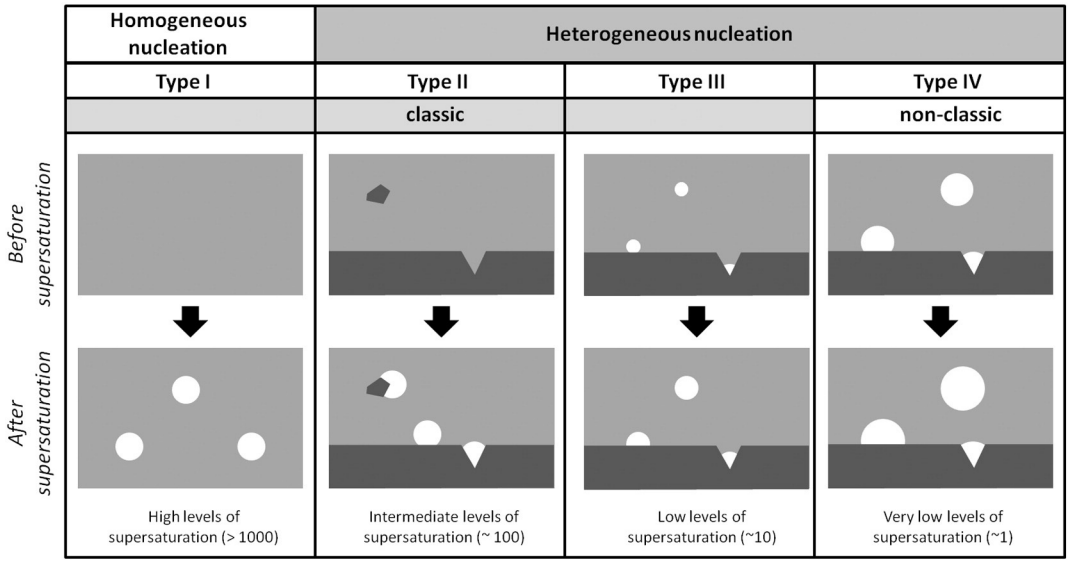

Fig. 22. Different types of nucleation and growth processes encountered in bubble formation (inspired from [90]).

isolated orifice in Section 2.4.1, a number of complex interactions occur between the closely spaced orifices on the plate or the disc which need to be taken into account [33,94]. These interactions may arise from a coupling through the reservoir or through the liquid by hydrodynamic flows or direct bubble contact. In an attempt to elucidate these complex interactions, researchers have started to look at more simplified systems of a few orifices of controlled spacing and dimensions (Section 3.2.1.2).

Characteristic bubble sizes with these kinds of techniques range from a few hundred micrometres to one centimetre. The foam can be very monodisperse, if identical orifices are driven under the right conditions (Section 3.2.1.2), or polydisperse, with polydispersities being typically up to 50%. Foam production rates depend on the number of orifices used. With porous discs one can easily generate 1 L/min/cm^2 of pore surface. Since the bubbles need to be generated in a liquid, the foam just after generation has generally a high liquid fraction. As bubbles rise away from the generation site the liquid is drained by gravity to create foams with low liquid fractions.

3.2.1.1. Complex bubbling regimes for one orifice. In Section 2.4.1 we considered periodic bubbling regimes only. However, even a single orifice can be driven in highly non-linear bubbling modes, depending on the bubbling conditions. As shown in Fig. 23a and b at intermediate gas flow rates the bubbling periods T (time between two bubble detachments) bifurcate, leading to two or more bubbling periods. In certain ranges a fully chaotic bubbling is observed with a random distribution of the bubbling periods [93,98–102]. Multiple bubbling periods can lead to bubble size distributions with several peaks (bi- or tri-disperse, etc.) while chaotic bubbling may generate polydisperse foams. Which one of the different regimes is selected, depends strongly on the liquid properties, the orifice conditions and the gas flow rate. At the outset, researchers believed that this complex behaviour resulted from intricate interactions between the detached bubble(s) and the one which is being generated, or from pressure fluctuations in the reservoir. The interpretation which seems to be emerging now is that it is rather the dynamics of the gas/liquid meniscus within and at the orifice which controls this interesting behaviour [93,100–102]. For example, Fig. 23b shows that the complexity is lost as soon as the orifice radius r_o is large enough.

3.2.1.2. Bubbling from several orifices/perforated plates. If one bubbles through several orifices in parallel, the resulting behaviour depends on whether the bubbles are blown from the same gas reservoir. At the outset let us consider two orifices which are fed by a separate gas injection. As long as they are sufficiently far away from each other within the fluid,

Table 3
Overview of the key features of some of the most commonly used foaming techniques.

Principle	Technique	Bubble size (mm)	Polydispersity (%)	Initial gas fraction φ	Production rate (L/min)	Section
Bubbling into a stationary liquid (active gas phase, passive fluid phase)	Individual orifice	0.1–10	2–40	<0.60	<1	2.4.1 and 3.2.1.1
	Many orifices/perforated plate	0.1–10	2–40	<0.60	<5 (per cm^2)	3.2.1.2
	Porous disc	0.1–10	10–50	<0.70	<5 (per cm^2)	3.2.1.3
Co-flow o of gas and liquid (active gas phase, active fluid phase)	Individual orifice	0.01–1	2–30	<0.99	<0.1	2.4.2 and 3.2.2.1
	Porous media	0.01–1	>30	<0.90	<1	3.2.2.2
	Static mixer	0.01–1	>30	<0.95	<15	3.2.2.3
	Straight tube	0.01–1	>30	<0.97	<10	3.2.2.4
Air entrainment and break-up under shear (passive gas phase, active fluid phase)	Ross–Miles (plunging jet)	0.1–5	10–40	<0.60	<1	3.2.3.2
	Venturi hose	0.01–0.1	<30	<0.90	<5	3.2.3.2
	Propeller	>1	<30	<0.97	<1000	3.2.3.2
	Kitchen blender	0.01–1	<40	<0.97	<1	3.2.3.3
	Rotor–stator-mixer	0.01–0.1	<30	<0.90	<10	3.2.3.3
	Foaming by shaking	0.1–10	<70	<0.80	Depends	3.2.3.4
Phase transition	Nucleation	0.001–0.01	10–40	<0.60	<1	3.3.1
	Aerosol cans	>0.01	>30	<0.99	<1	3.3.2
	Cavitation	≈ 0.001	>20	<0.60	<0.001	3.3.2
Electro-chemical	Electrolytic cell	0.001–0.01	10–30	<0.60	<0.001 (per cm^2)	3.3.3

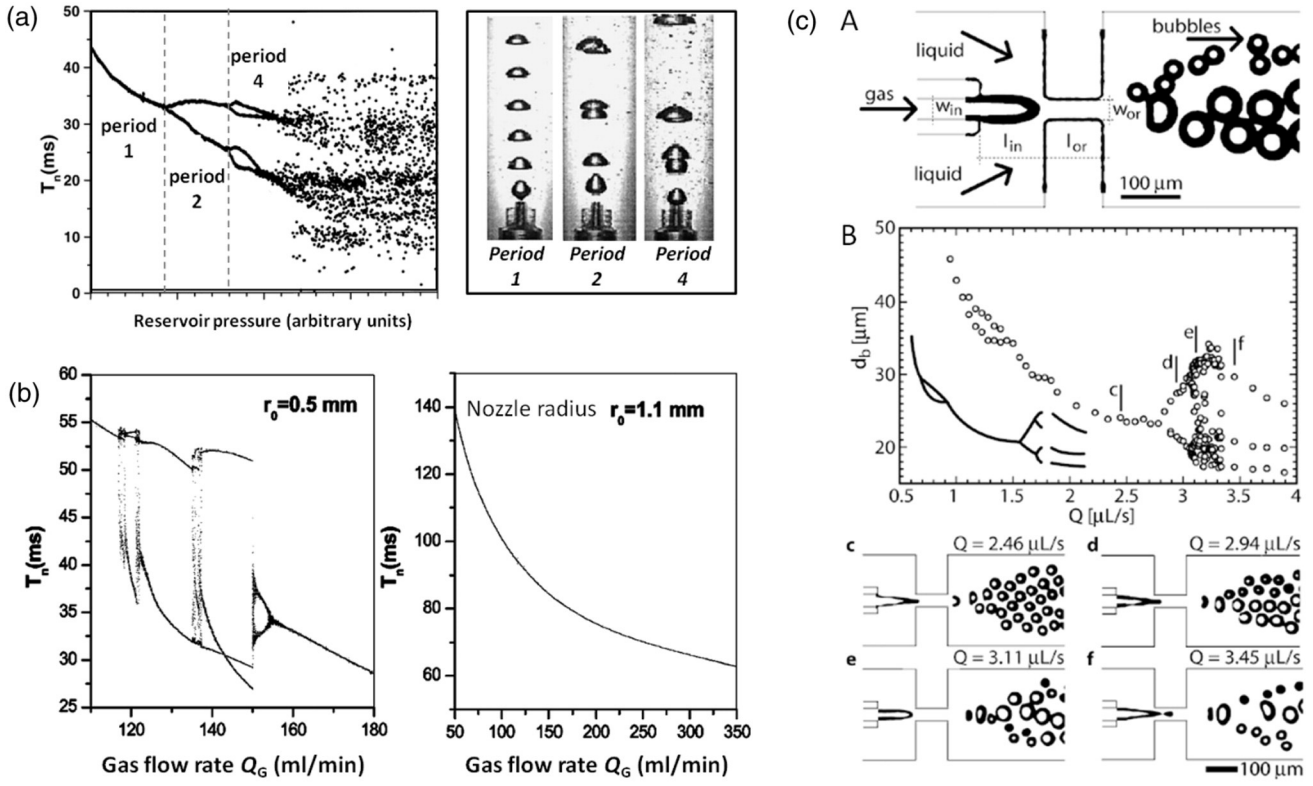

Fig. 23. Period doubling and chaotic bubbling behaviour upon gas injection into a stationary liquid (a, b) and in co-flow conditions (c). (a) Left: Bubbling periods T as a function of reservoir pressure. Right: Corresponding images for period-1, -2 and -4 behaviour (adapted from [99]). (b) Bubbling periods as a function of gas flow rate Q_G for two different orifice sizes. The complexity disappears for the larger orifice (adapted from [102]). (c) A: Bubbling device for the creation of co-flow conditions. B: Bifurcation diagram showing the bubble diameter d_b as a function of the liquid flow rate Q (at constant gas pressure) and corresponding photographs of the bubbling process (adapted from [65]).

both orifices function independently following the behaviour discussed in Section 2.4.1. However, below a critical spacing (which depends on parameters like the bubbling velocity), both orifices begin to communicate via hydrodynamic interactions [103,104] through the liquid. The result is that both orifices can synchronise such that the bubbles are generated in an alternating fashion as is shown in Fig. 24a with corresponding flow fields in Fig. 24b (from [103]). This synchronisation is sensitive to the bubbling speed and is generally lost at very low bubbling velocity and at very high bubbling speed, when the orifice is in the jetting mode.

If the orifices are fed from the same reservoir, as is the case for perforated plates (Fig. 24c–e), one adds an important coupling through fluctuations in the pressure and flow field of the gas within the reservoir. Let us imagine that at the beginning all orifices are closed. As the pressure increases in the reservoir, the gas/liquid interfaces at the orifices start to curve outwards until the maximum pressure is reached when the interface is a hemisphere (Fig. 6b). Beyond this point, the bubble grows at increasing speed (since the resisting Laplace pressure of the interface decreases with increasing bubble volume). The resulting rapid inflow into the bubble therefore leads to a pressure drop of a certain extension in the underlying reservoir. This pressure drop can be so strong and long-range, that a certain number of orifices around the one where the bubble is generated will not be able to reach the maximum pressure for bubble formation. The result is that at low flow rates on perforated plates only a certain number of holes are active in the bubbling process. A typical example is shown in Fig. 24d. The characteristic distance between the active holes depends on the influence length within the reservoir, which in turn depends on the flow rate. Which holes are active depends on which one manages to fire first, which generally depends on small fluctuations in the hole size, with larger holes firing first. As the flow rate is increased, more and more holes start to be involved in the bubbling process. Fig. 24e shows an example of the active hole fraction as a function of the injected gas velocity (from [105]). This increase is due to two reasons. The increase in gas flow velocity leads to an increasing dynamic pressure drop at each hole [106]. Once the dynamic pressure drop is of the order of the maximum capillary pressure, all holes should be able to generated bubbles. A second reason is that for sufficiently high gas flow velocities, i.e. beyond a characteristic Weber number (see Section 2.4.1.2), inertial forces play an important role leading to the formation of a gas jet. This implies that the holes remain open permanently and the maximum capillary pressure loses its meaning once the hole is firing. This can be seen in Fig. 24e, where all holes are active when the flow velocity is about 12 m/s which corresponds to $We \approx 2$ and therefore to the jetting regime (Section 2.4.1.2). Since the jets have a certain cross-section, the final number of active orifices may be smaller than 100% if the orifice spacing is smaller than a typical jet diameter [107]. The bubble size at each orifice can be approximated using the gas flow rate per active orifice and the relations provided in Section 2.4.1. However, one needs to keep in mind that the coupling can lead to flow rate fluctuations between the orifices and therefore to the generation of bubbles of different sizes.

For many purposes it is desirable to drive the porous plate in a slow bubbling mode to maintain the monodispersity of the bubbles. An elegant trick to avoid the pressure-coupling of the orifices is to increase the flow resistance between them in the reservoir. This can be done by increasing the flow resistance of each orifice (long slender orifices) or by replacing the part of the reservoir underneath the orifices by a fine porous medium [106]. Apart from the question of the number of active orifices, coupling of the bubble break-up can occur for sufficiently close orifices. Researchers find [108–110] that bubbling is synchronised at low and a high flow rates (jetting regime), while it is asynchronous for intermediate flow rates. The synchronisation depends on the orifice spacing and organisation.

Please cite this article as: Drenckhan W, Saint-Jalmes A, The science of foaming, Adv Colloid Interface Sci (2015), http://dx.doi.org/10.1016/j.cis.2015.04.001

3.2.1.3. Sparging from porous discs and more exotic sparger geometries. The most commonly used spargers for foam generation are probably of porous type, as shown in Fig. 24f. The most popular spargers are sintered glass discs, since they are hydrophilic, easy to clean and since they provide a wide range and a good control over the characteristic pore dimensions. In porous spargers, all of the previously discussed mechanisms interact simultaneously to give the final foam properties. The final bubble size distribution depends sensitively on the pore-size distribution, the wetting properties and the flow conditions. There are two important differences between porous spargers and perforated plates. The first lies in the wide distribution of pore sizes (as shown in Fig. 24f). Since the initial maximum capillary pressure to be overcome is inversely proportional to pore radius (Eq. (17)) the bubbling will occur through the largest pores. This is why at low flow rates, porous discs can produce foams of high monodispersity (Figure 24g from [111]). With increasing gas flow rate, the pressures at the smaller holes increase so that an increasing number of smaller pores are active, making the foam increasingly polydisperse. As in the case of a single orifice, as a rule of thumb, the average bubble size of a sparger is proportional to its average pore size. The second difference lies in the fact that the different pores of a sparger are less coupled by pressure fluctuations than the orifices of a perforated plate, since the gas encounters a high flow resistance as it passes through the complex pore network. However, this simplification regains complexity by the fact that depending on the dynamic conditions the gas may choose different preferred passages through the porous material. Depending on the flow conditions, bubble size distributions from porous spargers have been characterised by the presence of several peaks [112] or by a smooth Weibull distribution [113].

The gas fraction of the foam generated just above the sparger tends to be very low, the final gas fraction of the foam being created by a competition between foam rise and liquid drainage [114]. Care needs to be taken when the gas influx is so high that a foam is created right at the outlet of the sparger. In this case, bubble generation mechanisms may change dramatically, leading to a dependence of the bubble size with flow rate which may be completely different (even the inverse) to what has been discussed above.

A selection of more exotic spargers has been developed in the past, generally with the aim to obtain a better control over the bubble size distribution while increasing the foam production rate. Amongst the most elegant are techniques which employ the instability of gas/liquid interfaces in particular geometric conditions. Examples include periodic bubble generation at a narrow gap [116,117] or at a step [118,160], which can produce highly monodisperse bubbles, as shown in Fig. 25. Similar to the case of orifice bubbling, the bubble sizes may be varied via the gap/step width and the gas flow rate.

3.2.2. Foaming via co-injection of gas and liquid

As already discussed in Section 2.4.2, the bubbling techniques of the previous section are often improved by imposing a flow of the foaming solution. This helps in carrying the bubbles away from the bubbling site and in setting up additional stresses which provide improved control over the bubble sizes and the obtained gas fraction. Individual co-flow devices are often parallelised to increase the production rates (Section 3.2.2.1). One common approach of parallelising the co-flow mechanism is to let gas and foaming solution flow through complex pore geometries. In this case, both phases travel through an interconnected network of random or purpose-shaped pores (Sections 3.2.2.2 and 3.2.2.3), being exposed to a range of different mechanisms which turn one large gas pockets into many small bubbles. One of the key differences between co-flow in individual pores (as discussed in Section 2.4.2) and co-flow in more complex pore-networks, is that the

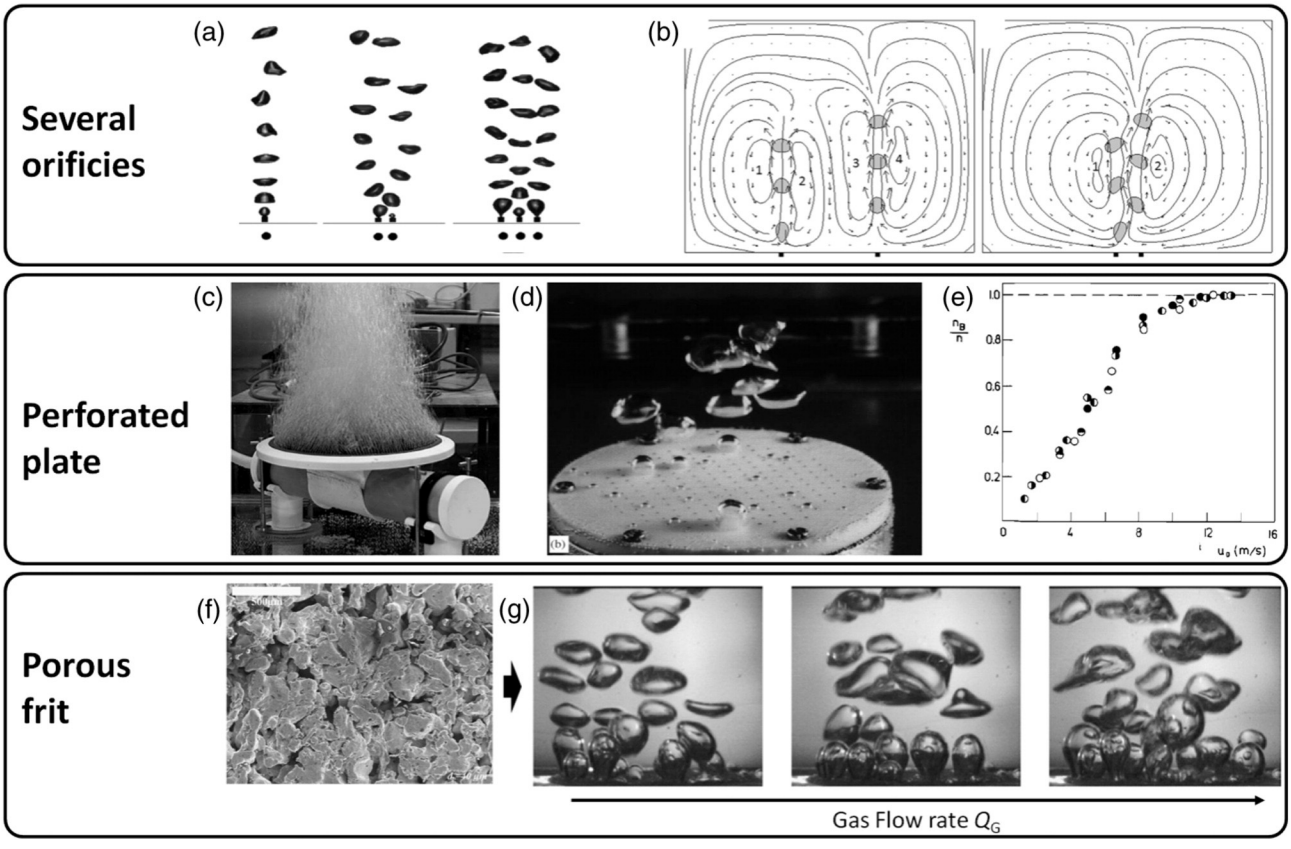

Fig. 24. Bubbling with increasing complexity. (a) Synchronisation of bubbling from neighbouring orifices via interaction through the liquid (from [103]). (b) Simulation of the flow-field around generated bubbles at two orifices for two different orifice spacing (from [103]). (c) Example of bubble generation on a perforated plate (adapted from [115]). (d) Bubbling at a perforated Teflon plate showing that bubbling occurs only via a limited number of holes [106]. (e) Variation of active hole fraction at which bubbles are generated with gas flow rate for different liquid heights (from [105]). (f–g) Image of a porous disc and of bubbles generated from it for increasing gas flow rate (from [111]).

Please cite this article as: Drenckhan W, Saint-Jalmes A, The science of foaming, Adv Colloid Interface Sci (2015), http://dx.doi.org/10.1016/j.cis.2015.04.001

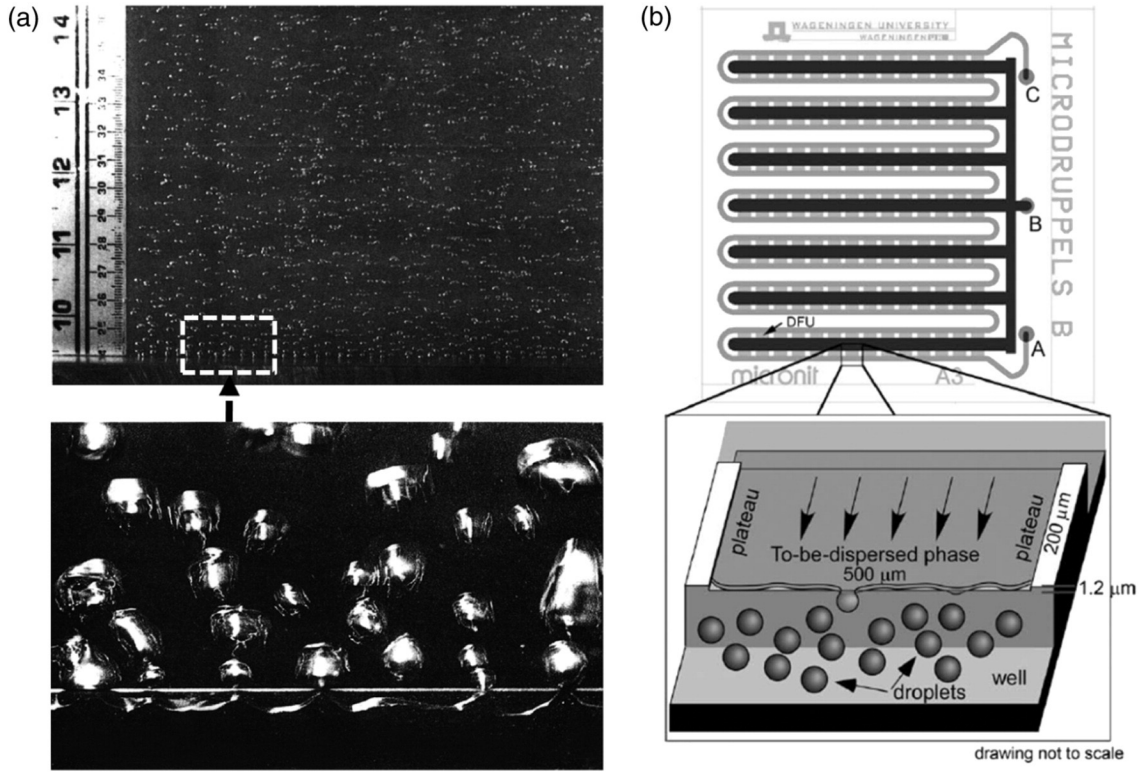

Fig. 25. (a) Sparging from a narrow gap (gap width: 75 µm (top image) & 100 µm (bottom image)) via an instability of the air/water interface (adapted from [116]). (b) Generation of equal-volume bubbles on a step using the same mechanism as in (a) (adapted from [118]).

system can choose between many different flow paths, adding yet another level of complexity. Different types of pore geometries and flow conditions can be used for efficient foam generation. We discuss some of them here.

3.2.2.1. Complex bubble generation and parallelisation of co-flow devices. As in the case of bubbling from an orifice into a stationary liquid (Section 3.2.1.1), even individual co-flow devices may exhibit a complex behaviour at intermediate bubbling regimes. An example is shown in Fig. 23c for the co-flow through a constriction, which shows period doubling and chaotic bubbling for certain ranges of liquid flow rates at constant gas pressure [65].

Even if co-flow devices can generate up to 10^6 bubbles/min, this tends to correspond to small foam production rates since bubble sizes are small. Efforts have therefore been made to parallelise the individual devices [62,119]. In the squeezing or dripping regime (Section 2.4.2) complex coupling is observed between the different orifices (Figure 26a from [119]), which is largely due to the compressibility of the air and the dynamics of the meniscus. As in the case of the porous disc (Section 3.2.1) this coupling can be reduced by increasing the pressures/flow rates and therefore moving towards the jetting regime, where most of the physics happens at the tip of the jet and not at the outlet of the orifice. An extreme example of parallelisation of the break-up of thin gas jets is shown in Fig. 26b [62]. These gas jets can become very thin under extreme co-flow conditions, and bubble sizes can therefore be of the order of a micrometre.

3.2.2.2. Foam generation in porous media. In the limit of very small pore sizes and low flow velocities one finds the application of foam generation in porous media (often sandstone) for enhanced oil recovery [120–124]. In this field, typical pore sizes are of the order of some micrometres, leading to strongly laminar flow which is dominated by surface tension and viscous forces (i.e. small *Re* and *We* numbers).

In a porous medium, at sufficiently low flow rates, both fluids may follow separate paths ("no-foam regime" in Fig. 27a and c), leading to a low flow resistance and hence a small pressure drop across the porous material. Upon increasing the flow rates, one observes an increase in the pressure drop, being associated with the creation of a coarse ("weak") foam (Fig. 27a and c). When a critical pressure gradient ∇P^* is reached in the porous medium upon further increase of the flow rates, the pressure drop jumps abruptly to a much higher value as a result of the onset of efficient foaming mechanisms taking place within the pores. Three different foaming mechanisms have been identified [120,121] which are shown in Fig. 27d. "Lamellea division" divides an already existing foam lamella, while "Leave-behind" creates one due to the flow around obstacles. The third mechanism is "Snap-off", which occurs in the pore throats (narrow section between two pores). Similar to the phenomena discussed in Section 2.4.2, pressure and flow conditions lead to a destabilisation of the gas thread in the pore, which breaks up to generate small bubbles. At this stage, about 10 different mechanisms of this snap-off have been identified [125], the most common one being probably "Roof-snap-off", which occurs when gas invades a liquid-filled pore, similar to the case of co-flow through a constriction (Section 2.4.2). The difference being here that one deals with a parallelisation of many co-flow devices of different dimension, i.e. a situation of even higher complexity than the one shown in Fig. 26a for the parallelisation of two identical devices. A lively debate is taking place in the community, whether "Snap-off" or "Lamellea division" is the main foaming mechanism [125].

Since foaming and foam flow in a porous medium are dominated by what happens in the pore throats (snap-off and lamella need to be pushed through the pore throats) the critical pressure gradient ∇P^* at which foaming occurs is related to the dimensions of the pore throats R_P [124]

$$\nabla P^* \sim R_P^{-2}, \tag{41}$$

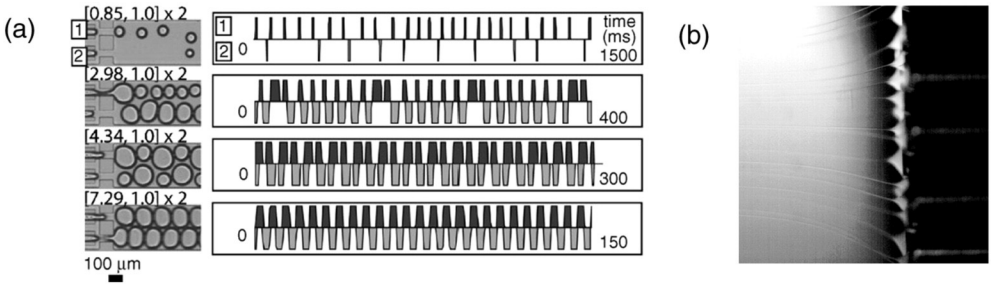

Fig. 26. Parallelisation of co-flow devices. (a) Complex coupling of parallel bubbling devices (from [119]). The left side shows photographs and the right side the bubbling activity of each hole. From top to bottom, the gas pressure is increased at constant liquid flow rate. The notation is [P_G (psi), Q_L (mL/h)]. (b) Parallelisation of micro-bubble generation in the jetting regime (from [62]). One can see thin gas threads formed by rapid gas/liquid co-flow coming out of capillaries in a tip-streaming manner (Section 2.3). These gas-threads break into micrometric bubbles further downstream.

and depends on the geometry of the pores. This means that for small pore throats, required pressure gradients for reliable foam production can be extremely high. Above this critical pressure gradient (and the associated critical flow rates), foam is generated efficiently with bubble sizes being of the order of the pore sizes, i.e. micrometric. Bubble sizes and gas fraction can be tuned by tuning the overall and the relative flow rates, with the bubble size being roughly inversely proportional to the total flow rate $Q = Q_G + Q_L$ in the porous medium [126]

$$R_B \sim Q^{-1}. \quad (42)$$

An example of this is shown in Fig. 28. Unfortunately, little systematic work has been done at this stage to establish a quantitative link between the porous material, the flow conditions and the final foam properties. In real porous media with microscopic pore sizes, pressures tend to become so high that they lead to frequent film rupture. Hence, an understanding of the global mechanisms needs to take into account coalescence.

An interesting (and for the practitioner important) finding is that there is a wide range of pressure gradients which lead to an unstable, often oscillatory flow, and hence oscillating foam properties. This is shown by the dotted line in Fig. 27a. Researchers associate this with the occurrence of intricate feedback mechanisms within the porous material [122,124]. Fig. 27b shows how the transition between the weak and the strong foam regime depends on the gas and the liquid flow rate. Anybody looking to generate a homogeneous foam should therefore strive for sufficiently high flow rates in order to be in the "strong foam" regime.

Most considerations of foam generation in porous media take into account individual bubbles only. As in the case of foam generation under shear (Section 3.2.3), researchers have recently been able to show that collective bubble effects may play a non-negligible role in encouraging the break-up of larger bubbles into smaller ones. An illustrative example (from [127]) is shown in Fig. 29, where one can see how the bubble which traverses the bottom of the constriction breaks the bubble which passes at the top, which then breaks the bubble at the bottom. An individual bubble of the same size which traverses this constriction at the same velocity does not break.

3.2.2.3. High-speed foaming through fibre matrices and static mixers. In order to obtain higher foaming rates, scientists use a range of purpose-designed porous-type media through which liquid and gas are co-injected at high velocities (up to several metres per second). In this case, bubble generation profits also from the presence of strong viscous and inertial forces. One class of devices is provided by static mixers (Fig. 30a–c) [129–131] which are purpose-designed such that a rapid flow of the gas and the liquid through the interconnected network of pores leads to an optimised shearing action on the bubbles, and hence to bubble break-up (Section 2.3). These mixers can be driven in the laminar regime, leading typically to bubble sizes of the order of 100 µm (Fig. 30d) with a wide range of gas fractions. Or they can be driven at high flow rates in the turbulent regime, leading to smaller bubble sizes and lower gas fractions. In [130,131], one can find a guideline for such static mixers, linking the type of mixer to be used as a function of the fluid properties and applications foreseen.

Other types of static mixers may include the passage through fine grids of different mesh sizes or through systems like compact steel wool [132] (or similar types of fibrous materials). The advantage of such systems is that they have a reasonably high permeability, despite having a small characteristic length scale which fixes the obtained bubble size. These "mixing units" may be positioned at the entry of a "foam homogeniser" which may simply consist of a very long tube which acts on the pre-foamed systems as discussed in Section 3.2.2.4. Such kind of combinations are often used in "compressed air foam systems", typically know for the generation of fire fighting foams [132,133]. The obtained foams can cover a wide range of bubble sizes (down to some tens of micrometres) and can have a wide range of gas fractions.

3.2.2.4. High rate co-injection in straight tubes. Efficient foaming does not necessarily require complex foaming geometries. Under certain conditions, a simple tube is sufficient. Co-injection of gas and liquid into a straight tube at sufficiently high flow velocities leads to complex patterns of two phase flow (Fig. 31a) [134], many of which generate bubbles and therefore foams, especially in the presence of surfactants. The physics of these processes is highly complex, mixing different types of air entrainment (Section 2.4.4) and bubble break-up. Until recently, this has been studied mostly for engineering purposes where bubble generation needs to be avoided or at least understood to optimise pressure drops and heat flow problems. Researchers have now realised that some of these regimes are extremely efficient foam generators (Fig. 31b and c), providing foams with small bubbles and well-controlled gas fractions [87,132,133,135].

One example consists of the co-injection of gas and foaming solution at constant pressure (or flow rate) into a straight tube of typically millimetric dimensions [87,135] (Fig. 31b). The tube needs to be much longer than its diameter (typically a few hundred times longer than thick) in order for the mechanism to work efficiently. Moreover, the Weber numbers *We* of the flow need to be sufficiently high so that inertial forces play a role in the foaming process. Upon choosing the right flow conditions, foams can be obtained with very small bubble sizes (order of 10 µm) (Fig. 31d), at very high production rates (litres per second) and over nearly the entire range of gas fractions.

Smaller quantities of foams, but with a very precise control over the gas fraction, can be obtained using the "Double-Syringe technique" (Fig. 31c) [87,161]. This uses a similar mechanism as in the previous case, but here two syringes are connected to either side of a short tube in order to push the two-phase mixture back and forth through the tube. At the outset, one syringe contains the gas, while the other one contains the foaming liquid. Both mix efficiently after a few cycles, giving rise to foams with very small bubbles (around 10 µm) and with

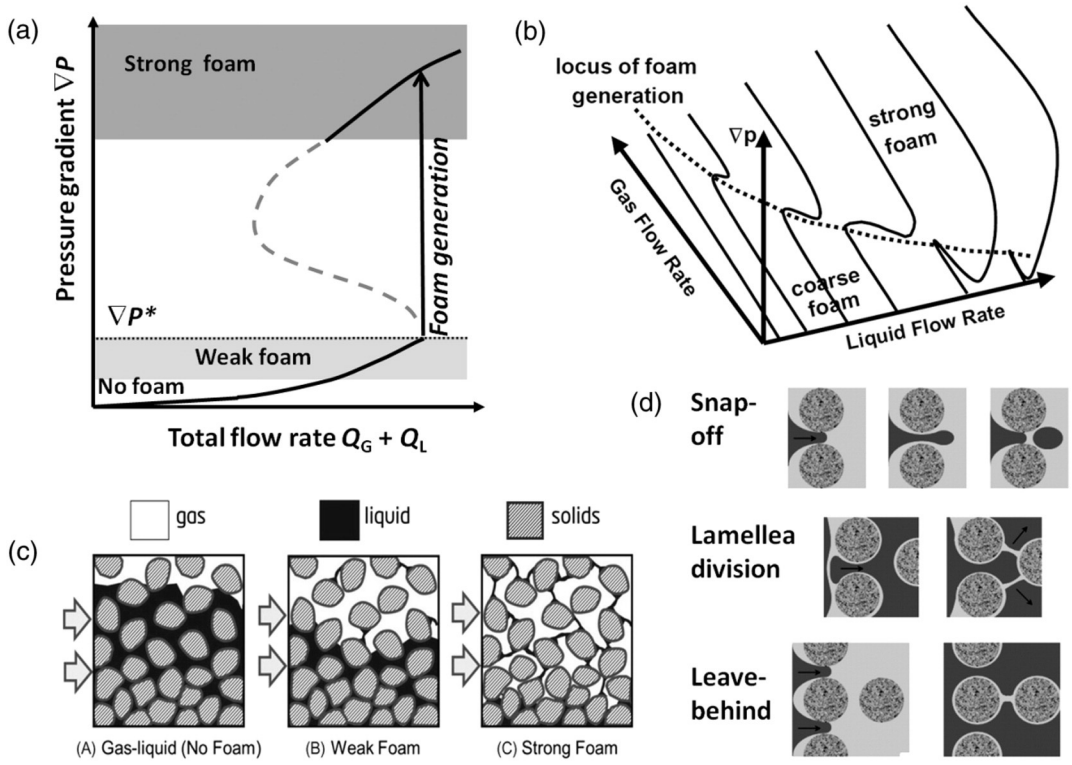

Fig. 27. Foam generation in porous media in the low velocity limit. (a) Sketch of the variation of the pressure gradient across the porous material as a function of the total flow rate (inspired by [124]) showing the different foaming regimes. (b) 3D-illustration of (a) considering the gas and liquid flow rate independently (from [124]). (c) Different flow scenarios encountered in the porous material (from [122]). (d) The three main mechanisms responsible for foam generation (from [127], adapted from [120]).

extremely well-controlled gas fractions (Fig. 31e). Obtained bubble size distributions are similar to those obtained in the continuous flow. Most interestingly, as can be seen in Fig. 31e, they are independent of the final liquid fraction of the foam [87].

3.2.3. Gas entrainment at free surfaces and bubble break-up under shear

3.2.3.1. Breaking waves and hydraulic jumps. As discussed in Section 2.4.4, gas entrainment is mostly associated with high fluid velocity and/or under abrupt variations of the velocity field of the flow. This occurs in many natural processes, a well-known example being that of cascades. It is also at the origin of foaming at the shore break on the sea [13,80] or at hydraulic jumps. In these processes, many of the basic situations described in Section 2.4.4 may simultaneously occur, and any understanding of such complex flows relies on how far it can be described by combining the elementary mechanisms. Researchers have developed a number of lab-scale prototypes in an attempt to simplify the complexity of the processes [80,136].

In the case of *foam generation by wave breaking*, as shown in Fig. 32b, a full description of how exactly the waves trap the surrounding air has not yet been obtained. Nevertheless, the main time-sequences of the phenomenology are known and summarised in Fig. 32a [80]. First, a major part of air entrainment occurs as the plunging wave hits its front face (Fig. 32a — image A). This is the most studied and understood mode of entrainment (Section 2.4.4), as one might expect to link it to the physics of a plunging jet configuration (Section 3.2.3.2). However, it significantly differs from the prototypal scenario discussed in Section 2.4.4 since the impacting jet is not continuous, its geometry is much more complex (with angles of impact changing with time) and the liquid receiving the impact undergoes itself a complex flow (parallel to the surface and moving upslope). With such complexity, simulations have been a powerful source to provide some preliminary insights of how much air can be entrainment by this first impact of the wave (see references in [80]). Then, there are several post-jet impact entrainment modes, all mostly linked to the splash of the first impact. This is schematised in Fig. 32a — images B and C where subsequent impacts of the forward and backward splashes entrapped some air. Lastly, some turbulent entrainments occur all over the various subsequent splashes, and at the leading edge of the turbulent region (Fig. 32a — image D). Going much beyond a phenomenological description of this process is rendered challenging also because the breaking wave situation corresponds to flows of low-viscosity fluids, which adds further complexity (disturbances, instabilities) as discussed before for the basic plunging jet configuration (see Section 2.4.4).

Let us mention that while a plunging wave is a reasonably efficient mean to incorporate large amounts of air into water (as

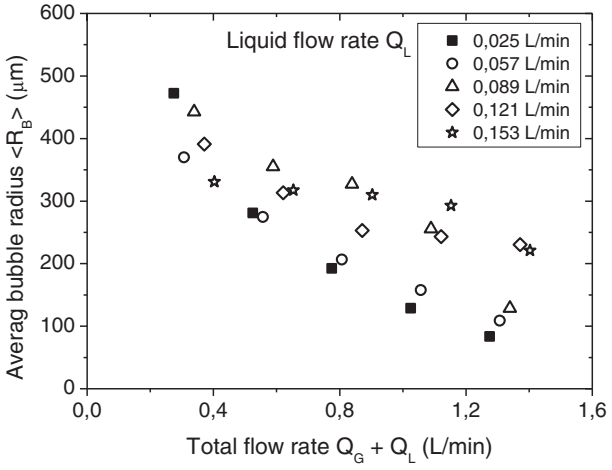

Fig. 28. Dependence of average bubble radius of foam generated by co-flow of gas and liquid through a porous medium generated by closely packing 2 mm glass spheres. Data courtesy of R.-M. Guillermic, pre-work to [128].

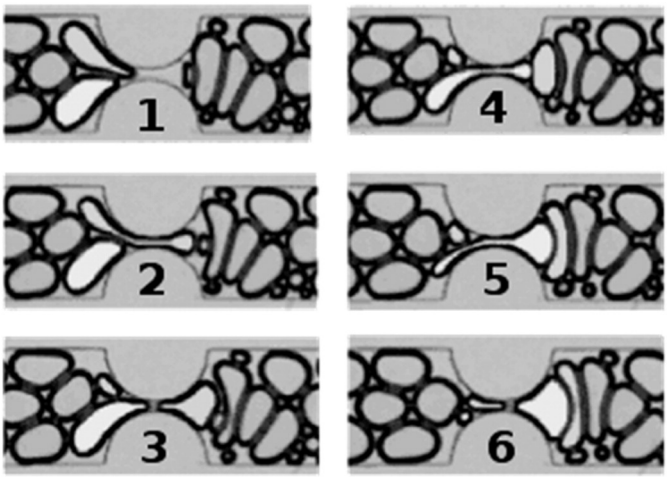

Fig. 29. Bubble–bubble interactions may play an important role in bubble break-up. Here it can be seen that the bubble passing through the bottom of the constriction breaks the one passing on the top, which then breaks the one on the bottom.
From [127].

everyone can experience while looking at the shore break on a beach), it has not (yet) been transformed into a dedicated foaming device.

Gas entrainments within hydraulic jumps (Fig. 17c) belong to the same family of self-aerated situations, where air is incorporated as a consequence of rapidly flowing jets associated to strong free-surface deformations. It is clear that not all hydraulic jumps provide air entrainment. Usual jumps in a sink give no signs of foaming or bubbling. However, if one increases the velocity of the impacting jet, one can start to see the first bubbles entrained in the fluid, originating at the jump where the fluid thickness abruptly varies, as shown in Fig. 32c. In fact, it is only for high enough Froude number *Fr* (typically $Fr > 3$) that air is entrained [137], and this can become an efficient foaming mechanism, as seen in Fig. 32d. Experiments show that in order to obtain significant air entrainment, a large turbulent shear region — usually called a 'roller' — needs to be formed. This roller is located at the top of the thick fluid region, as shown in the scheme of Fig. 32c [137]. The gas is then entrained at the toe of this high shear region, characterised by intensive turbulence. The length of this roller is directly related to the Froude number (see references in [137]). Similarly, the amount of gas entrained also increases with the Froude number. However, there are still no clear models unambiguously describing this effect, and only phenomenological laws are proposed which lack satisfying agreement with experimental data. In fact, the geometry of the experimental setup plays a role, as well as the amount of pre-entrained gas in the impacting jet.

Even though the entrainment conditions by both mechanisms, wave breaking and hydraulic jumps, have been investigated intensively in the past, what is lacking almost entirely at this stage are thorough investigations into the obtained bubble size distributions, which would be important for foaming applications.

3.2.3.2. Plunging jets and foaming hoses. One foaming technique which makes systematic use of air entrainment and bubble break-up under shear by a plunging jet (Section 2.4.4) in a controlled manner has been turned into a standardised test method: the Ross–Miles test [138]. The historic set-up is shown in Fig. 33a with some typical example curves (Fig. 33b) and images of the entrainment process (Fig. 33c). This foaming test belongs to the ASTM databank of test methods (identified under the number ASTMD1173-53(2001)). In practice, 50 ml of the solution is placed in a cylinder. Using a pipette and a funnel fixed at a height of 90 cm, 200 ml of the same solution is allowed to fall into the cylinder. As soon as all of 200 ml solution has fallen, the foam height is recorded. Note that if the impact is initially on the liquid layer, this is no longer the case once the few first layers of bubbles are created. During the process, bubbles might also be destroyed (or not) by the falling liquid, thus mixing foaming and stability issues at the same time. Foams produced with this technique can be highly monodisperse or highly polydisperse, with polydispersity increasing with impact velocity of the jet. Average bubble sizes tend to be of the order of a few hundred micrometres all the way up to a few millimetres. Foam production rates are low, of the order of 1 L/min. The initially obtained gas fractions are very low and generally increase by gravity-driven drainage of the fluid as the foam accumulates at the liquid surface. The most popular use of this foaming technique is probably that of filling our bathtub with foam.

Other techniques have been developed to use air entrainment in a more systematic and controlled manner for foam generation. This air entrainment may happen at the outlet of nozzles (Fig. 34a) or at specifically designed cross-sections of Venturi-type nozzles, in which the fluid flow creates an underpressure and therefore entrains surrounding air (Fig. 34b). With this approach, low to intermediate gas fractions can be obtained. In order to increase the gas fraction of the foam, air needs to be injected actively. This can be done using compressed air (Fig. 34d) or a propeller system (Fig. 34d–g). In the latter case, an air/water mixture is projected at high speed onto a fine mesh. This generates a mixture of bubble blowing/air entrainment through the mesh and bubble break-up by shear. Foam production rates can reach more than a cubic metre per minute. However, bubble sizes tend to be millimetric in this case, giving rise to a reasonably coarse foam.

3.2.3.3. Breakup under active shear. In order to obtain smaller bubbles, a wide range of foaming devices has been developed by engineers which use more actively the fundamental mechanisms of bubble break-up

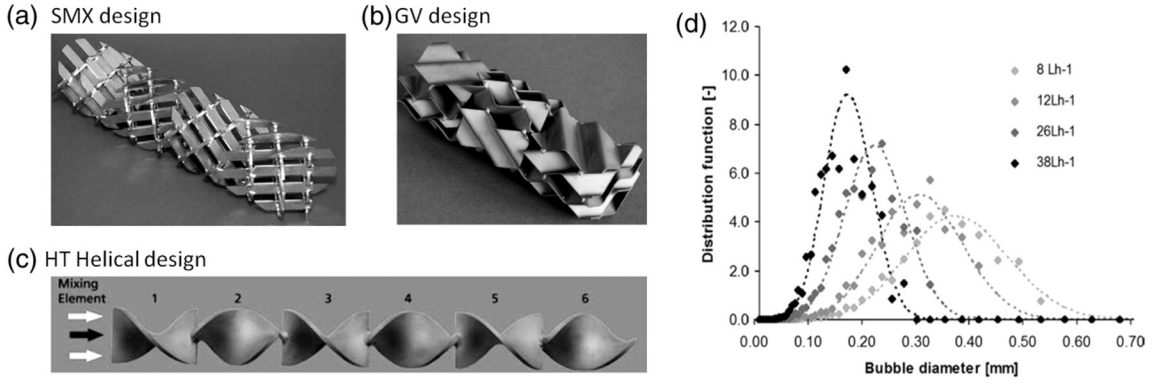

Fig. 30. High speed co-flow of gas and liquid through purpose-designed static mixers generates efficiently foams. (a–c) Examples of static mixer geometries. (d) Typical bubble size distributions obtained in a static mixer for different total flow rates at constant gas fraction ($\Phi = 0.92$) (from [130]).

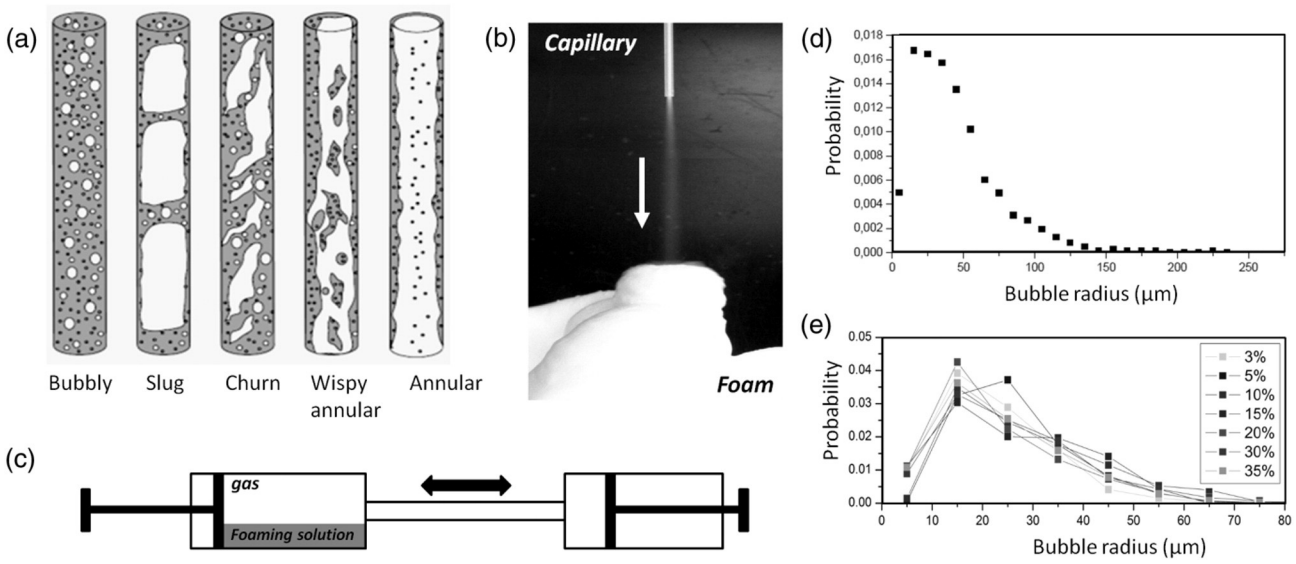

Fig. 31. (a) Typical two-phase flow patterns in straight tubes with increasing ratio of gas to liquid flow rate. Some of these regimes can be used to generate foams at high production rates and with small bubble sizes. One example is the continuous flow in a simple capillary (or larger tube) shown in (b), a second example pushes the gas/liquid mixtures repeatedly back and forth through a tube using a double syringe shown in (c). Both techniques provide access to a wide range of gas fractions and to extremely small bubble sizes. Examples of size distributions are shown in (d) for the straight tube and in (e) for the double syringe.
Panels b–e from. [87]

under shear described in Section 2.4.3. In these devices, the foaming fluid and the gas are drastically and heterogeneously sheared in order to efficiently create a foam with sub-millimetric bubbles. The main issue in designing and optimising such devices is not only to obtain the desired foam in terms of bubble size and gas fraction, but also to ensure that the device is efficient (rapid foaming at low power consumption).

One highly popular foaming device which is based on air entrainment and systematic bubble-breakup under shear is certainly known to most of the readers: the kitchen blender. In this device, air is entrained at the free surface of the blended liquid (Section 2.4.4), which creates large bubbles, which are then broken under the continuous shearing action of the blender. The interaction between air entrainment and bubble break-up leads to a gradual increase of the gas fraction (as shown in Fig. 35a) and a decrease of the average bubble size over time — this is noticed by the user as the foam becomes increasingly white and solid-like. This process happens until an equilibrium state is reached, whose characteristic gas fraction and bubble size depend on the rheological properties of the liquid and the rotating velocity of the blender. As a rule of thumb, the higher the viscosity of the liquid, the smaller the bubbles and the lower the gas fraction which can be obtained (Fig. 35b). Depending on the beating time and the beating speed, obtained bubble sizes can range between some tens of micrometres and a few millimetres. Extreme shearing conditions and unusual foam formulations may lead to sub-micron bubble sizes [139]. As can be seen

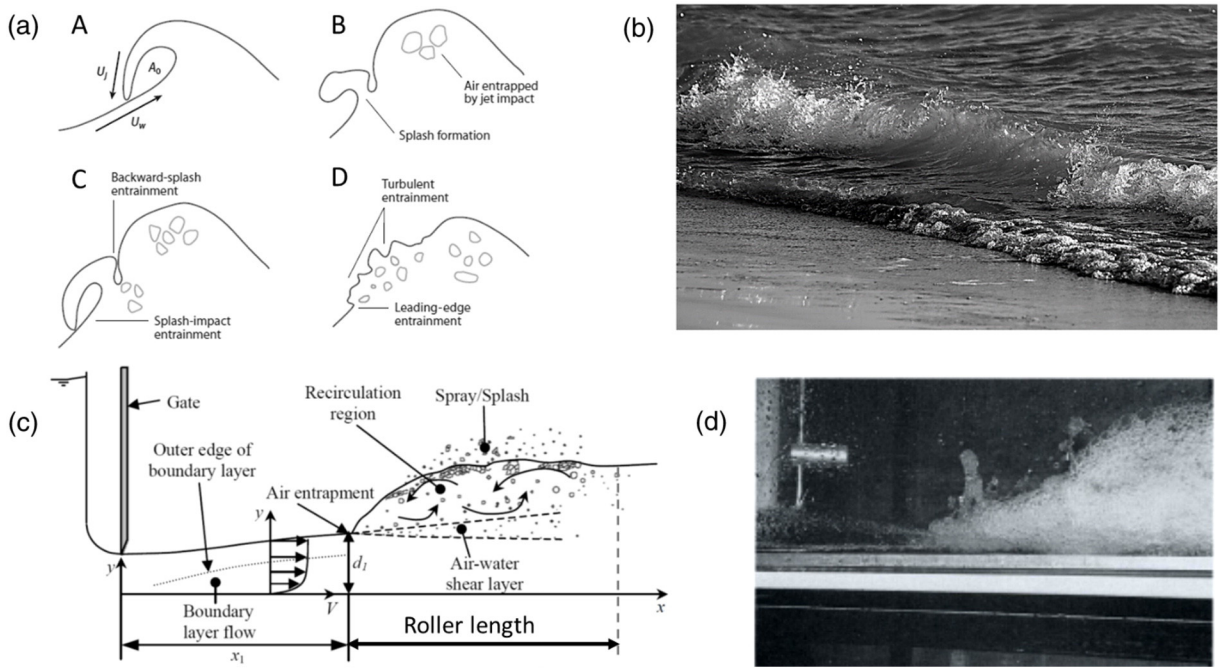

Fig. 32. (a) Scheme (from [80]) and (b) photograph of air entrainment by wave breaking. (c) Scheme and (d) photograph of air entrainment at a hydraulic jump (both from [13]).

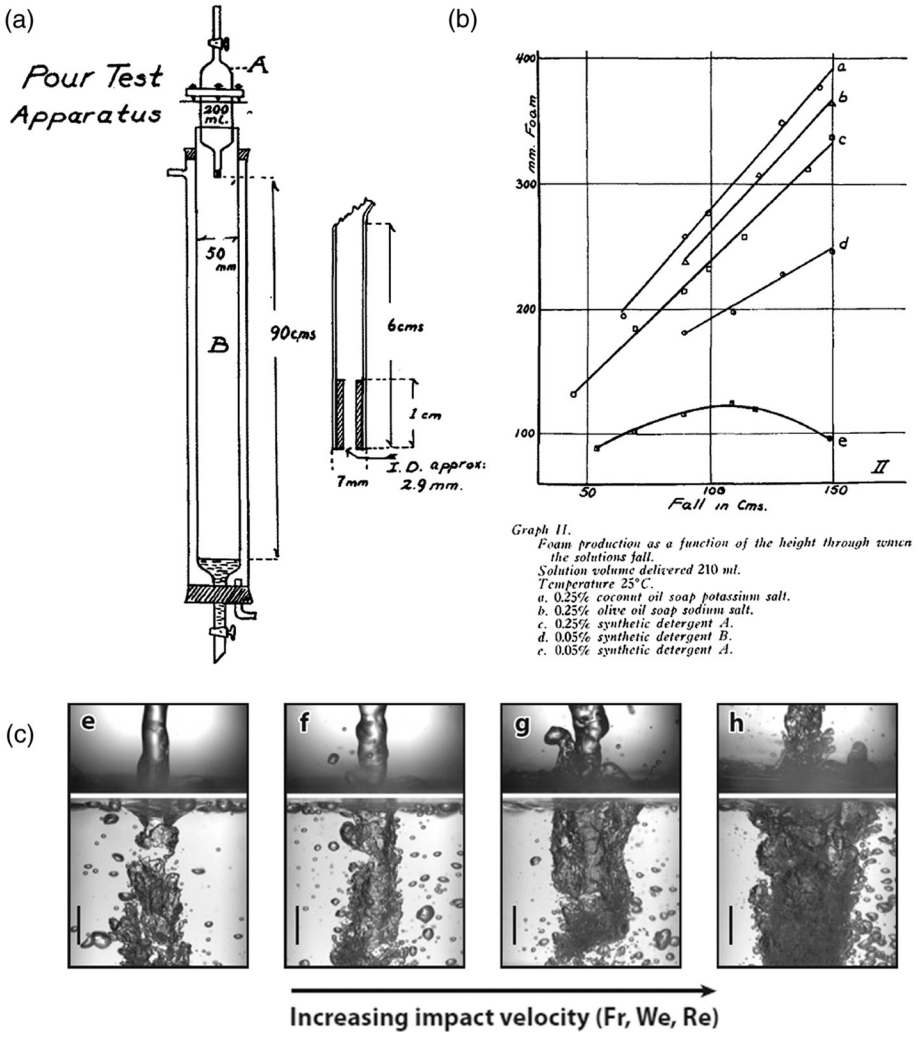

Fig. 33. Foam generation by a plunging jet. (a) The historic Ross–Miles test which lets a foaming solution of defined volume drop into the same solution from a well-defined height and measures the obtained foam height (from [138]). (b) Examples of the evolution of foam height with height over which the solutions fall (from [138]). (c) Images of plunging jets and the accompanying bubble generation with increasing impact velocity (from [80]).

in Fig. 35a, the initial foaming rate in the case of low-viscosity liquids can be quite rapid (about 1 L/min), but the final bubble break-up may take much longer. The main issue with the kitchen blender for larger scale applications is the fact that it is a non-continuous process.

In order to obtain continuity and a more explicit control over the air input (rather than relying on passive air entrainment) and the shearing process, a number of advanced blenders have been developed in the past. A first class of devices are rotor–stator mixers (Fig. 36a–d) which consist of a set of narrowly-spaced static "stators" and rapidly rotating "rotors" through which the foaming solution and the gas are pressed simultaneously. A large body of literature deals with the optimal design of the rotor/stator as a function of the fluids to be sheared [141–143]. In this context, the Newton number (*Ne*) (defined as the ratio between the mechanical driving force and the inertial force) is often used to describe the device behaviour [141–143].

In these devices one finds that the mechanical energy input is the most influential parameter which controls the properties of the obtained foam. It is a function of the rotor speed, the fluid viscosity and the time which the gas/liquid mixture spends in the device [142–145]. The widely-used "Ultra-Turrax®" (Fig. 36e) belongs to this category of rotor–stator mixers, with the specialty that it typically contains only one rotor–stator pair. Bubble sizes obtained in these kind of devices can be very small, down to the order of a few micrometres, with reasonably high foam production rates.

Another class of devices is based on the "Narrow Annular Gap Unit" shown in Fig. 37a and b. In these devices, gas and liquid are generally pre-mixed using a porous plate (Section 3.2.1.3). This pre-foam is then injected between the impellers. Souidi et al. [79] could show that one of the main mechanisms of bubble generation in this device appears to be "tip streaming" (as discussed in Section 2.3 and shown in Fig. 15) which leads to very small bubble sizes of the order of 10 μm (Fig. 37c). The main advantage is that this device requires much lower rotation speeds (lower energy input) than the more classic rotor–stator devices [79,146].

Beside engineering issues concerning the design of such kind of mixers, one has to be aware of the effect of bubble "cooperativity", as already mentioned in the introduction. As the bubbles begin to be closely packed they cannot be considered any more as isolated objects (as done in Section 2). The effect of the gas volume fraction has been investigated in controlled model experiments using a shear rheometer [17,147,148] (Fig. 38a). The authors evidence different break-up regimes. In particular, as in the case of cooperative bubble breakup in constrictions (Fig. 29), they realised that bubble–bubble interaction becomes important and leads to critical capillary numbers well below those of an isolated bubble/drop (Fig. 38b). The authors explain this enhanced instability by a "microstructure-induced" instability which leads to a pinch-off of an elongated bubble by its neighbours (Fig. 38c) and to a *critical stress* which needs to be obtained in the foam (rather than a critical capillary number) [149].

Please cite this article as: Drenckhan W, Saint-Jalmes A, The science of foaming, Adv Colloid Interface Sci (2015), http://dx.doi.org/10.1016/j.cis.2015.04.001

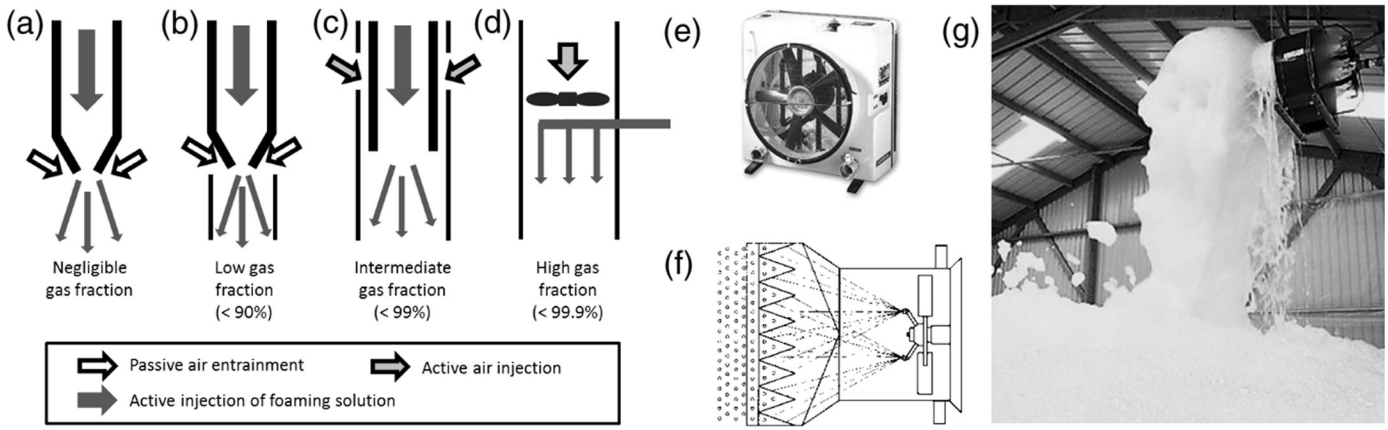

Fig. 34. Controlled air entrainment for foam generation: Air can be entrained by the liquid flow (Ventouri-type effect) (b, c), leading to low and intermediate gas fractions. (c–g) Gas fractions can be increased significantly by actively injecting air, for example through the use of a propeller system. The air/water mixture is then propelled onto a grid, where strong shear forces turn the water droplets into air bubbles. (e–f) Jet-X from ASUL. (g) ALPHA HF+ de LEADER in action with up to 1000 L of foam/min.

3.2.3.4. Foaming by shaking. One of the simplest techniques to foam a solution consists of shaking a closed container which is partially filled with the solution. If this is done in a controlled manner, the container is shaken at specific frequency, amplitude and for a controlled duration. The foamability of the solution is then determined by the amount of foam created, and the bubble size can also be monitored as a function of the shaking parameters. This is often referred to as the "Bartsch test". In the "Bartsch test" the shaking is performed by a controlled flipping of the cell at controlled (and variable) frequency. Note that this shaking can also be done by hand, and this usually provides a good and cheap estimation of the foamabilities of various solutions.

Foam generation by shaking mixes about all the different mechanical foaming effects which we have discussed until now and is therefore difficult to describe quantitatively. To disentangle the different effects, more simple experiments have been developed. Flat cells were used by Caps et al. [150,151], in association with a rotation setup providing consecutive upside-down flips of the cell. As shown in Fig. 39a, the cells are so flat that they generate a quasi-2D foam, i.e. only monolayers of bubbles. This configuration allows us to visualise all the bubbles, as a function of the number of flips (Fig. 39b). A sequence of images of the obtained foams with increasing number of flips n_f is shown in Fig. 39a, showing how the bubble size (and hence the number of bubbles N) decreased systematically with the number of flips. These experiments and further analysis of this setup [150–152] finally demonstrate that, thanks to these series of successive flips of the flat cell, a spatially homogeneous foam can be produced. Moreover, the bubble size distribution eventually saturates with a Gamma distribution. The obtained average bubble size depends on the initial amount of liquid and can be linked to the capillary length of the foaming solution.

3.3. Foaming through phase transitions and by electro-chemistry

3.3.1. Nucleation and growth of bubbles in supersaturated liquids

The great classics which make use of bubble generation through nucleation and growth of bubbles in a supersaturated liquid are known to most of us from the beverage industry: cola, champagne or beer foams. In most cases, the supersaturated gas is CO_2 due to its high solubility in water. The supersaturation is either achieved by explicitly applying high pressures when filling and closing the bottles (fizzy drinks), or it arises naturally as a result of the fermentation process (champagne, beer). In most of these cases, researchers have been able to show that bubbles are generated by heterogeneous nucleation (types III and IV) at the wall or at impurities (Section 2.5) [11,153]. As is obvious to the careful observer, continuous bubble streams nucleate from individual nucleation sites, as is shown in Fig. 40a. Thanks to this effect, supersaturation in these beverages can be kept low and is typically of the order of 5–10 only. A champagne bottle, for example, is typically at a pressure of 5–10 bar and releases around 5 L of CO_2 to enhance our pleasure.

Similar phenomena are used in cosmetic or other food products. A classic example is the whipped cream dispenser which decorates some kitchens (Fig. 40c). In this case, it is the 'laughing gas' (nitrous oxide) which is dissolved under high pressure and then released to create the bubbles in the cream.

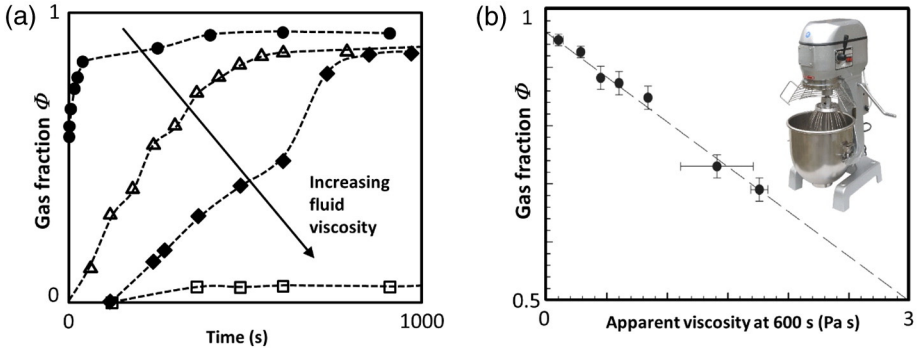

Fig. 35. Foaming with a kitchen blender (all data from [140]). (a) Change of air volume fraction with time for different foaming mixtures containing particles. The variation of the ratio between the surfactant concentration CS and the particle concentration CP leads essentially to a variation in the bulk viscosity of the liquid. (b) Linear decrease of the maximum obtained air volume fraction with the viscosity of the foamed liquid.

Please cite this article as: Drenckhan W, Saint-Jalmes A, The science of foaming, Adv Colloid Interface Sci (2015), http://dx.doi.org/10.1016/j.cis.2015.04.001

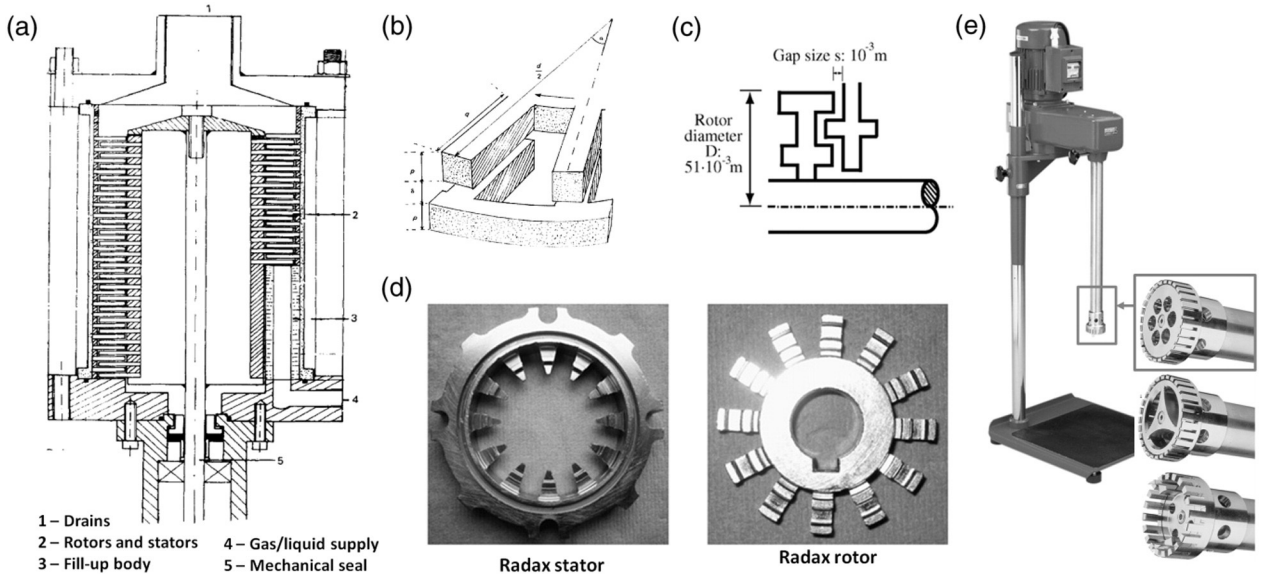

Fig. 36. A classic amongst the foaming devices: the rotor–stator mixer. (a) Overall sketch of the device containing the rotating "rotor" and the static "stator" (from [141]) (b) Side-view (from [141]) and (c) top view (from [70]) of an elementary unit of a rotor–stator mixer. (d) Photographs of a typical stator and rotor (from [70]). (e) The "Ultra-Turrax®" — a widely used rotor–stator device containing only one rotor/stator pair.

In order to foam highly viscous liquids and large quantities, one often uses classic extruder screws (Fig. 40b) to exert high pressures on the foaming liquid. This is also the method of choice in order to foam thermosensitive polymers, which are mixed with the gas at high temperatures under high pressures, to give a rapid foaming (and simultaneous solidification) as the liquid is released to ambient pressure.

3.3.2. Cavitation and boiling

As far as we know, foaming through boiling is currently little used in a systematic manner. It is rather known to most of us as an unpleasant surprise when the soup or the milk are left unwatched a little too long on the stove. The only systematic use known to us is that of gels which foam when in contact with the skin. These gels contain substances (for example isopentane) which are liquid at room temperature, but gaseous at body temperature. Hence, the contact with the skin (shaving gels, tooth pastes, etc.) makes these gels foam. Shearing the gel on the skin helps to break the micro-structure and to get the nucleation process going.

A similar foaming system is found in three-phase aerosol cans, the most classic being shaving foam cans. In this case the phase transition is driven by a pressure change, rather than a temperature change. The overall system consists of two immiscible liquids creating an emulsion under pressure (see bottom of Figs. 2 and 40d, B). The dispersed phase is a liquid of low vapour pressure (most commonly butan/propan mixtures) which remains liquid under the pressure conditions of the containing vessel. Once the pressure is released, the dispersed liquid changes phase and the entire emulsion droplet turns into a gas bubble. The final bubble size is therefore determined by the initial droplet volume [154]. This is why it is recommended to shake the can before use in order to re-emulsify the mixture. Bubble sizes in these applications are typically around 50 μm.

An increasingly popular foaming technique employs cavitation (Section 2.5). This is of particular interest when foams with micron-

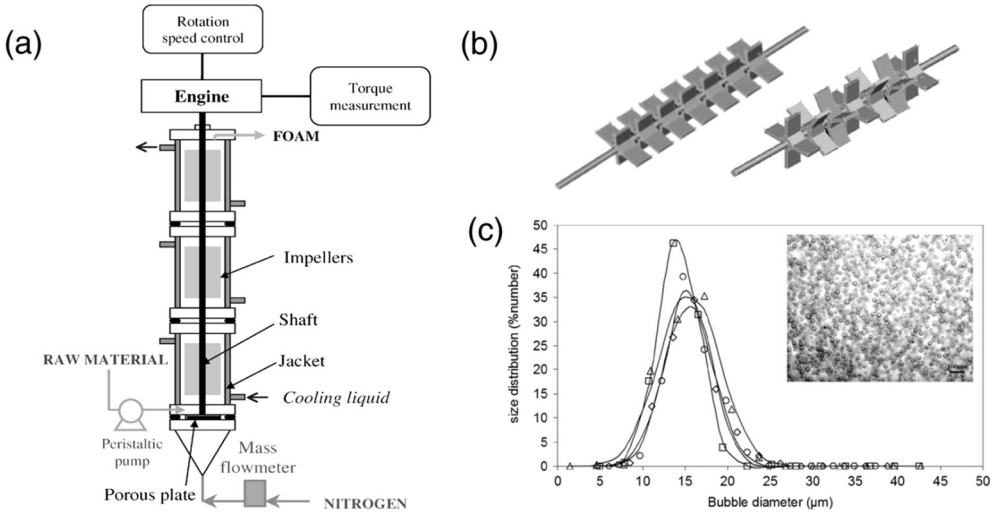

Fig. 37. The Narrow Annular Gap Unit (NAGU). (a) Overall device configuration (from [146]). (b) Examples of propellers used for the shearing action (from [79]). (c) Examples of bubble size distributions obtained for different propeller geometries (rotation speed: 1600 rpm, $Q_G = 10$ mL/min, $G_L = 30$ mL/min) (from [79]).

Please cite this article as: Drenckhan W, Saint-Jalmes A, The science of foaming, Adv Colloid Interface Sci (2015), http://dx.doi.org/10.1016/j.cis.2015.04.001

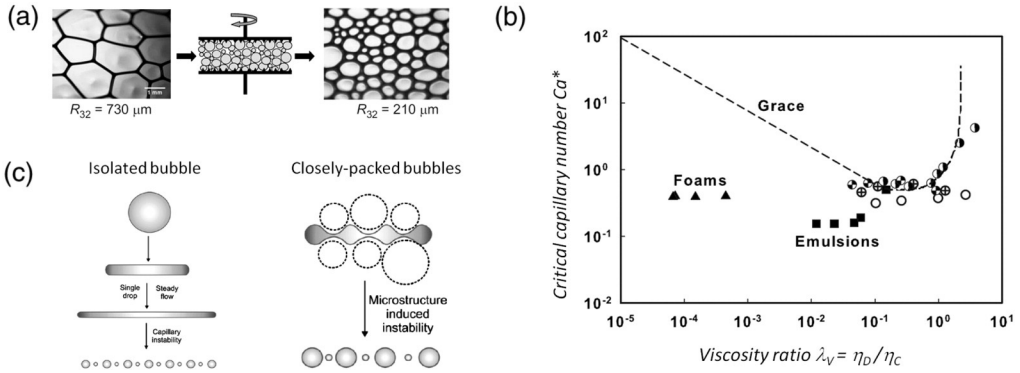

Fig. 38. (a) Break-up of bubbles under shear in a foam with closely packed bubbles (from [149]), which occurs at capillary numbers well below those of isolated bubbles (b) from [149]. (b) Comparison between the critical capillary number required for break-up of individual droplets ("Grace curve" Section 2) and associated data (circles) and between densely packed bubbles ("Foams") and droplets ("Emulsions") (c) Proposed reasoning for the earlier break-up of bubbles in the presence of neighbouring bubbles: a micro-structure induced instability (from [149]).

sized bubble are desired. Historically, such kinds of bubbles were generated using acoustic pressure fields (sonication). However, since the production rates are too low, hydrodynamic cavitation is making its way into foaming devices [155,156]. Different devices exist to use a rapid flow of the foaming liquid in a manner that a sudden, strong pressure drop occurs which leads to the generation of cavitation bubbles. The most popular scenario consists of rapid flow through a constriction, leading to a pressure drop just behind the constriction. Special care needs to be taken to render these bubbles stable as they are swept away with the flow. A certain degree of supersaturation with another gas helps. The most important ingredients are stabilising agents [156].

3.3.3. Foaming by electrolysis

An electro-chemical way of producing gas bubbles is provided by electrolysis. For this purpose, a voltage is applied across two electrodes placed within the same water reservoir (Fig. 41a), turning one of the electrodes into a cathode (negatively charged) and one into an anode (positively charged). Since water molecules decay and recombine permanently ($2H_2O \leftrightarrow 2\,H^+ + 2OH^-$), the resulting H^+ protons will combine with electrons from the cathode to form hydrogen gas (H_2), while the OH^- ions will liberate electrons at the anode to form water and oxygen:

$$\begin{aligned} &\text{Cathode}: \quad 4H^+ + 4e^- \leftrightarrow 2H_2 \\ &\text{Anode}: \quad 4OH^- \leftrightarrow 2H_2O + O_2 + 4e^-. \end{aligned} \tag{43}$$

Hence, hydrogen bubbles are created at the cathode, while oxygen bubbles are created at the anode. In both cases, the bubbles are blown at the surface of the electrode, meaning that either gravity or an external flow needs to detach them from the site where they grow [162]. The bubble size is therefore controlled by the same mechanisms discussed in Sections 2.4.1 and 2.4.2, the key difference being that the gas is blown by an electro-chemical reaction. A second key difference is that the blowing sites occur generally on small defects on the electrode surface. The bubbles are therefore only weekly attached to the surface (as if they were blown from a tiny orifice) and the resulting bubble sizes are therefore of at least an order of magnitude smaller than bubbles blown from orifices (typically some tens of micrometres, as shown in Fig. 41b [157]). Since the number of bubbling sites can be very high on an electrode, this is an efficient technique to produce reasonable quantities of foams with tiny bubbles. For this reason, one of the main applications of this foaming technique is electro-flotation. Flotation efficiency increases with decreasing bubble size since the total interfacial area is inversely proportional to the bubble size. A typical flotation cell is shown in Fig. 41c [157]. A common use is that of waste water treatment or mineral flotation (on small scales). The number of sites and the bubble size can be varied by tuning the current density (Fig. 41b), which is convenient for applications.

Particular control and even the generation of highly monodisperse bubbles can be obtained by working with strongly pointed electrodes which can produce micron-sized bubbles (Figure 41c from [158]). As usual, this gain in control needs to be paid by a strongly reduced production rate.

The key constraint for applications of bubble and foam formation by electrolysis is the restricted choice of gases which can be produced. This is commonly oxygen or hydrogen, which restricts quite significantly their field of use.

3.4. Conclusions and outlook

We hope that this review shows that there are many ways of incorporating bubbles into a liquid phase. We have concentrated here on

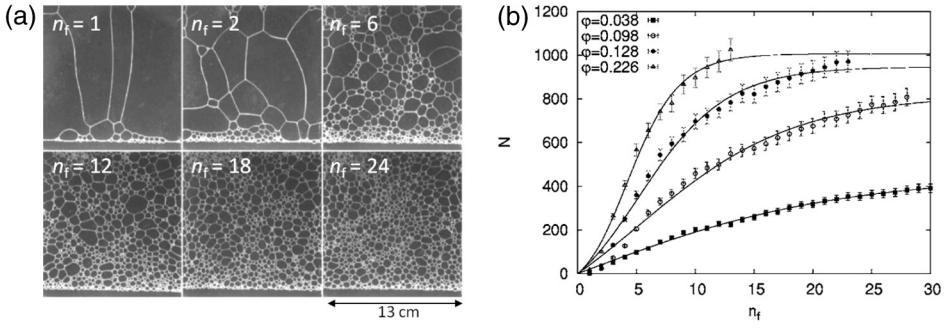

Fig. 39. Foaming by flipping a shallow cell (adapted from [150]). (a) Consecutive images of the foam in the cell after $nf = 1, 2, 6, 12, 18$, and 24 flips. (b) Evolution of number of bubbles with number of flips for different contents of liquid (φ) in the cell.

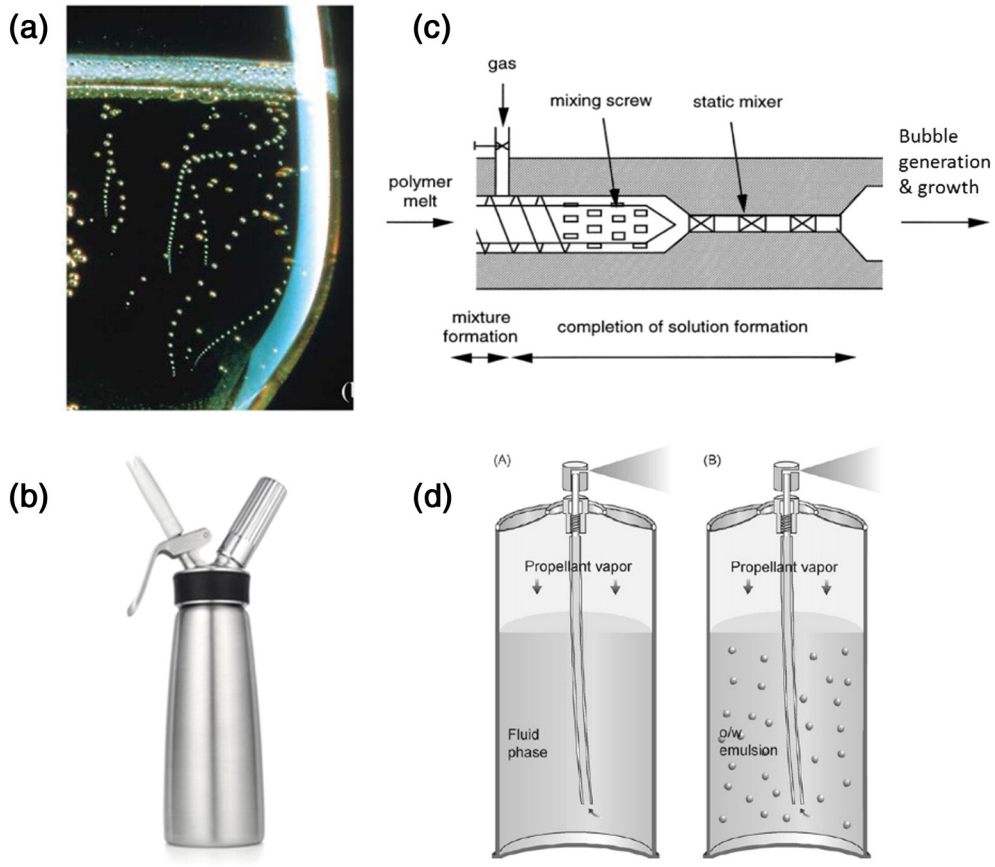

Fig. 40. Examples of foam generation via bubble nucleation and growth. (a) Continuous bubble generation and rise at nucleation sites at the wall of a champagne glass (image from [11]). (b) A whipped cream dispenser uses nitrous oxide. (c) A foam extruder is typically used to foam highly viscous liquids bringing the gas (often CO_2) into solution at high pressure. (d) Aerosol cans are typically used for cosmetic applications. The gas can either be in solution (case A) or it can be chosen such that it is an insoluble liquid under the pressure condition in the bottle. In both cases, upon release of the liquid into ambient pressure, the gas comes either out of solution or evaporates (from [154]).

physical effects, but the reader should be aware that a wealth of chemical and biological foaming techniques is also available. It needs to be added that there exists a large number of "natural foaming techniques", where foams occur naturally in nature (on the beach, in waterfalls, etc.) or in industrial processes. In both cases, this natural foam production may pose serious problems. Understanding the mechanisms at their origin can therefore be very helpful to avoid the foam formation.

It is important to keep in mind that for a given fluid any foaming technique leads to a characteristic bubble size distribution, gas fraction and foam production rate (Table 3). The generation of foams with a wide range of these parameters generally requires the application of different foaming techniques.

A wealth of literature is available to capture certain key properties of different foaming techniques. However, at this stage only the most simple configurations are beginning to be explained in a systematic manner — for example bubbling from individual nozzles or bubble breakup under shear. And even in these simple cases, many important questions remain open.

Much more systematic work within a coherent physical framework needs to be done in the future to shed more light on the more complex foaming mechanisms. Such work needs to establish the role of the different dynamic forces. As we hope to have shown in this chapter, a highly appropriate framework for taking into account these different forces is provided by working with dimensionless hydrodynamic numbers, as listed in Table 2. The use of these numbers allows us to group a wide range of observations by the main physical mechanisms of a process.

The physical mechanisms of the bubbling process are generally well reflected by the obtained bubble sizes and size distribution. Due to the difficulty of measuring bubble size distributions in foams, much of this information is lacking in the past literature. Modern characterisation techniques provide a more straightforward access to this information, which should be exploited more heavily in the future. These techniques include light scattering, X-ray and NMR tomography or high speed imaging. The availability of the size distributions should help us to grasp more profoundly the physical mechanisms which control the bubble formation. However, great care needs to be taken in this exercise: obtained bubble sizes and size distributions may depend more on the foam stability than on the foaming technique used! Coalescence and gas exchange [1,3] between bubbles may completely change the size distribution within a few seconds of the life time of the foam. Much of the past literature has therefore mixed measures of foaming and foam stability — which capture very different physical phenomena.

A number of key challenges remain to be tackled in this subject. The first challenge requires to establish a description of foaming which allows us to move away from the dilute limit of individual bubbles in order to take properly into account the many types of bubble interactions which occur in most commonly used foaming techniques. The second challenge is to consider the influence of the complex visco-elastic properties of gas/liquid interfaces which contain stabilising agents. The presence of these agents leads to a number of interfacial stresses which need to be taken into account in a proper dynamic description. First steps into combining the physics of bubble break-up in dense foams and the influence of the interfacial viscoelasticity have been taken by evidencing the importance of a *critical stress* in the foam, rather than a critical capillary number [149]. A final key challenge will be the description of the foaming of liquids with non-Newtonian flow

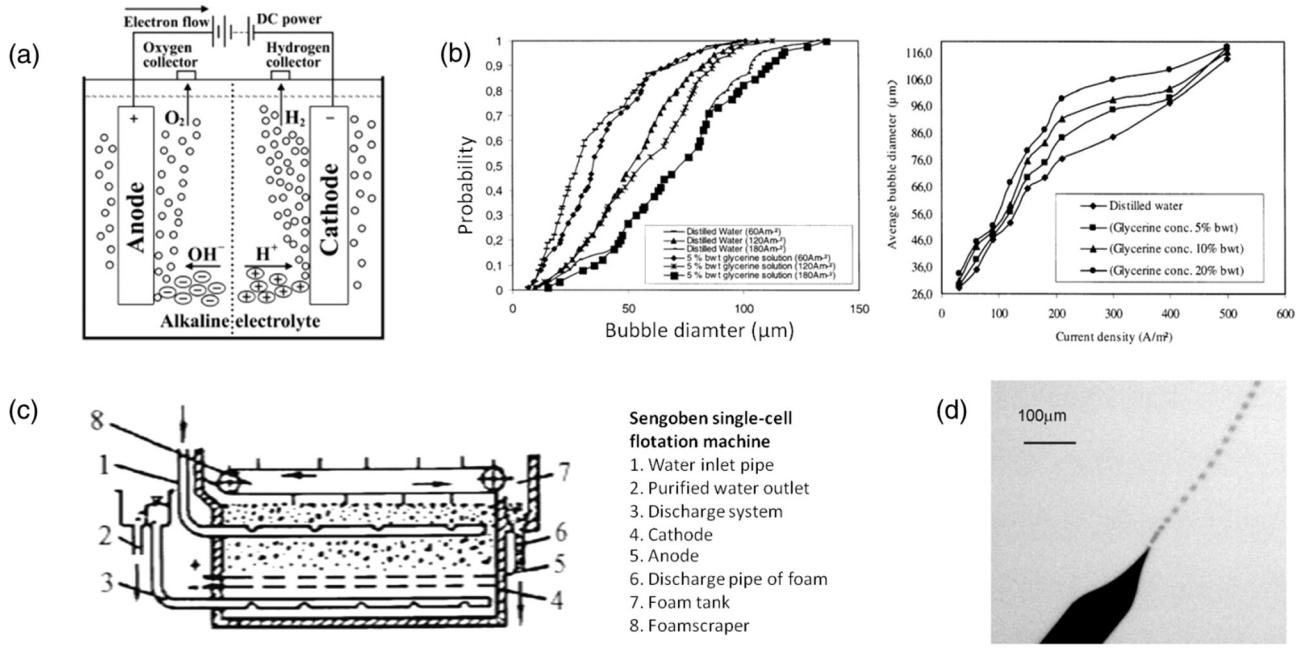

Fig. 41. Bubble and foam generation via electrolysis (a) General concept of the generation of oxygen and hydrogen bubbles at the anode and cathode, respectively. (b) Examples of cumulative bubble size distributions and variation of mean bubble size with current density in an electroflotation cell for different solutions containing glycerine (from [157]) (c) Electroflotation device (from Deryagin Dukhin 1986). (d) Generation of extremely small and monodisperse microbubbles from an electrode tip (from [158]).

properties, which change their flow properties upon deformation and with deformation rate. In fact, many processes require the successful foaming of complex fluids (polymer melts and solutions, particle suspensions, emulsions, etc.).

Of great importance in the future will be to develop foaming techniques which push beyond current limits. The foaming of highly viscous liquids, for example, remains a great challenge due to the important influence of the fluid viscosity on the different flow instabilities. Another boundary to be pushed will also be that of the obtained bubble sizes — especially towards small bubbles and low gas fraction. Low density foams with bubble sizes well below 1 μm have giant surface to volume ratios (1 cm^2 of "nano-foam" can contain the surface of an entire football field!) which is of interest for catalytic reactions. Moreover, thermal conduction is reduced by orders of magnitude, when the bubble size is smaller than the mean free path of the gas molecules (about 0.1 μm for air at room temperature and ambient pressure).

To sum up, decades of considerable engineering work have provided us with a wide range of reliable foaming techniques. The current and future challenge is to be able to arrive at a satisfying description and prediction of the complex foaming processes. On the one hand, this should help to optimise current foaming processes, on the other hand, this should provide us with the possibility to generate controlled foams with a wider range of properties, stimulating new research directions and leading to the emergence of new applications of foams.

Acknowledgements

The authors would like to thank Reinhard Miller for motivating the writing of this article and for his important contributions to research on bubbles. We also thank Bill Rossen, Stubenrauch, Emmanuelle Rio, Dominique Langevin, Nikolai Denkov and Jean-Eric Poirier for very useful comments on this manuscript. W. Drenckhan acknowledges funding from an ERC Starting Grant (agreement 307280-POMCAPS).

References

[1] Weaire D, Hutzler S. The physics of foams. Oxford: Clarendon Press; 1999.
[2] Exerova D, Kruglyakov PM. Foam and foam films; theory, experiment, application, vol. 5. Amsterdam: Elsevier Science B.V.; 1998.
[3] Cantat I, Cohen-Addad S, Elias F, Graner F, Hohler R, Pitois O, et al. Foams — structure and dynamics. In: Cox S, editor. Oxford, UK: Oxford University Press; 2013. p. 300.
[4] Stevenson P. Foam engineering: fundamentals and applications. Chichester, UK: John Wiley & Sons, Ltd; 2012.
[5] Tcholakova S, Denkov ND, Lips A. Comparison of solid particles, globular proteins and surfactants as emulsifiers. Phys Chem Chem Phys 2008;10(12):1608–27.
[6] Hsu S-H, Lee W-H, Yang Y-M, Chang C-H, Maa J-R. Bubble formation at an orifice in surfactant solutions under constant-flow conditions. Ind Eng Chem Res 2000;39:1473–9.
[7] Miller R, Liggieri L. Interfacial rheology. In: Miller R, editor. Progress in colloid and interface science. Boca Raton: CRC Press; 2009.
[8] Chhabra RP. Bubbles, drops, and particles in non-Newtonian fluids. CRC Press; 2007.
[9] Li HZ, Mouline Y, Midoux N. Modelling the bubble formation dynamics in non-Newtonian fluids. Chem Eng Sci 2002;57(3):339–46.
[10] Dietrich N, Mayoufi N, Poncin S, Li HZ. Experimental investigation of bubble and drop formation at submerged orifices. Chem Pap 2013;67(3):313–25.
[11] Liger-Belair G, Polidori G, Jeandet P. Recent advances in the science of champagne bubbles. Chem Soc Rev 2008;37(11):2490–511.
[12] Testouri A, Honorez C, Barillec A, Langevin D, Drenckhan W. Highly structured foams from chitosan gels. Macromolecules 2010;43(14):6166–73.
[13] Chanson H. Air bubble entrainment in free surface turbulent shear flows; 1995.
[14] Stone HA, Bentley BJ, Leal LG. An experimental study of transient effects in the breakup of viscous drops. J Fluid Mech 1986;173:131–58.
[15] De Gennes PG, Brochard-Wyart F, Quere D. Capillarity and wetting phenomena: drops, bubbles, pearls, waves. New York: Springer-Verlag New York Inc.; 2003.
[16] Langevin D. Influence of interfacial rheology on foam and emulsion properties. Adv Colloid Interface Sci 2000;88(1–2):209–22.
[17] Golemanov K, Tcholakova S, Denkov ND, Ananthapadmanabhan KP, Lips A. Breakup of bubbles and drops in steadily sheared foams and concentrated emulsions. Phys Rev E 2008;78(5):051405.
[18] Saulnier L, Boos J, Stubenrauch C, Rio E. Comparison between generations of foams and single vertical films — single and mixed surfactant systems. Soft Matter 2014;10(29):5280–8.
[19] Burton JC, Waldrep R, Taborek P. Scaling and instabilities in bubble pinch-off. Phys Rev Lett 2005;94(18).
[20] Thoroddsen ST, Etoh TG, Takehara K. High-speed imaging of drops and bubbles. Annu Rev Fluid Mech 2008:257–85.
[21] Savart F. Ann Chim 1833;53:337.
[22] Plateau JF. Acad Sci Brux Mem 1843;16:3.
[23] Rayleigh L. Proc. London Math. Soc. 1879;10:4.
[24] Eggers J. non-linear dynamics and breakup of free-surface flows. Rev Mod Phys 1997;69:865–929.
[25] Weber C. Zum zerfall eines flussigkeitsstrahles. ZAMM 1931;11:136.
[26] Driessen T, Jeurissen R, Wijshoff H, Toschi F, Lohse D. Stability of viscous long liquid filaments. Phys Fluids 2013;25:062109.
[27] Son Y, Martys NS, Hagedorn JG, Migler KB. Suppression of capillary instability of a polymeric thread via parallel plate confinement. Macromolecules 2003;36(15):5825–33.

[28] Duclaux V, Clanet C, Quere D. The effects of gravity on the capillary instability in tubes. J Fluid Mech 2006;556:217–26.
[29] Tomotika S. On the instability of a cylindrical thread of a viscous liquid surrounded by another viscous fluid. Proc R Soc Lond A 1935;150:322–37.
[30] Eggers J, Villermaux E. Physics of liquid jets. Rep Prog Phys 2008;71:036601 [79 pp.].
[31] Dollet B, Van Hoeve W, Raven JP, Marmottant P, Versluis M. Role of the channel geometry on the bubble pinch-off in flow-focusing devices. Phys Rev Lett 2008;100(3).
[32] Kumar R, Kulorr NR. The formation of bubbles and drops. Adv Chem Eng 1970;8:228–368.
[33] Kulkarni A, Joshi J. Bubble formation and bubble rise velocity in gas–liquid systems: a review. Ind Eng Chem Res 2005;44(16):5873–931.
[34] Di Bari S, Robinson AJ. Experimental study of gas injected bubble growth from submerged orifices. Exp Therm Fluid Sci 2013;44:124–37.
[35] Elias F, Hutzler S, Ferreira MS. Visualisation of sound waves using regularly spaced soap films. Eur Phys J 2007;28:755.
[36] Gnyloskurenko SW, Byakova AV, Raychenko OI, Nakamura T. Influence of wetting conditions on bubble formation at orifice in an inviscid liquid. Transformation of bubble shape and size. Colloids Surf A 2003;218:73–87.
[37] Lin JN, Banerji SK, Yasuda H. Role of interfacial tension in the formation and the detachment of air bubbles 1. A single hole on a horizontal plane immersed in water. Langmuir 1994;10(3):936–42.
[38] Davidson JF, Schueler BOG. Bubble formation at an orifice in a viscous liquid. Chem Eng Commun 1960;38:335.
[39] Pamerin O, Rath H-J. Influence of buoyancy on bubble formation at submerged orifices. Chem Eng Sci 1995;50(19):3009–24.
[40] Berghmans J. Stability of gas bubbles rising in iviscid fluids. Chem Eng Sci 1973;28:2005–11.
[41] Zhao YF, Irons GA. The breakup of bubbles into jets during submerged gas injection. Metall Trans B 1990;21(6):997–1003.
[42] Jamialahmadi M, Zehtaban MR, Muller-Steinhagen H, Sarrafi A, Smith JM. Study of bubble formation under constant flow conditions. Chem Eng Res Des 2001;79(A5):523–32.
[43] Bragg L, Nye JF. A dynamical model of a crystal structure. Proc R Soc Lond A Math Phys Sci 1947;190(1023):474–81.
[44] Smith CS. On blowing bubbles for Bragg's dynamic crystal model. J Appl Phys 1949;20(6):631.
[45] Martinez CJ. Bubble generation in microfluidic devices. Bubble Sci Eng Technol 2009;1(1–2):40–52.
[46] Christopher GF, Anna SL. Microfluidic methods for generating continuous droplet streams. J Phys D Appl Phys 2007;40:R319–36.
[47] Marmottant P, Raven JP. Microfluidics with foams. Soft Matter 2009;5(18):3385–8.
[48] Garstecki P, Ganan-Calvo AM, Whitesides GM. Formation of bubbles and droplets in microfluidic systems. Bull Pol Acad Sci Tech Sci 2005;53(4):361.
[49] Whitesides GM. The origins and the future of microfluidics. Nature 2006;442(7101):368–73.
[50] Seemann R, Brinkmann M, Pfohl T, Herminghaus S. Droplet based microfluidics. Rep Prog Phys 2012;75(1):016601.
[51] Nunes JK, Tsai SSH, Wan J, Stone HA. Dripping and jetting in microfluidic multiphase flows applied to particle and fibre synthesis. J Phys D Appl Phys 2013;46:114002.
[52] Baroud CN, Gallaire F, Dangla R. Dynamics of microfluidic droplets. Lab Chip 2010;10(16):2032–45.
[53] Raven JP, Marmottant P, Graner F. Dry microfoams: formation and flow in a confined channel. Eur Phys J B 2006;51(1):137–43.
[54] Lorenceau E, Sang YYC, Hoehler R, Cohen-Addad S. A high rate flow-focusing foam generator. Phys Fluids 2006;18(9):097103.
[55] Raven J-P, Marmottant P. Microfluidic crystals: dynamic interplay between rearrangement waves and flow. Phys Rev Lett 2009;102(8):084501.
[56] Hoehler R, Sang YYC, Lorenceau E, Cohen-Addad S. Osmotic pressure and structures of monodisperse ordered foam. Langmuir 2007;24(2):418–25.
[57] Fu T, Ma Y, Funfschilling D, Zhu C, Li HZ. Squeezing-to-dripping transition for bubble formation in a microfluidic T-junction. Chem Eng Sci 2010;65(12):3739–48.
[58] De Menech M, Garstecki P, Jousse F, Stone HA. Transition from squeezing to dripping in a microfluidic T-shaped junction. J Fluid Mech 2008;595(1):141–61.
[59] Utada AS, Fernandez-Nieves A, Stone HA, Weitz DA. Dripping to jetting transitions in coflowing liquid streams. Phys Rev Lett 2007;99:094502.
[60] Guillot P, Ajdari A, Goyon J, Joanicot M, Colin A. Droplets and jets in microfluidic devices. C R Chim 2009;12(1–2):247–57.
[61] Ganan-Calvo AM, Herrada MA, Garstecki P. Bubbling in unbounded coflowing liquids. Phys Rev Lett 2006;96(12):124504.
[62] Marín AG, Campo-Cortés F, Gordillo JM. Generation of micron-sized drops and bubbles through viscous coflows. Colloids Surf A Physicochem Eng Asp 2009;344(1–3):2–7.
[63] Castro-Hernandez E, Van Hoeve W, Lohse D, Gordillo JM. Microbubble generation in a co-flow device operated in a new regime. Lab Chip 2011;11(12):2023–9.
[64] Ganan-Calvo AM. Perfectly monodisperse microbubbling by capillary flow focussing: an alternate physical describtion and universal scaling. Phys Rev E 2004;69(027301).
[65] Garstecki P, Fuerstman MJ, Whitesides GM. Nonlinear dynamics of a flow-focusing bubble generator: an inverted dripping faucet. Phys Rev Lett 2005;94(23):234502.
[66] Hinch EJ, Acrivos A. Steady long slender droplets in two-dimensional straining motion. J Fluid Mech 1979;91:401–14.
[67] Acrivos A. The breakup of small drops and bubbles in shear flows. Ann N Y Acad Sci 1983;404:1–11.
[68] Bentley BJ, Leal LG. An experimental investigation of drop deformation and breakup in steady, two-dimensional linear flows. J Fluid Mech 1986;167:241–83.
[69] Stone HA. Dynamics of drop deformation and breakup in viscous fluids. Annu Rev Fluid Mech 1994;26:65–102.
[70] Muller-Fischer N, Tobler P, Dressler M, Fischer P, Windhab EJ. Single bubble deformation and breakup in simple shear flow. Exp Fluids 2008;45:917–26.
[71] Grace HP. Dispersion phenomena in high viscosity immiscible fluid systems and application of static mixers as dispersion devices in such systems. Chem Eng Commun 1982;14(3:6):225–77.
[72] Stone HA. Dynamics of drop deformation and breakup in viscous fluids. Annu Rev Fluid Mech 1994;26:65–102.
[73] Cristini V, Tan YC. Theory and numerical simulation of droplet dynamics in complex flows — a review. Lab Chip 2004;4(4):257–64.
[74] Lorenceau E, Restagno F, Quere D. Fracture of a viscous liquid. Phys Rev Lett 2003;90(18).
[75] Suryo R, Basaran OA. Tip streaming from a liquid drop forming from a tube in a co-flowing outer fluid. Phys Fluids 2006;18(8) [p. –].
[76] Anna SL, Mayer HC. Microscale tipstreaming in a microfluidic flow focusing device. Phys Fluids 2006;18(12).
[77] Lee W, Walker LM, Anna SL. Competition between viscoelasticity and surfactant dynamics in flow focusing microfluidics. Macromol Mater Eng 2011;296(3–4):203–13.
[78] Baret J-C. Surfactants in droplet-based microfluidics. Lab Chip 2012;12(3):422–33.
[79] Souidi K, Mardaru A, Roudet M, Marcati A, Dellavalle D, Djelveh G. Effect of impellers configuration on the gas dispersion in high-viscosity fluid using narrow annular gap unit. Part 1: experimental approach. Chem Eng Sci 2012;74:287–95.
[80] Kiger KT, Duncan JH. Air-entrainment mechanisms in plunging jets and breaking waves. Annu Rev Fluid Mech 2012;44.
[81] Lorenceau E, Quere D, Eggers J. Air entrainment by a viscous jet plunging into a bath. Phys Rev Lett 2004;93(25).
[82] Charu F, De Forcrand-Millard P. Hydrodynamic instabilities. Cambridge texts in applied mathematics. Cambridge: Cambridge University Press; 2011.
[83] Bremond N, Villermaux E. Bursting thin liquid films. J Fluid Mech 2005;524:121–30.
[84] Villermaux E. Fragmentation. Annu Rev Fluid Mech 2007;39:419–46.
[85] Shinjo J, Umemura A. Simulation of liquid jet primary breakup: dynamics of ligament and droplet formation. Int J Multiph Flow 2010;36:513–32.
[86] Delteil J, Vincent S, Erriguible A, Subra-Paternault P. Numerical investigations in Rayleigh breakup of round liquid jets with VOF methods. Comput Fluids 2011;50:10–23.
[87] Gaillard T, Honorez C, Jumeaux M, Balan A, Roché M, Drenckhan W, unpublished results
[88] Fundamentals of cavitation. In: Franc J-P, Michel J-M, editors. Fluid mechanics and its applications. Kluwer Academic Publisher; 2011.
[89] Brennen CE. Cavitation and bubble dynamics. Oxford: Oxford University Press; 1995.
[90] Jones SF, Evans GM, Galvin KP. Bubble nucleation from gas cavities — a review. Adv Colloid Interface Sci 1999;80(1):27–50.
[91] Lugli F, Zerbetto F. An introduction to bubble dynamics. Phys Chem Chem Phys 2007;9(20):2447–56.
[92] Weaire D, Kermode JP. Computer-simulation of a two-dimensional soap froth. 1. Method and motivation. Philos Mag B 1983;48(3):245–59.
[93] Mosdorf R, Shoji M. Chaos in bubbling—nonlinear analysis and modelling. Chem Eng Sci 2003;58.
[94] Deckwer W-D. Bubble column reactors. Wiley; 1992.
[95] Kantarci N, Borak F, Ulgen KO. Bubble column reactors. Process Biochem 2005;40:2263–83.
[96] Clarke AN. Foam flotation: theory and applications. Chemical industries. Marcel Dekker Inc.; 1983
[97] Stevenson P, Li XL. Foam fractionation: principles and process design. CRC Press; 2014.
[98] Tritton DJ, Egdell C. Chaotic bubbling. Phys Fluids A 1993;5(2):503–5.
[99] Tufaile A, Sartorelli JC. Chaotic behavior in bubble formation dynamics. Physica A 2000;275(3–4):336–46.
[100] Stanovsky P, Ruzicka MC, Martins A, Teixeira JA. Meniscus dynamics in bubble formation: a parametric study. Chem Eng Sci 2011;66:3258–67.
[101] Ruzicka MC, Bunganic R, Drahos J. Meniscus dynamics in bubble formation. Part I: experiment. Chem Eng Res Des 2009;87:1349–56.
[102] Pereira FAC, Colli E, Sartorelli JC. Period adding cascades: experiment and modeling in air bubbling. Chaos 2012;22:013135.
[103] Mosdorf R, Wyszkowski T. Self-organising structure of bubble departures. Int J Heat Mass Transf 2013;61:277–86.
[104] Pereira PAC, Colli E, Sartorelli JC. Synchronization of two bubble trains in a viscous fluid: experiment and numerical simulation. Phys Rev E 2013;87:022917.
[105] Zahradnik J, Kastanek F. Gas holdup in uniformly aerated bubble column reactors. Chem Eng Commun 1979;3:413–29.
[106] Loimer T, Machu G, Schaflinger U. Inviscid bubble formation on porous plates and sieve plates. Chem Eng Sci 2004;59:809–18.
[107] Bowonder B, Kumar R. Studies in bubble formation — IV: bubble formation at porous discs. Chem Eng Sci 1970;25:25–32.
[108] Ruzicka MC, Drahos J, Zahradnik J, Thomas NH. Structure of gas pressure signal at two-orifice bubbling from a common plenum. Chem Eng Sci 2000;55:421–9.
[109] Ruzicka M, Drahos J, Zahradnik J, Thoams NH. Natural modes of multi-orifice bubbling from a common plenum. Chem Eng Sci 1999;54:5223–9.
[110] Xie S, Tan RBH. Bubble formation at multiple orifces — bubbling synchronicity and frequency. Chem Eng Sci 2003;58:4639–47.
[111] Kazakis NA, Mouza AA, Paras SV. Experimental study of bubble formation at metal porous spargers: effect of liquid properties and sparger characteristics on the initial bubble size distribution. Chem Eng J 2008;137(2):265–81.

Please cite this article as: Drenckhan W, Saint-Jalmes A, The science of foaming, Adv Colloid Interface Sci (2015), http://dx.doi.org/10.1016/j.cis.2015.04.001

[112] Mohammed TJ, Hanna FZ, Hamawand IB. Bubble size distribution in gas–liquid dispersion column. J Eng 2012;18(7):799–818.
[113] Stevenson P, Sederman AJ, Mantle MD, Li X, Gladden LF. Measurement of bubble size distribution in a gas–liquid foam using pulsed-field gradient nuclear magnetic resonance. J Colloid Interface Sci 2010;352(1):114–20.
[114] Feitosa K, Halt OL, Kamien RD, Durian DJ. Bubble kinetics in a steady-state column of aqueous foam. Europhys Lett 2006;76(4):683–9.
[115] Hasanen A, Orivuori P, Aittamaa J. Measurements of local bubble size distributions from various flexible membrane diffusers. Chem Eng Process 2006;45:291–302.
[116] Wraith AE, Li R-Q, Harris R. Gas bubble volume at a narrow slot nozzle in a liquid. Chem Eng Sci 1995;50(6):1057–8.
[117] Li R-Q, Wraith AE, Harris R. Gas dispersion phenomena at a narrow slot submerged in a liquid. Chem Eng Sci 1994;49(4):531–40.
[118] Van Dijke KC, Schroën K, Van Der Padt A, Boom R. EDGE emulsification for food-grade dispersions. J Food Eng 2010;97(3):348–54.
[119] Hashimoto M, Shevkoplyas SS, Zasonska B, Szymborski T, Garstecki P, Whitesides GM. Formation of bubbles and droplets in parallel, coupled flow-focusing geometries. Small 2008;4(10):1795–805.
[120] Kovscek AR, Radke CJ. Fundamentals of foams transport in porous media. In: Schramm LL, editor. Foams: fundamentals and applications in the petrolium industry. American Chemical Society; 1994.
[121] Rossen WR. Foams in enhanced oil recovery. In: Prud'homme RK, editor. Foams: theory, measurements, and applications. Marcel Dekker, Inc.; 1996
[122] Lee S, Kam SI. Enhanced oil recovery by using CO_2 foams: fundamentals and field applications. In: Sheng J, editor. Enhanced oil recovery field case studies. Gulf Professional Publishing; 2013.
[123] Schramm LL, Isaacs EE. Foams in enhancing petroleum recovery. In: Stevenson P, editor. Foam engineering: fundamentals and applications. Wiley-Blackwell; 2012.
[124] Gauglitz PA, Friedmann F, Kam SI, Rossen WR. Foam generation in homogeneous porous media. Chem Eng Sci 2002;57(19):4037–52.
[125] Rossen WR. A critical review of roof snap-off as a mechanism of steady-state foam generation in homogeneous porous media. Colloids Surf A Physicochem Eng Asp 2003;225(1–3):1–24.
[126] Friedmann F, Jensen JA. Some parameters influencing the formation and propagation of foams in porous media; 1996.
[127] Liontas R, Ma K, Hirasaki GJ, Biswal SL. Neighbor-induced bubble pinch-off: novel mechanisms of in situ foam generation in microfluidic channels. Soft Matter 2013;9:10971–84.
[128] Guillermic R-M, Volland S, Faure S, Imbert B, Drenckhan W. Shaping complex fluids—how foams stand up for themselves. J Rheol 2013;57:333.
[129] Paglianti A. Recent innovations in turbulent mixing with static elements. Recent Pat Chem Eng 2008;1:80–7.
[130] Talansier E, Dellavalle D, Loisel C, Desrumaux A, Legrand J. Elaboration of controlled structure foams with the SMX static mixer. AIChE J 2013;59:132–45.
[131] Fradette L, Li H-Z, Choplin L, Tanguy P. Gas/liquid dispersions with aSMXstatic mixer in the laminar regime. Chem Eng Sci 2006;61:3506–18.
[132] Gardiner BS, Dlugogorski BZ, Jameson GJ. Rheology of fire-fighting foams. Fire Saf J 1998;31(1):61–75.
[133] Magrabi SA, Dlugogorski BZ, Jameson GJ. Bubble size distribution and coarsening of aqueous foams. Chem Eng Sci 1999;54(18):4007–22.
[134] Cheremisinoff N. Encyclopedia of fluid mechanics: gas–liquid flows. Encyclopedia of fluid mechanics, vol. 3. Gulf Publ. Company; 1536 1536.
[135] Saint-Jalmes A, Vera MU, Durian DJ. Uniform foam production by turbulent mixing: new results on free drainage vs. liquid content. Eur Phys J B 1999;12(1):67–73.
[136] Loewen MR, O'Dor MA, Skafel MG. Bubbles entrained by mechanically generated breaking waves. J Geophys Res 1996;101(C9):20,759–69.
[137] Chanson H. Air bubble entrainment in free surface turbulent shear flows. Academic Press; 1996.
[138] Ross J, Miles GD. An apparatus for comparison of foaming properties of soaps and detergents. Oil and Soap 1941;18(5):99–102.
[139] Dressaire E, Bee R, Bell DC, Lips A, Stone HA. Interfacial polygonal nanopatterning of stable microbubbles. Science 2008;320(5880):1198–201.
[140] Lesov I, Tcholakova S, Denkov N. Factors controlling the formation and stability of foams used as precursors of porous materials. J Colloid Interface Sci 2014;426:9–21.
[141] Kroezen A, Wassink JG. Foam generation in rotor–stator mixers. JSDC 1986;102:397–403.
[142] Hanselmann W, Windhab E. Flow characteristics and modelling of foam generation in a continuous rotor/stator mixer. J Food Eng 1999;38:393–405.
[143] Muller-Fischer N, Suppiger D, Windhab EJ. Impact of static pressure and volumetric energy input on the microstructure of food foam whipped in a rotor–stator device. J Food Eng 2007;80:306–16.
[144] Garrett PR. Recent decelopments in the understanding of foam generation and stability. Chem Eng Sci 1993;48(2):367–92.
[145] Mary G, Mezdour S, Delaplace G, Lauhon R, Cuvelier G, Ducept F. Modelling of the continuous foaming operation by dimensional analysis. Chem Eng Res Des 2013;91(12):2579–86.
[146] Thakur RK, Vial C, Djelveh G. Influence of operating conditions and impeller design on the continuous manufacturing of food foams. J Food Eng 2003;60:9–20.
[147] Tcholakova S, Lesov I, Golemanov Konstantin, Denkov Nikolai D, Judat Sonja, Engel Robert, et al. Efficient emulsification of viscous oils at high drop volume fraction. Langmuir 2011;27:14783–96.
[148] Tcholakova S, Lesov I, Golemanov K, Denkov ND. Drop size in concentrated emulsions, obtained by rotor–stator homogenization. Proceedings of the world congress on emulsion 2010; 2010.
[149] Golemanov K, Tcholakova S, Denkov ND, Ananthapadmanabhan KP, Lips A. Breakup of bubbles and drops in steadily sheared foams and concentrated emulsions. Phys Rev E 2008;78:051405-1.
[150] Caps H, Vandewalle N, Broze G. Foaming dynamics in Hele–Shaw cells. Phys Rev E 2006;73:065301.
[151] Caps H, Vandewalle N, Broze G, Zocchi G. foamability and structure analysis of foams in Hele–Shaw cell. Appl Phys Lett 2007:214101-1–3.
[152] Tufaile A, Tufaile APB. Stretching and folding mechanism in foams. Phys Lett A 2008;372(42):6381–5.
[153] Vignes-Adler M. The fizzling foam of champagne. Angew Chem Int Ed 2013;52(1):187–90.
[154] Arzhavitina A, Steckel H. Foams for pharmaceutical and cosmetic application. Int J Pharm 2010;394(1–2):1–17.
[155] Gogate PR, Pandit AB. Hydrodynamic cavitation reactors: a state of the art review. Rev Chem Eng 2001;17(1):1–85.
[156] Raut JS, Stoyanov SD, Duggal C, Pelan EG, Arnaudov LN, Naik VM. Hydrodynamic cavitation: a bottom-up approach to liquid aeration. Soft Matter 2012;8(17):4562–6.
[157] Mansour LB, Chalbi S, Kesentini I. Experimental study of hydrodynamic and bubble size distributions in electroflotation process. Indian J Chem Technol 2007;14(3):253–7.
[158] Hammadi Z, Morin R, Olives J. Field nano-localization of gas bubble production from water electrolysis. Appl Phys Lett 2013;103(22) [p. –].
[159] McGuinness P, Drenckhan W, Weaire D. The optimal tap: three-dimensional nozzle design. J Phys D Appl Phys 2005;38(18):3382–6.
[160] Vladisavljević GT, Kobayashi I, Nakajima M. Production of uniform droplets using membrane, microchannel and microfluidic emulsification devices. Microfluid Nanofluid 2012;13(1):151–78.
[161] Anthony David Harman, Jan Willem Marinus Mijers, Nikki Robinson. Preparation of therapeutic foam 2006 EP 1898860 A1.
[162] Fernandez D, Maurer P, Martine M, Coey JMD, Moebius ME. Bubble Formation at a Gas-Evolving Microelectrode. Langmuir 2014;30(43):13065–74.

Please cite this article as: Drenckhan W, Saint-Jalmes A, The science of foaming, Adv Colloid Interface Sci (2015), http://dx.doi.org/10.1016/j.cis.2015.04.001